UNIVERSITY OF SOUTHAMPTON

FACULTY OF ENGINEERING AND THE ENVIRONMENT

Bioengineering Science Research Group

Modelling nutrient transfer across the placenta

by

Simone Perazzolo

Thesis for the degree of Doctor of Philosophy

April 2017

UNIVERSITY OF SOUTHAMPTON

ABSTRACT

FACULTY OF ENGINEERING AND THE ENVIRONMENT

Bioengineering Science Research Group

Thesis for the degree of Doctor of Philosophy

MODELLING NUTRIENT TRANSFER ACROSS THE PLACENTA

by Simone Perazzolo

The placenta is a fetal organ that separates the maternal from the fetal circulation and mediates the transfer of nutrients between the mother and the fetus. Placental transfer of nutrients occurs across the placental villi, which are finely branched tree-like structures. Nutrients from the maternal blood in the intervillous space cross the villous barrier and then enter the fetal capillaries. A healthy pregnancy outcome is dependent on adequate placental transfer of gases and nutrients from the maternal to the fetal circulation. Impairments in nutrient transfer lead to altered fetal growth, which also has health implications in later life. While the transport mechanisms that mediate this transfer are known, the ways in which these interact as a system are not well understood.

Mathematical modelling provides a tool to enhance the interpretation of placental transfer experiments. In this thesis, physiologically based compartmental models were employed for the study of nutrient transfer between the mother and the fetus and validated with data from ex vivo placental perfusion and in vivo clinical experiments. With respect to previous models, a more extensive range of modelling applications is presented in this thesis including several different transport mechanisms. Model implementation was carried out for fatty acids, amino acids and cortisol. In particular, fatty acids were studied extensively in vivo and in vitro. In addition, a 3D image based modelling approach of the placental microstructures was carried out. The main novelty compared to previous approaches was that the transport of nutrients in the maternal blood was modelled explicitly and a study of nutrient uptake with respect to different maternal blood flow rates was performed.

The main objectives of this thesis were to increase the biological understanding of placental transfer and to provide a platform for quantification, prediction and evaluation of nutrient transfer across the placenta. This may ultimately form the basis for clinical tools to help physicians to prevent, recognise, intervene and cure problematic pregnancies.

The main results of the thesis were that placental metabolism was found to play a rate-limiting role in fatty acid and amino acid transfer and that the flow environment in the placental microstructure had a significant effect on limiting transfer. Examples of application of the proposed models to experimental data from external collaborators was successful and enhanced their interpretation and value.

Future work needs to focus on the further investigation of placental metabolism, such as the localisation and characterisation of metabolic sub compartments. Moreover, future modelling investigation of the 3D microstructure of the placenta should focus on the inclusion of both maternal and fetal capillary flow and the implememntation of more complex transport mechanisms. The models developed in this thesis could equally be used to study the transfer of other substances, e.g. drugs or toxins, in normal and altered pregnancies. In this respect, the models presented should be integrated as part of the realisation of a "virtual" placenta.

Table of Contents

List of Tables

List of Figures

List of Publications

JOURNAL PAPERS

S Perazzolo, RM Lewis, BG Sengers. Modelling the effect of intervillous flow on solute transfer based on 3D imaging of the human placental microstructure. Submitted to *Annals of Biomedical Engineering*, 2017.

S Perazzolo, B Hirschmugl, C Wadsack, G Desoye, RM Lewis, BG Sengers. The influence of placental metabolism on fatty acid transfer to the fetus. *Journal of Lipid Research,* V58-2 443-454, American Society for Biochemistry and Molecular Biology, 2016.

E M Lofthouse, S Perazzolo, S Brooks, IP Crocker, JD Glazier, ED Johnstone, N Panitchob, CP Sibley, KL Widdows, BG Sengers, RM Lewis. Phenylalanine transfer across the isolated perfused human placenta: an experimental and modelling investigation. *American Journal of Physiology-Regulatory, Integrative and Comparative Physiology,* V310-9 828-838, American Physiological Society, 2015.

CONFERENCE PAPERS

S Perazzolo, RM Lewis, BG Sengers. Modelling nutrient transfer based on 3D imaging of the human placental microstructure. *Engineering in Medicine and Biology Society (EMBC), 38th Annual International Conference of the IEEE*, 2016.

S Perazzolo, B Hirschmugl, C Wadsack, G Desoye, RM Lewis, BG Sengers. Computational modelling of fatty acid transport in the human placenta. *Engineering in Medicine and Biology Society (EMBC), 37th Annual International Conference of the IEEE*, 2015.

Acknowledgements

First, I should like to thank God. I should like to thank, as ever, my parents Graziella and Vasco Perazzolo and my brother Daniel for their continual patience and unwavering support, which I have had and always will be blessed with. I am grateful to all the good friends that I have met along the way. I should also like to express my earnest gratitude to my supervisors, Bram and Rohan, for accompanying me on this educational journey. Finally, I would like to thank the Bioengineering Science Research Group, the Faculty of Engineering and the Environment faculty and the Graduate School for providing me with the best research environment as possible.

I would like to acknowledge my funding partners: The University of Southampton Institute of Life Science and EPSRC DTP. In addition, I would like to acknowledge all the experimental collaborators for providing me with the biological and clinical data upon which I built and tested my models, as part of the European Union Seventh Framework Programme (FP7/2007-2013), project EarlyNutrition 289346: Birgit Hirschmugl, Christian Wadsack and Gernot Desoye from the Medical University of Graz, Austria; Antonio Gazquez Garcia and Elvira Larque from University of Murcia, Spain.

List of Abbreviations

AAL	Aleuria Aurantia Lectinto: tracer binding to the capillary endothelium
ARA	Arachidonic acid: a long chain poly-unsaturated fatty acid (C20:4n6, omega-6)
BM	Basal Membrane: syncytiotrophoblast fetal facing membrane
BSA	Bovine Serum Albumin: experimental albumin for fatty acid binding in plasma
CE	Cholesteryl ester: cholesterol esterified to a fatty acid
DSL	Datura Starmonium Lectin: tracer binding to the syncytiotrophoblast
DHA	Docosahexaenoic acid: a very long chain poly-unsaturated fatty acid (C22:6n3, omega-3)
FABP	Fatty Acid Binding Protein: family of fatty acid transporters in the cytosol
FABP(pm)	Fatty Acid Binding Protein (plasma membrane): extruding membrane protein from the syncytiotrophoblast MVM and involved in the transport of the very long chain fatty acids
FAT/CD36	Fatty Acid Translocase (Cluster of Differentiation 36): a transmembrane membrane protein involved also in the fatty acid transport
FATP	Fatty Acid Transport Protein: family of membrane fatty acid transporters
FEA	Finite Element Analysis
FEM	Finite Element Modelling
IUGR	Intra-Uterine Growth Restriction
GC-MS	Gas Chromatography-Mass Spectrometry
LA	Linoleic acid: a long chain poly-unsaturated fatty acid (C18:2n6, omega-6)
LCPUFA	Long Chain Polyunsaturated Fatty Acids
LGA	Large for Gestational Age
MVM	Microvillous Membrane: syncytiotrophoblast maternal facing membrane
NEFA	Non-Esterified Fatty Acids

OA Oleic acid: a long chain mono-unsaturated fatty acid (C18:1)

PA Palmitic acid: a long chain saturated fatty acid (C16:0)

PL Phospholipid: lipid class formed by esterification of glycerol, 2 fatty acids and at least one compound with one phosphate group

PBPK Physiological Based Pharmacokinetics

PBS phosphate-buffered saline

PSA Pisum Sativum Agglutin: tracer binding to stromal tissue

SA Stearic acid: a long chain saturated fatty acid (C18:0)

TG Triglycerides: lipid class formed by esterification of glycerol and 3 fatty acids

List of Symbols

R Maternal reservoir

M Maternal intervillous space

S Syncytiotrophoblast

P Metabolic Pool

F Fetal capillary volume

Q_M Maternal flow

Q_F Fetal flow

u Mass measurement of uptake of fatty acids

d Mass measurement of delivery of fatty acids

J_{MVM} Net flux of fatty acids across the MVM

V_{MVM} Maximum net rate flux capacity of fatty acids across MVM

V_{BM} Maximum net rate flux capacity of fatty acids across BM

K Association/dissociation constant of membrane carrier and fatty acids.

J_{BM} Net flux of fatty acids across the BM

k_a Accumulation rate of fatty acids into metabolic pool

k_r Release rate of fatty acids from metabolic pool

J_{uptake} Uptake flux of fatty acids from maternal plasma to placenta *in vivo*

$J_{delivery}$ Flux of fatty acids from placenta to fetal plasma *in vivo*

$J_{fetaltissue}$ Deposition flux of fatty acids from fetal plasma to fetal tissue *in vivo*

$J_{A,ex}^{I\rightarrow II}$ Net flux of amino acids in membrane exchanger from side I to side II of membrane

$J_{A,fa}^{I\rightarrow II}$ Net flux of amino acids in membrane facilitated transporter from side I to side II of membrane

k_c Rate of conversion cortisol-cortisone enzyme

κ Hydraulic permeability in placental 3D sample

q Estimated placental uptake in placental 3D sample

α_{tot} Total estimated uptake in placental cotyledon as repetition in series of averaged 3D placental samples

Chapter 1: Introduction

Pregnancy is a critical period of physiological change for the mother while the feto-placental unit develops within the uterus. Pregnancy lasts around 39 weeks. During the pregnancy, the placenta is the organ separating the maternal from the fetal blood, while supporting the normal growth and development of the fetus. Fetal growth is dictated by interaction between the fetuses genetic potential and the supply of maternal nutrients via the placenta [1]. Placental pathologies are the main cause (65%) of intrauterine fetal death after the 20th week of pregnancy [2]. Thus, analysing the placenta is of great interest as it may help to determine the origin of pregnancy outcomes, which spans from abnormalities in placental physiology (*e.g.* maternal floor infraction), to diseases that do not originate in the placenta but cause abnormal placental function (*e.g.* maternal under-perfusion) and to abnormalities in the intrauterine environment (*e.g.* altered expression of nutrient transporters). Although the placenta is usually discarded after birth, it is a unique source of information and can be studied immediately after birth (*e.g. ex vivo* perfusions or tissue analysis).

Nutrient flux across the placenta is dependent on the accessibility of the placental structure (micro- and macro-structure), nutrient-specific transporters, utero-placental and umbilical blood flows. Transfer of highly permeable molecules, such as oxygen, is particularly dependent on flow, while for less permeable substances, such as fatty acids, the placenta possesses specific membrane transport systems that will be rate determining.

Fatty acids are the building blocks for cell membranes and precursors for several biosynthetic pathways. They serve many critical roles in fetal life including the development of the fetal brain and fat accretion [3-5]. It has been shown an association between the percentage of maternal plasma omega-3 fatty acid during gestation and the development of cognitive functions in the neonate [6]. Nonetheless, fatty acids are hydrophobic compounds in a hydrophilic environment and their passive transport mechanisms across biological membranes is not well understood, placental transport included. A novel multi-compartmental model of the placental fatty acid transfer will be presented in the thesis. This model will be adapted to two experimental studies by external collaborators to simulate placental fatty acid transfer under different operating conditions.

Another important class of nutrients for a healthy fetal growth are the amino acids. They are the building blocks of proteins. Impaired fetal growth, such as intrauterine growth restriction (IUGR), has been shown to be associated with inadequate placental amino acid transfer [7-9]. Amino acid transport across the placental membranes is actively mediated by a range of distinct membrane transporters, however the ways in which these transporters interact as a system is hard to predict intuitively. An adaptation of a pre-existent multi-compartmental model of the placental amino acid transfer, including several transport mechanisms, will be presented in the thesis and for the first time compared to experimental data.

Not only nutrients get across the placenta, also hormones. Cortisol is a hormone secreted by the mother that is increased in response to stress. Perinatal exposure to higher levels of cortisol retards the fetal growth leading to low weight offspring [10]. In order to protect the fetus, the placenta activates an enzyme, 11β-hydroxysteriod dehydrogenase 2 (11β-HSD2), which converts cortisol into its inactive form, cortisone. This protects the fetus from exposure to maternal cortisone. Nonetheless, the efficiency of this biochemical "barrier" is not clear. A novel compartmental model of the placental cortisol and cortisone transfer will be presented in the thesis, including the enzymatic conversion from cortisol to cortisone.

Placental morphology may become a major factor limiting transfer for small solutes [11]. For example, severe abnormal placental physiology can compromise oxygen transport with immediate fetal impact and may lead to permanent fetal brain damage and death [12]. It was, therefore, a major objective to use modelling to evaluate the effect of the placental geometry, especially by including the microscale features where the transfer is thought to occur. Nonetheless, placental morphology is highly complex, and its representation has previously mainly consisted of 1D or 2D structures or simplified 3D continuum approaches [11]. In this thesis, an innovative method employing 3D image based modelling using finite element analysis will be implemented, with the focus on the impact of the maternal blood flow on placental transfer, which has not been considered previously.

Overall, computational methods will provide useful tools in helping to understand the underlying biology, to provide predictive methods that can be integrated into the design of experimental studies and ultimately to provide a support platform to facilitate clinical decisions. Although most of the effort in this project was invested in modelling placental transfer of specific nutrients (in particular fatty acids), the approach could be equally applied to other nutrients or drugs. In addition, the 3D image-based finite element

modelling (FEM) approach presented at the end of the thesis, not only complements the compartmental modelling approaches but also represents a very innovative field with significant potential to be expanded into further multiscale modelling studies, going from the microscale to the entire placenta.

1.1 Summary of the aims of the thesis

The main aims of this thesis are:

1) Propose a novel compartmental model for the transfer of fatty acids across the placenta
2) Apply the fatty acid model to
    a. compare lean and obese pregnant mothers
    b. analyse *in vivo* experimental data
3) Extend the compartmental approach to the placental transfer of amino acids and cortisol
4) Develop microscale 3D models for the placental transfer of a diffusive solute

A general modelling paradigm will be followed, where possible, throughout the thesis as outlined in Fig. 1.1.

1.2 Thesis structure

The text is structured as follows: the present introductory Chapter 1, followed by a Background Chapter 2 providing an overview of the placental physiology, nutrient transport, perfusion experiments and previous modelling work. The model of fatty acids transfer is presented in Chapter 3 and applied to an *ex vivo* placental perfusion experiment. A further *ex vivo* application of this fatty acid transfer model was presented in Chapter 4, where an investigation was carried out to compare the transfer of fatty acids between lean and obese mothers. An example of an *in vivo* application of the fatty acid model was presented in Chapter 5, where the model was adapted to study the placental transfer of fatty acids in pregnant women. A modelling evaluation of the effect of placental blood flow on the transfer of amino acids is presented in Chapter 6. A first modelling exploration of cortisol transfer is presented in Chapter 7. The 3D image based model for the effect of the placental microstructure on transfer is presented in Chapter 8. Finally, in Chapter 9, the thesis concludes with an overall discussion of the modelling results, including perspectives for future work.

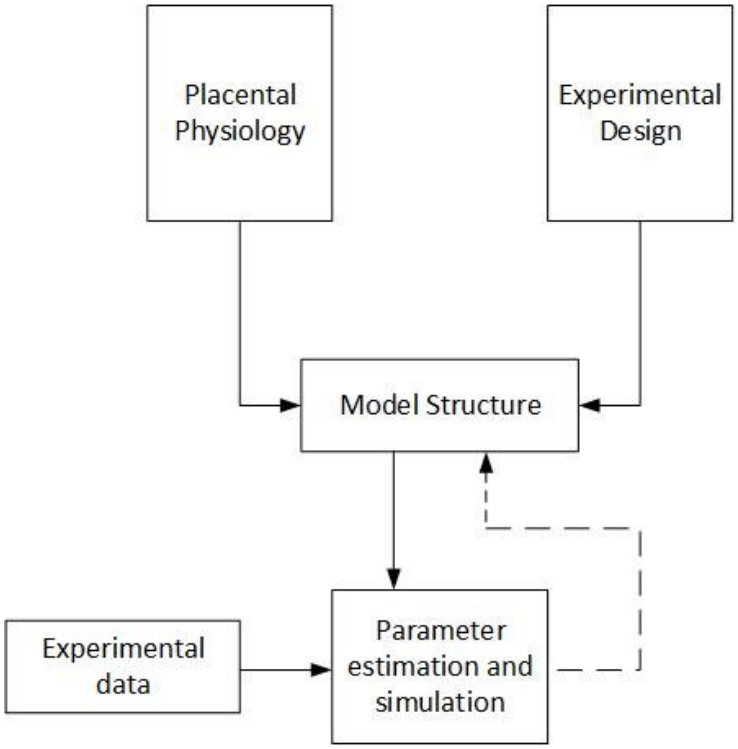

Figure 1.1. *Workflow paradigm for developing the placental models in this thesis. The model needs to incorporate aspects of the placental transfer system alongside the experimental design. As part of the modelling process, a number of necessary simplifications and assumptions will be selected in accordance with the scope of the investigation and the level of available knowledge. Once the model structure has been determined, simulations are carried out and a set of parameters of interest can be estimated from the experimental data. If required, as indicated by the simulation results, the model structure can be refined in an iterative loop (dashed line).*

Chapter 2: Background

The placenta is the interface between the mother and the growing fetus. It supplies the fetus with water, nutrients and oxygen, while clearing carbon dioxide and other wastes from the fetal circulation. It is a selective barrier between the maternal and fetal circulations and has metabolic and endocrine roles, thus fulfilling functions of multiple organs. Understanding the placental function is important in order to understand fetal development. Studying the placenta may help the assessment of baby health risks as a valuable source of information about the development of the baby during pregnancy. The rate of nutrient transfer is greatest in the third trimester of pregnancy (from 24th week of gestation until birth) and the mature placenta will be the focus of the work presented in this work.

2.1 Structure of the placenta

The placenta is a fetal organ developed by almost all mammals during pregnancy, including *Homo Sapiens* (Fig. 2.1). A healthy human placenta is a disk-like with an average diameter of 22 cm [13]. The average thickness of the delivered organ is 2.5 cm and the average weight is around 450 g [13]. The two faces of the placenta are the chorionic plate (which stems the umbilical cord, Fig. 2.2A) and the basal plate (which attaches to the uterine wall, Fig. 2.2B). The placenta separates the maternal from the fetal blood and it is subdivided into functional transfer units, called cotyledons or lobules. It is estimated that a healthy placenta has more than twenty cotyledons [13].

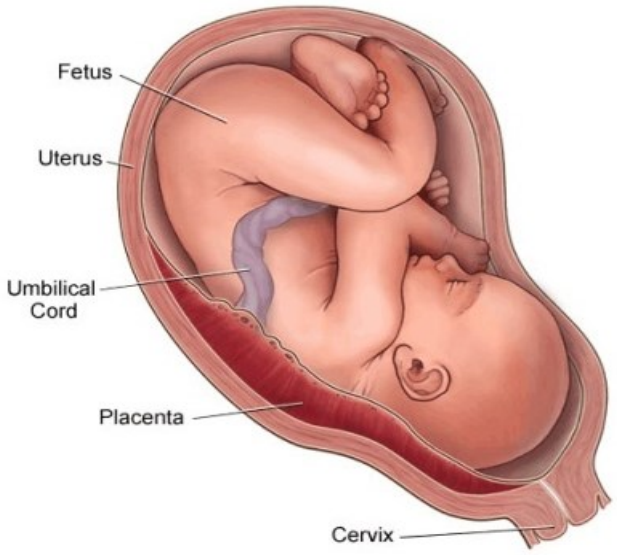

Figure 2.1. *Overview of the placental location and womb anatomy. Image adapted from* [13].

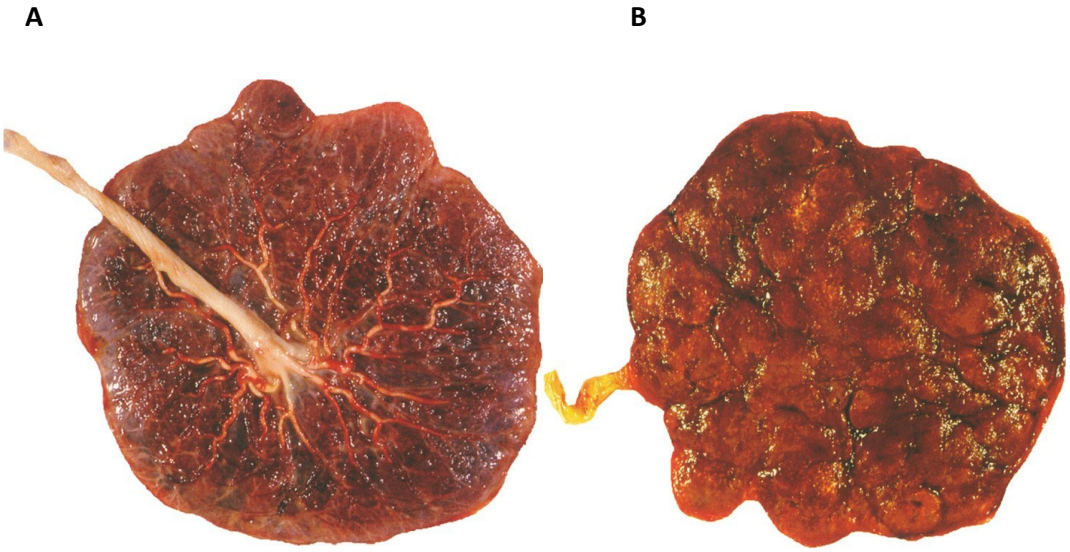

Figure 2.2. *Appearance of the human placenta*. (***A***) *Chorionic plate.* (***B***) *Basal plate. Image adapted from* [13].

The placenta is derived from embryonic tissues and does not contain any maternal tissue as part of its structure. Maternal blood leaves the maternal vascular system when it spills out into the intervillous space from uterine spiral arteries. The maternal blood then percolates between the placental villi leaving via openings into uterine veins where it re-enters the maternal vascular system. The oxygenated blood flows in by the uterine spiral arteries and the deoxygenated blood is drained by the uterine decidual veins (Fig. 2.3). Although many years of human placenta studies have passed, the exact number of spiral arteries and decidual veins perfusing the placenta is still unknown owing to the difficulty finding the vessels and distinguish between arteries and veins at the delivery [13]. The physical space in which the spiral arteries bring the blood is called intervillous space that is the space between the fetal villi.

The placenta has a villous structure, where the villi have a tree-like shape. The villi form the intervillous space in a conformation that augment their surface available for exchange, which is estimated to be around 13 m^2 [14]. As a tree, it has several generations of branches that differ by their calibre, stromal structure, vessel structure and location within the villous tree. According to these criteria, five villi types are distinguished: stem villi (300–3000 µm of calibre), immature intermediate villi (60–200 µm of calibre), mature intermediate villi (40–80 µm of calibre), terminal villi and mesenchymal villi (30–80 µm of calibre) [13]. Inside of each villus, fetal capillaries stream fetal blood from the umbilical arteries to the umbilical vein. All the nutrient exchange between the mother and the baby take place at the surface of the villi (Fig. 2.5). In particular, the exchange mainly occurs in the smallest branches of the tree, i.e. the terminal villi (at the micro-scale level of the placental structure, Fig. 2.4 A, B, C).

Inside the terminal villi the fetal capillaries are located close to the Syncytiotrophoblast [13], and sometimes the distance between the villi membrane and the capillary is further reduced (vasculo-syncytial membranes [13]). Generally, between the villous and inner fetal capillaries, there are three main structural layers (Fig. 2.3, 2.6): (1) The **syncytiotrophoblast** is a thin trophoblastic cover in the form of a syncytium (a single cell or cytoplasmic mass containing several nuclei in which the cytoplasm of constituent cells is continuous), characterized by a mother-facing brush border membrane, and named micro-villous membrane (**MVM**) which is in direct contact with the intervillous space. On the fetal side of the syncytiotrophoblast there is the basal membrane (**BM**) [15]; (2) The **stroma** is a connective tissue with structural functions and contains few fibroblasts and macrophages (called Hofbauer cells). (3) The fetal **capillary endothelium**, whose endothelial cells surround the vessel, are characterized by clefts between them.

Nutrient transfer from mother to fetus passes through the different compartments and barriers in this order: maternal arterial blood, uterine spiral artery, intervillous space, MVM of the syncytiotrophoblast, BM of the syncytiotrophoblast, stroma, fetal capillaries, umbilical vein, and fetal arterial blood. This pathway is reversed for transfer of fetal wastes to the mother.

The role of the fetal capillaries endothelium as a barrier is unclear [16, 17]. For nutrients such as glucose and amino acids, it is believed they simple diffuse through the junctions between endothelial cells. However, it is less clear how hydrophobic nutrients, such as fatty acids, cross this barrier, as they need to be bound to a carrier protein. Among the physical components of the placental system, the syncytiotrophoblast has a very dynamic environment possessing metabolic and regulatory pathways. The syncytiotrophoblast is considered the main transport barrier [18-20].

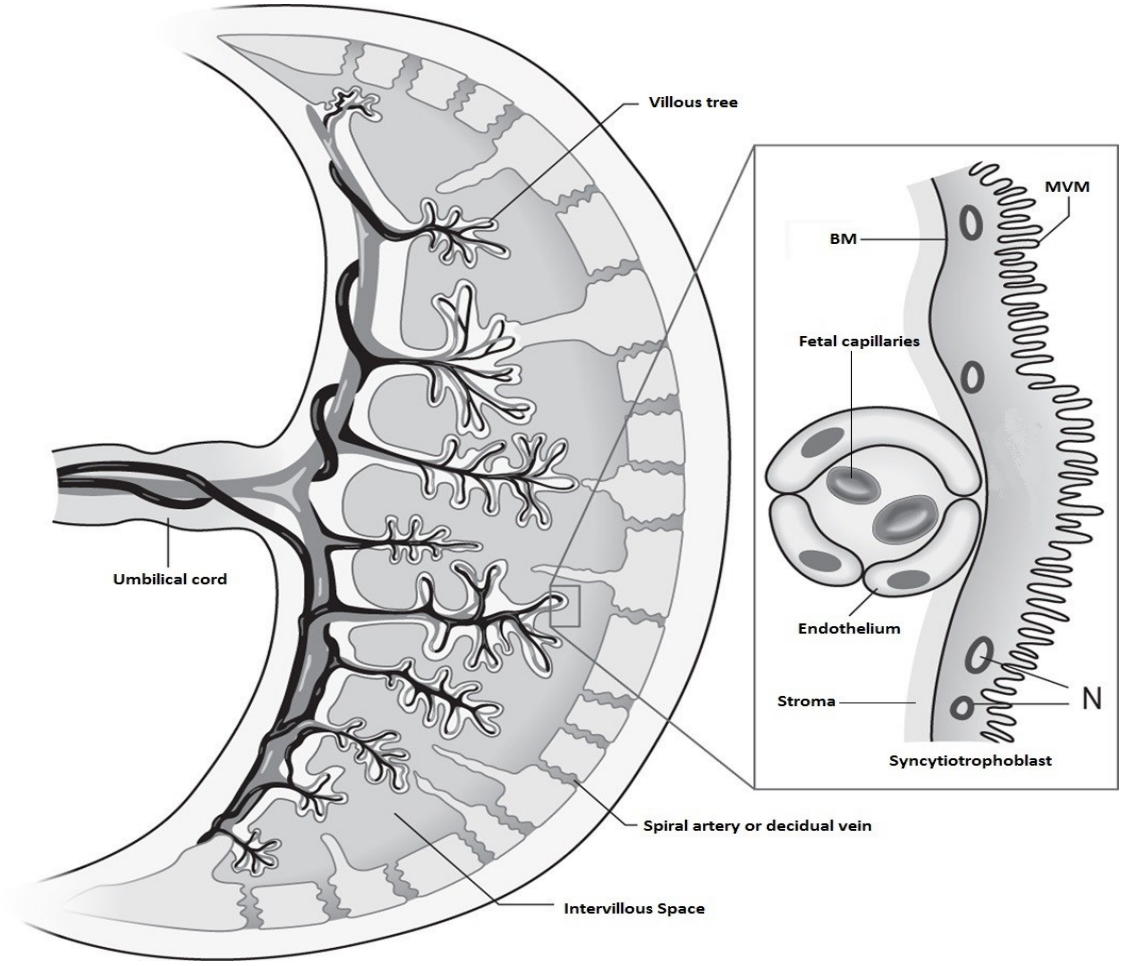

Figure 2.3 *A schematic cross-section of the human placenta.*

The maternal side of the placenta originates from the uterus wall and has vessels (spiral arteries) bringing the oxygenated maternal blood into the intervillous space, which is the space between each villous tree and the spiral arteries outlet. The deoxygenated blood is drawn from the intervillous space into the decidual veins. The fetal side of the placenta is represented by the fetal capillaries and originates from the fetus. The villi are in a tree-like configuration and they have branches of several calibres. The insert to the right shows in detail a schematic cross-section structural layer of the placenta. They are the syncytiotrophoblast layer (where some nuclei are illustrated (N)) possessing two membranes, the microvilli membrane (MVM) and the basal membrane (BM), respectively facing the maternal and the fetal blood; The inner villous is vascularized by the fetal capillaries (FC), which are surrounded by the endothelial cells (EC), with a thin layer of connective tissue (stroma). Note that, although this is a commonly used schematic, the actual structure possesses more discretely divided lobules (cotyledons). Image modified from [21].

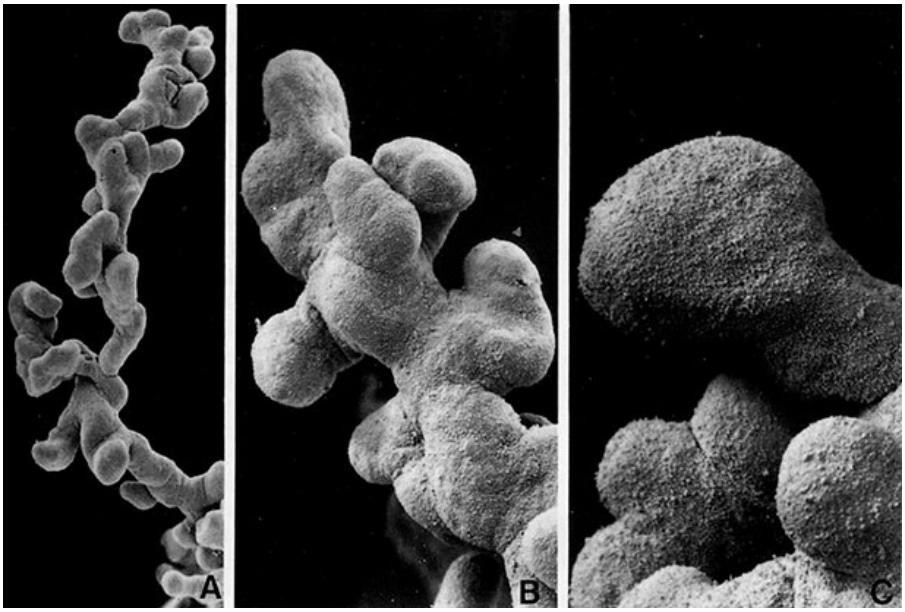

Figure 2.4. *Placental villous type microscope photographs.*
*(**A**) Mature **intermediate villus**. (**B**): Zoom of the mature intermediate villus showing the branching into **terminal villi**. (**C**): A group of terminal villi, with the central one showing a typically constricted neck region and a dilated final portion. Image taken with permission from* [13].

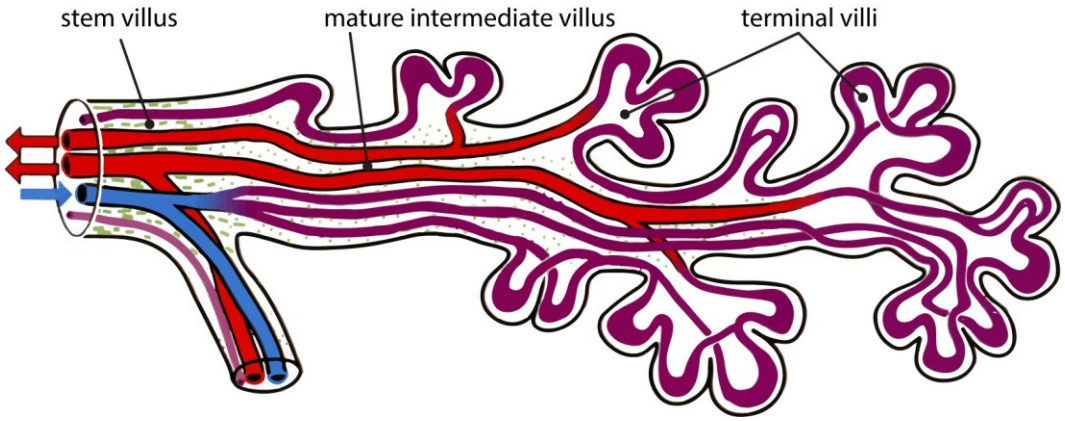

Figure 2.5. *Schematic of the typical structure of the inside of a placental villous.*
Location of fetal vessels inside a villous tree. The blue colour represents the fetal arteries and arterioles (de-oxygenated blood). The red represents the fetal venules and veins (oxygenated blood). Green stands for the stroma. Image adapted from [13].

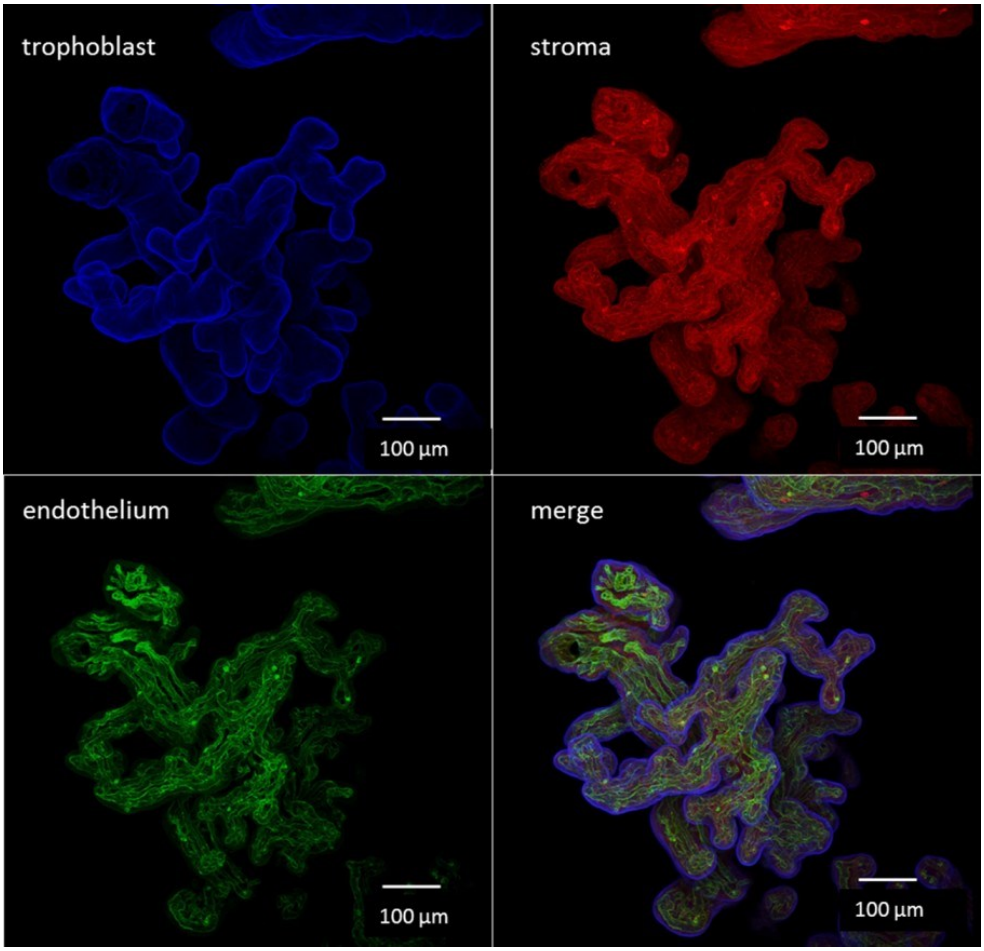

Figure 2.6. *Terminal villi 3D images.*

Confocal 3D projection images of placental terminal villi from term human placenta showing the three structural layers: The outer layer trophoblast localizing the MVM (in blue). The connective stroma (in red). The fetal capillary endothelium (in green). Image courtesy of Prof. R.M. Lewis, University of Southampton.

2.2 Placental functions

The placenta has multiple roles, mediating selective transfer of various types of molecules: nutrients, gases and wastes as well as being an endocrine organ that secretes the hormones, which adapt maternal physiology to support the pregnancy.

2.2.1 Transfer of substances and gasses between maternal and fetal circulations

Factors that influence transport across the placenta include uterine and umbilical blood flow, the area available for exchange, placental metabolism and the membrane transport system. Altered fetal growth is likely to occur as a consequence of one or more impairments of these factors [15, 16]. Transfer of highly permeable molecules, such as oxygen and carbon dioxide is particularly influenced by the flow [17]. For less permeable substrates, the placenta possesses both active and

passive transport mechanisms [18] (Fig. 2.7). There is also a paracellular route across the placenta that is not well defined due to the syncytiotrophoblast's lack of junctions between cells that normally mediate paracellular diffusion. However, despite an absence of an obvious physical route, there is clear evidence that such a route exists [22].

The primary barrier for the transport is commonly thought to be the syncytiotrophoblast layer. Therefore, the characteristics of both MVM and BM will have a major influence on the net placental nutrient transport.

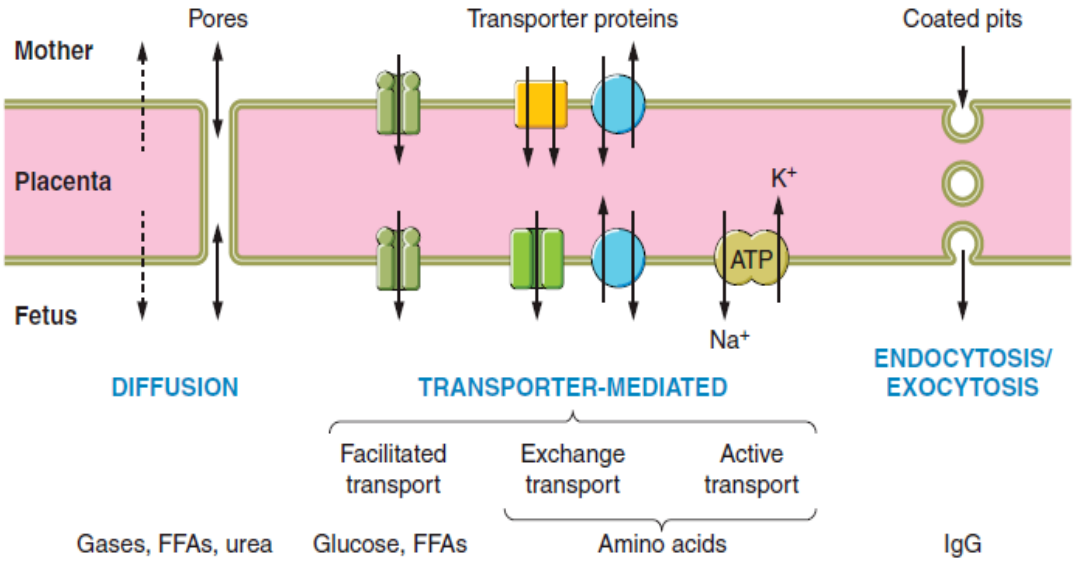

Figure 2.7. *Diagram of the main processes of transport typically found in the placental membranes.*

Diffusion is the passage of simple molecules through the lipid bilayers or pores following the thermodynamic gradient (e.g. this is the case for O_2). Transporter-mediated refers to transport across the membranes dependent on carrier proteins embedded in the membrane, which commonly facilitate the transport across the lipid bilayer of hydrophilic molecules. Transported-mediated can be passive (Facilitated transport, e.g. for glucose, and Exchange transport, e.g. for specific amino acids) or active (Active transport, e.g. for certain amino-acids or ions), in which the transporter pumps against the gradient. Active transport can be a combination of primary Exchange transport and secondary Active transport (e.g. for specific amino acids). Endocytosis/exocytosis is the process of invagination/expulsion of vesicles containing molecules (e.g. immunoglobulin G, IgG). Note that, although no one has ever found actual pores in the placental membranes, they are sketched here to represent potential mechanisms for the paracellular route. Image adapted from [23].

2.2.2 Fatty acids

A fatty acid is a carboxylic acid with an aliphatic chain characterised by the presence of single (saturated) or double bonds (unsaturated). Fatty acids form lipids (i.e. fat) when one or many (non-esterified) fatty acids (NEFA) esterify with an alcohol, such as glycerol, forming the compound called ester. The most common esters are the triglycerides (TG), cholesteryl esters (CE) and phospholipids (PL). Mainly, TG form the lipid deposit in the tissue and it is used as cellular fuel, CE and PL form the membranes, and all of them have several metabolic functions. Fatty acids vary in length and they can be short-chain ($C < 14$) or long-chain ($C \geq 14$) fatty acids. They can also be classified according to the degree of double bonds in their carbon chain as saturated (no double bonds), monounsaturated (one double bond) and poly-unsaturated fatty acids (PUFA, multiple double bonds). Long-chain fatty acids are found in appreciable amounts in the humans, and the PUFA are of particular metabolic and immune response importance. When PUFA have their first double bond in the third carbon, they are called omega-3 (similarly, when they have the first bound on the sixth carbon, they are called omega-6). Another classification of fatty acids (typical for the PUFA) is if they are "essential", i.e. if the human body cannot synthetize them but they are still necessary for the regular maintenance of the body. Many omega-6 and omega-3 are essential fatty acids. For example, Linoleic Acid (LA) is an essential omega-6 PUFA and Docosahexaenoic Acid (DHA) is an essential omega-3 PUFA. The essential PUFA are considered of critical importance for a correct fetus growth [5]. For sake of terminology, when using the term fatty acids we will refer to the long-chain fatty acids in –cis conformation, as the -trans configuration is not found in nature.

2.2.2.1 Fatty acids in the placenta

Although the fetus might be able to synthesize saturated fatty acids and simple unsaturated fatty acids *de-novo* from glucose [24], the fetus cannot make long chain polyunsaturated fatty acids and these must be transported from the mother across the placenta [25]. The fetus needs these long chain polyunsaturated fatty acids to maintain the composition of its cell membranes and deficiency leads to neurodevelopmental impairment.

Once ingested as part of the diet, lipids are broken down into fatty acids that are absorbed by the gut endothelium where they are predominantly converted into TG. As TG is not water soluble, it is released into the body encapsulated into a form of lipoprotein called chylomicron [26]. Chylomicrons transport this exogenous dietary triglyceride to the body tissues, especially muscle and adipose, where the fatty acids are released by lipases. The chylomicron remnants are then taken up by the liver.

Within the body, endogenous lipid metabolism is controlled by the liver that secretes esterified fatty acids in lipoproteins that transport them around the body. Lipoproteins are classified upon

their density, which is inversely proportional to the amount of triglyceride they contain (very low-density lipoproteins VLDL, low density lipoproteins LDL, medium density lipoproteins MDL and high density lipoproteins HDL). Lipases act on the chylomicron and lipoproteins to release fatty acids, some of which are taken up by the tissue in which the lipases work. Lipases catalyse the dissociation of esters (*e.g.* TG) into NEFA. NEFA is the primary form in which a fatty acid can move across plasma membranes. Other routes include lysophospholipid transporters and endocytosis of lipoproteins. The lipases are found in several tissues, such as adipose tissue, muscles, heart, liver and placenta [27, 28].

During a healthy pregnancy, the maternal lipid profile shifts from an anabolic to a catabolic state and this results in gestational hypertriglyceridemia. This elevates the plasma concentrations of triglycerides (+300%), cholesterol (+25-50%) and the lipoprotein, all this favouring their availability for the fetus [5]. The placenta takes up and transports fatty acids in their non-esterified form (NEFA), however, the availability of NEFA is limited since the majority of the fatty acids are in the lipoproteins [29]. Lipases on the MVM degrade the TG within the lipoproteins into NEFA and make them available to the placenta for uptake. There are specific lipases for TG (lipoprotein lipase, LPL) and PL (endothelium lipase, EL) [27, 30] to break down the lipases to provide NEFA at the MVM (Fig. 2.8A). For the sake of terminology, from now on, when we refer to fatty acids, we mean the non-esterified fatty acids (NEFA).

2.2.2.2 Fatty acid transport in the placenta

Because fatty acids have low solubility in aqueous solutions such as blood plasma and interstitial fluids (e.g. intervillous space or syncytiotrophoblast cytosol), fatty acids require binding proteins to increase their concentration in those compartments [31, 32]. Plasma albumin binds the majority of the fatty acids in the blood. Since albumin cannot cross the plasma membrane, the fatty acids detach forming a local fatty acid transport gradient across the membrane [33]. The albumin association-dissociation with NEFA is in equilibrium. However, the mechanisms of dissociation of NEFA from albumin for the membrane transport is under debate, where dissociation may either occur before approaching the membrane [33] or in the proximity of the membrane [34]. Some authors have speculated the existence of a specific membrane mediator for albumin [33].

Experimental evidence exists for both simple (e.g. flip-flop [35]) and protein mediated transport of fatty acids across the plasma membranes [31]. Simple diffusion is thought sufficiently rapid to supply the cell when the fatty acids are non-ionized and primarily in the situation of fatty acids concentrations ratio with albumin concentration greater than 3 [36]. However, if the unbound fatty acids adjacent to the membrane they are ionized at physiological pH and the fatty acid to albumin ratio was found in pregnant mothers to be in the range of 0.78-1.3 [5, 37]. Thus, the placental

membranes were found to preserve saturable kinetics [38] and membrane transport proteins for fatty acids are expressed in the placenta (Fig. 2.8A, B):

- FABP (fatty acid binding protein): Family of membrane proteins that have been shown to be the most outwardly located acceptor in the plasma membrane. They facilitate the diffusion by increasing the local extra-to-intracellular fatty acid gradient and decreasing the diffusion distance in the unstirred bilayers [39].
- FATP (fatty acid transport protein): Integral membrane proteins that present CoA-synthetase activity and may directly translocate free fatty acids across the membrane and also direct them to acyl-CoA conversion, facilitating their metabolism within the syncytiotrophoblast. Present in both MVM and BM[40].
- FAT/CD36 (Fatty acid translocase): Multi-functional protein, involved also in the placental fatty acid transfer. It is unclear whether it might directly function as a translocase or if it binds the fatty acids to then transfer them to FATP. Present in both MVM and BM [40, 41].

Inside of the cell, in the syncytiotrophoblast cytosol, the fatty acids may bind to carriers to improve their transportability in an aqueous environment [32]. The intracellular-FABPs were found in the placenta (H-, L-) [42]. The function of these proteins is to transport the fatty acids around within the cell to each possible destination, e.g. oxidation, nuclear signal, to BM in order to pass to the fetal circulation *etc*. [43] (Fig. 2.8B).

Overall, the fatty acids transport is driven by the concentration gradient (see example Fig. 2.9) and it is believed to primarily rely on facilitated transport to supply the fetus with fatty acids, however, the contribution of the simple diffusion is not known. In addition, the contribution of lipases, albumin and internal carriers (e.g. L-FATP) to the overall transfer is not clear. To complicate things, the different fatty acids may behave differently in uptake, metabolism and release.

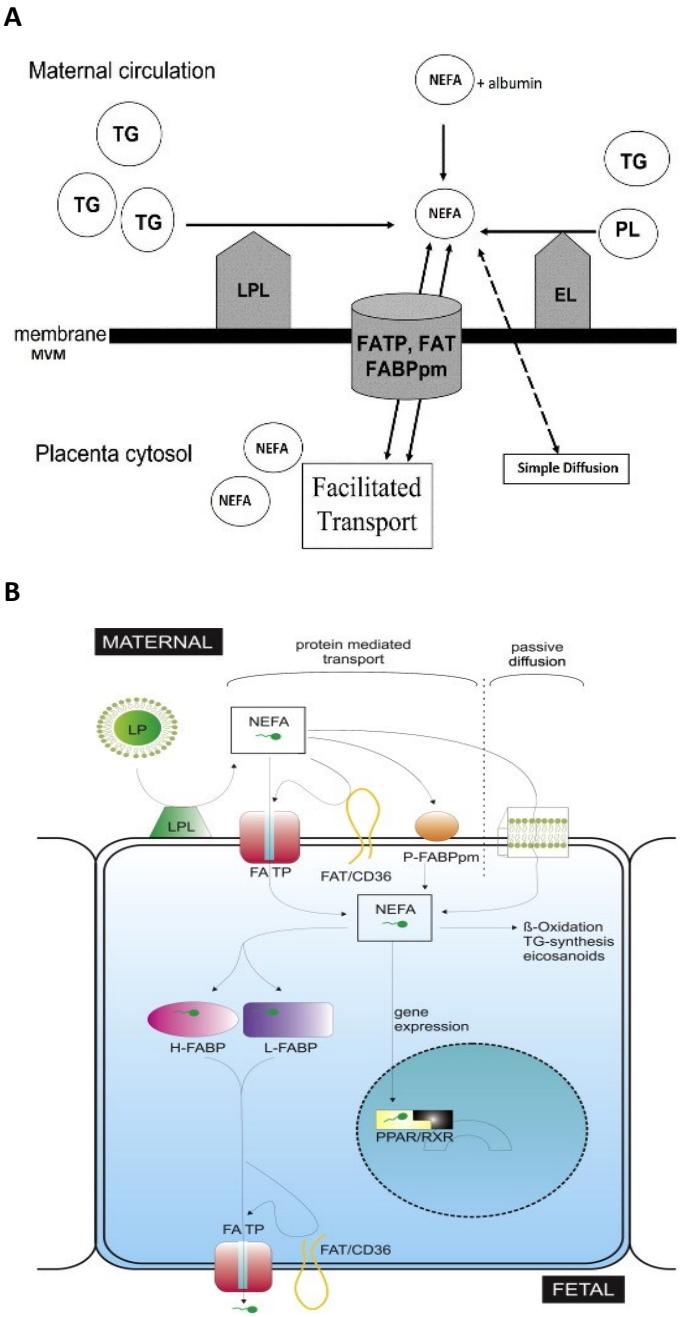

Figure 2.8. *Uptake and cytosol regulation of fatty acid in the placenta.*

*(**A**) Mechanisms involved in the uptake of circulating maternal fatty acids by placental tissue. Circulating TG and PL are degraded to free fatty acids by specific lipases (LPL and EL) found on the MVM. Then, NEFA can enter the cytosol via the membrane proteins (facilitated transport) or passive facilitated diffusion. Image modified from* [25]. *(**B**) An overview of the fatty acid transport across the placenta. Membrane proteins mediate fatty acid uptake into the syncytiotrophoblast (or this may occur by simple diffusion). Within the cell, the NEFA are bound by different fatty acid binding proteins trafficking the lipids towards the basal membrane, β-oxidation, TG esterification, eicosanoid synthesis, activation of nuclear transcription factors like PPAR/RXR etc. Image modified from* [40]. *In both (A) and (B) the NEFA is the only lipid capable of crossing the plasma membranes.*

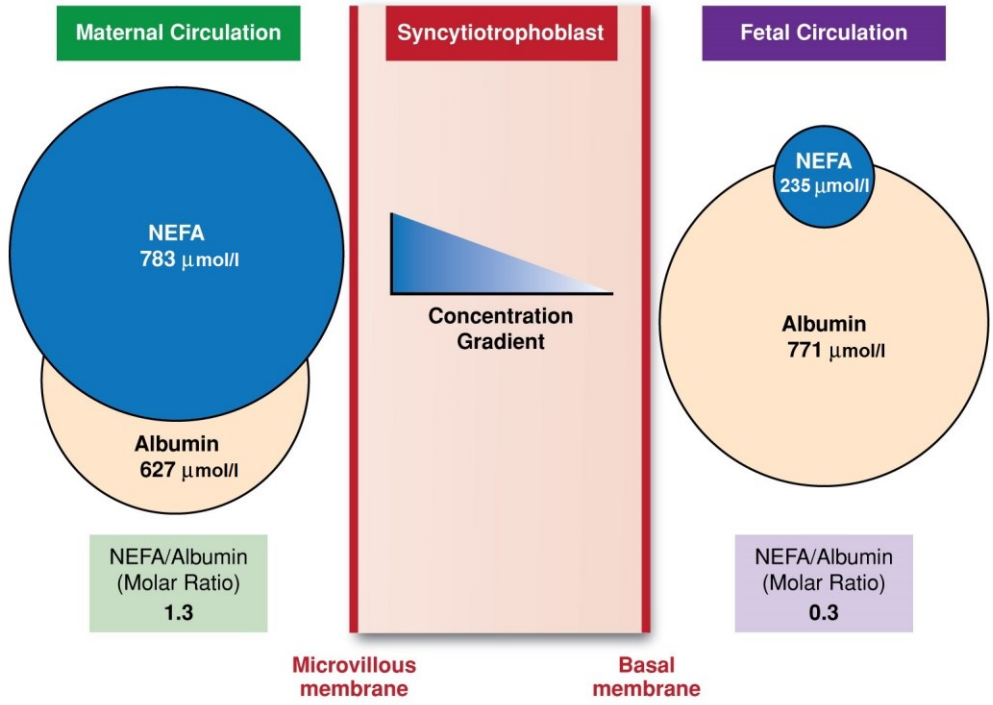

Figure 2.9. *Example of fatty acid gradient and concentrations.*
The net direction of the gradient is from mother to fetus. The albumin ratios are different as the fetal circulation may be more disposed to sequestrate the inlet fatty acids (each albumin can bind 5-7 NEFA [33]*). Image adapted from* [5].

2.2.3 Amino acids

Amino acids are the building blocks of proteins that form the cellular machinery. The fetus cannot make essential amino acids and therefore there must be a net transfer of essential and non-essential amino acids. Transfer of non-essential amino acids is also important as these can only be made by using amino groups from other amino acids. Amino acids uptake across cellular membranes is mediated by specific membrane transport proteins [44, 45] (Fig. 2.10):

- Accumulative transporters, which accumulate amino acids in the intracellular pool against their transmembrane concentration, usually by co-transporting extracellular sodium.
- Exchangers alter the intercellular amino acid composition by exchanging amino acids between the inside and outside of the cell.
- Facilitated transporters, which allow net transfer of amino acids across the basal membrane

For example, System A (accumulative transporter) transports glycine against its gradient via a coupling with the intracellular sodium gradient. Once inside the cell, the glycine can then be exchanged with another extracellular amino acid via System L (exchanger). This mechanism is an example of secondary active transport [45]. The placenta expresses more than 20 different amino

acids transporters. In addition, the paracellular route remains a possibility [22] and the BM has been suggested to possess also facilitated efflux transporters [46].

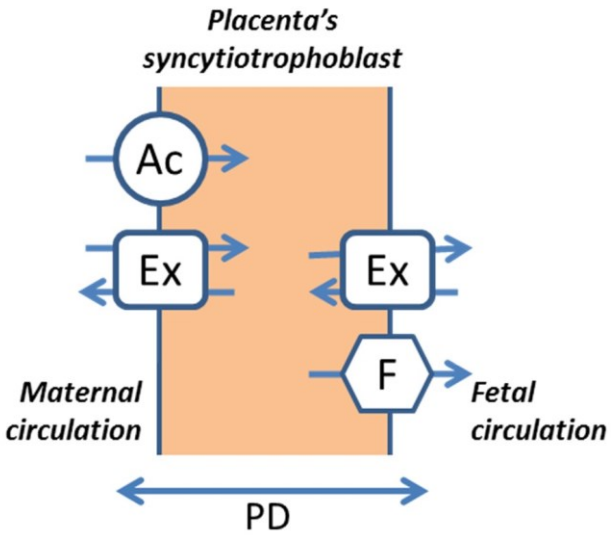

Figure 2.10: *Schematic of the amino acids transporters in the placental membranes. Transport proteins mediating amino acid transport are depicted in both MVM and BM. Categorized by their transport mechanisms, these transport proteins include accumulative transporters (Ac), exchangers (Ex), and facilitative transporters (F). Paracellular diffusion (PD) is also depicted as a potential route. Image taken with permission from [47].*

2.2.4 Cortisol

Cortisol is a steroid hormone that is produced in humans by the zona fasciculata of the adrenal cortex within the adrenal gland. It is released in response to stress and low blood-glucose concentration. Cortisol is not soluble in water and most of circulating cortisol in the bloodstream is bound to the plasma proteins (90% with corticosteroid binding protein) [48]. Little is known about the nature of the transmembrane transport of cortisol although this is likely to be a key process in the tissue-specific regulation of cortisol action. Currently, no specific transporter is known for cortisol; it is therefore still assumed that this hormone moves through the plasma membrane by passive simple diffusion when it has to exert its cytosol functions. Nevertheless, there is evi dence of saturable kinetics in liver cells [49]. In the placenta the enzyme 11ß-hydroxysteriod dehydrogenase 2 (11ß-HSD) converts the cortisol into an inactive form cortisone, thus it has been proposed as the mechanism guarding the fetus against over-exposure of cortisol during the pregnancy [50].

2.2.5 Respiratory gasses, water and ions

Oxygen and carbon dioxide freely cross the plasma membrane following their gradient. Gradients are thus maintained by the placental flows [51]. Nonetheless, the 99% of oxygen in the blood is transported bound to haemoglobin, and association-dissociation binding limits the transfer [52]. Interestingly, the oxygen affinity of fetal haemoglobin is higher than that of the maternal haemoglobin, which some researchers believe to facilitate oxygen transport from the mother to the fetus and carbon dioxide transfer from the fetus to the mother [53].

Water is believed to passively cross the placenta, with the transfer rate defined by the hydrostatic and osmotic pressures. Water transfer may be also facilitated by water-channel-forming integral protein as found expressed in the membranes of the syncytiotrophoblast [54]. The filtration is the process by which water and hence its solutes cross the membrane due to the hydrostatic pressure. Osmosis refers to the passive diffusion of water across a solvent-only permeable membrane. Most of the ions are actively transported across the placental membrane, e.g. sodium and chloride [54].

2.3 Endocrine and immune functions of the placenta

The placenta is an endocrine organ secreting hormones into both the maternal and fetal circulations. These hormones contribute to the maintenance of pregnancy and the maternal adaptations required to support the pregnancy (e.g. the hyperglycaemia and lipidemia). For example, the oestrogen causes breast enlargement in preparation for the lactation and uterine growth for the fetus and it is produced by the placenta [55].

The placenta protects the fetus from being infected by several diseases thus providing a protective interface between the two blood circulations that cannot mix [56]. Although some xenobiotics can be transferred by some of the placental transport mechanisms, the placenta arranges several protective mechanisms that diminish fetal exposure to dangerous agents. On one hand, there are special export pumps, on the other, special enzymes [57, 58]. Nevertheless, there are other substances (such as alcohol) that can still cross the placenta and have adverse effects on the fetus [53].

2.4 Placental insufficiency

During pregnancy, the fetus requires adequate nutrition for growth and development, while nutrient deficiency or surplus supply may result in abnormal fetal growth and dise ases in future life. Intrauterine growth restriction, (IUGR) affects 10% of all pregnancies and the placenta is reported to be under-perfused, small in overall size, with reduced cell volumes, decreased intervillous space and villous surface area and abnormal villous angiogenesis [59-61]. These conditions contribute to reduced overall placental transfer of amino acids and oxygen (which may lead to hypoxia) causing retardation of fetal growth in IUGR that can result in disease such as impaired neurological development after birth [59]. On the other hand, an oversupply of nutrients may occur when the mother is diabetic, gestational diabetic or obese yielding a condition in which the baby is large for gestational age (LGA). LGA may predispose to develop obesity in later life and raises the possibility of an intergenerational cycle of obesity [62]. Moreover, pathological disorders can also occur to the mother. For example, maternal anemia and preeclampsia were reported to be related to under-perfused placentas that also have low villous surface area [63].

In the third trimester of pregnancy, the rate of accretion of fatty acids in the fetus is 7 g per day. The fetal brain is composed of lipids at 50-60% and includes high proportions of very-long fatty acids, especially docosahexaenoic acid (DHA) and arachidonic acid (ARA) [64, 65]. DHA and ARA also are highly concentrated in the membranes of the retina [65, 66]. Impaired transfer of LCPUFA is associated with defects in the development of the fetal brain, hormonal environment, increased risk of abnormal development of the lungs [67, 68], and cardiovascular systems [69]. In particular, the DHA was found of particular importance due to its involvement in the fetal neurodevelopment, learning ability and visual acuity [6, 70].

Amino acid transport and restricted amino acid transfer have been associated with impaired fetal growth [71]. Prenatal exposure to corticoids retards the fetal growth leading to low weight offspring that might lead to diverse health problems in future life [72].

2.5 Experimental approaches to study placental transfer

Modern technologies provide numerous ways to study the placenta. However, few measurements are ethical in humans, to the extent that even oxygen content in the umbilical arteries and vein (which is a general and imprecise characteristic of the placental oxygen transport function) is rarely available. Moreover, the internal placental structure has been only obtained after birth, but even for a delivered human placenta, no high-resolution large-scale 3D structure is available. Depending on the question of interest, the following methods can be employed:

- *In vivo* flux technique which measures the net effect on nutrient concentrations from blood samples;
- Cultured cell methods, which investigate the transport regulation separated from other cells and other endocrine influences.
- Membrane vesicle techniques that observe the behaviour of the spherical cell membranes prepared from the placental tissue.
- The *ex vivo* perfusion, where an explanted placenta is connected to tubes to replicate *in vivo*-like conditions in a perfusion chamber.

Obviously, each method has its strengths and weakness. The cell culture methods and the membrane vesicle techniques are preferred for the membrane transport. They can provide kinetics data even for a specific transporter. Oocytes, which are induced to over-express specific human transporter proteins, are used for observing uptake of the substrate into the cells from the external environment while maintaining normal intracellular cell operations (*e.g.* metabolism and intracellular concentrations) [73]. Intra-vesicular and extra-vesicular buffer solutions could be added to maintain a normal environment as well as to pre-set the desired experimental conditions [74]. Nonetheless, when the experimentalist wants to extract summary conclusion about the overall transfer of a substance the organ perfusion is preferred, since the extracellular environment is far much more complex than represented *in vitro*. The perfusion of the entire placenta is not necessary: the lobular organization of the placenta permits the perfusing of only one lobule (cotyledon) instead of the whole organ. Cotyledon perfusion is not only considered accurate but easier to set up [75].

There are three main components making up the perfusion system, a maternal reservoir, a fetal reservoir and the organ chamber (Fig. 2.11). The maternal reservoir contains the solution to transfer which is well mixed before perfusing. This reservoir represents the maternal blood. The placenta is collected as soon as possible after birth, and a cotyledon catheterised in the fetal artery and vein, and catheters inserted in the basal plate to represent the maternal spiral arteries. Maternal and fetal arterial perfusion is established from the respective reservoirs and the maternal and fetal venous exudate collected separately. Depending on the experiment, the venous outflow can be reconnected to the artery (a closed system) or not (an open system). The schematic of an actual perfusion set-up is presented in Fig. 2.12.

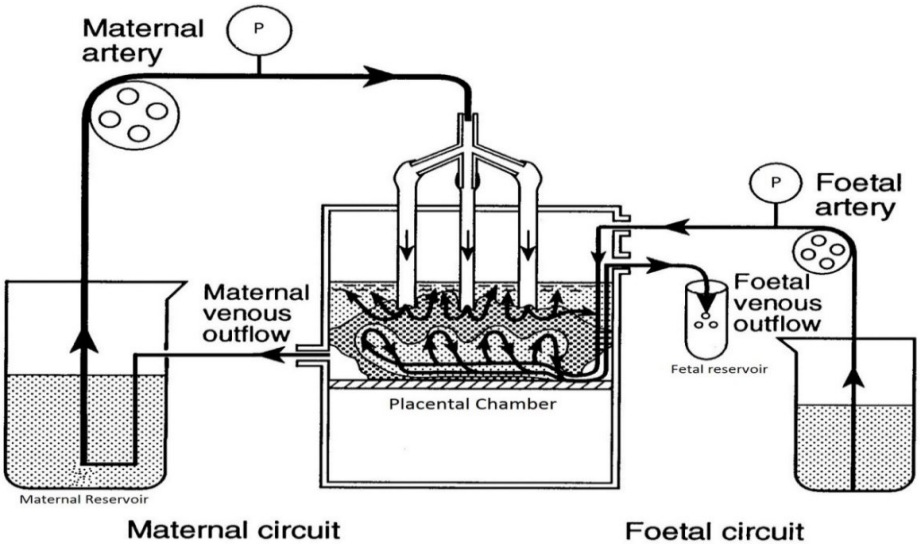

Figure 2.11: *Typical ex vivo placental perfusion schematic.*

Starting from the left, the maternal reservoir in a closed loop configuration. In the middle, the placental chamber containing the cannulated cotyledon. On the right, the fetal reservoirs, one collecting the transferred solute and the other containing the fetal input buffer. P stands for pump. Image modified from [13].

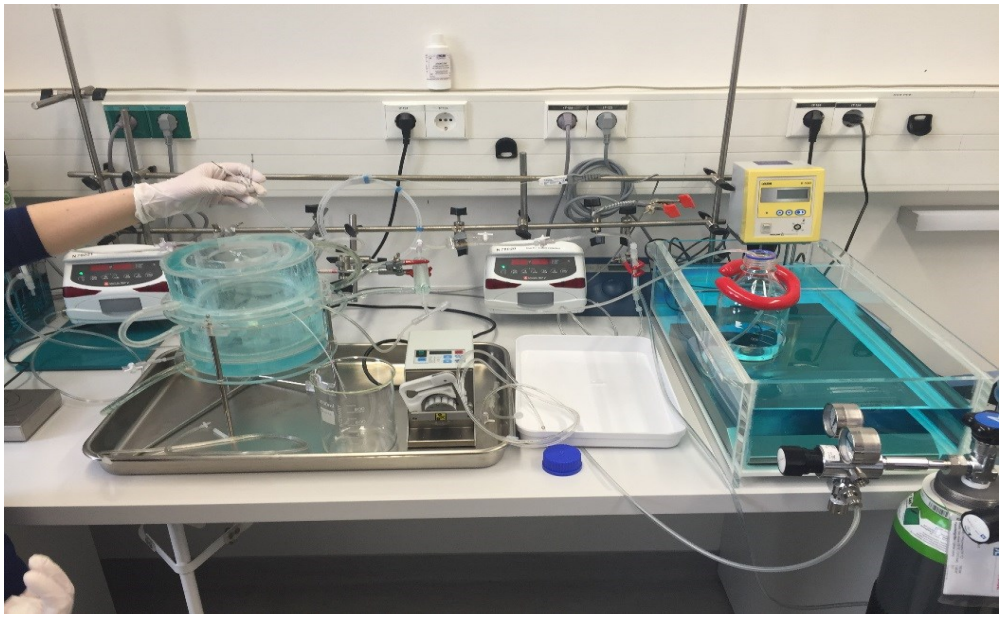

Figure 2.12: *Ex vivo perfusion system.*

Cylinder shaped box is the perfusion chamber, where the explanted placenta is placed. Two pumps (white devices) are the maternal (right) and fetal (left) circulation pumps. The maternal reservoir is the glass bottle on the right, which is weighted down by a red circle and immersed in a blue solution, which has maintaining functions. A beaker (in front of the chamber) collects the fetal exudate containing the substances that crossed the placenta. The beaker is then moved for measurement. Image taken in the Medical University of Graz, Perfusion Laboratory, Austria, March 2015.

In the perfusion experiments, the measurements are usually extracted as:

- The concentration of solute in the maternal reservoir (after a mixing phase);
- Depending on the configuration of the maternal circulation, measurements can be made of the concentration of solute in the maternal efflux (open loop), or the concentration of solute flowing through the tube going from the chamber to the reservoir (closed loop).
- The concentration of solute in the efflux coming from the fetal side of the placenta.

Tracers and labelled compounds are usually used as solutes in transfer studies together with unlabelled and endogenous substances. The tracers can be boluses or infused continuously. Obviously, the choice of experimental conditions may require modifications to the perfusion set-up described here.

Overall, the perfusion system provides an excellent model in which to study placental transfer [76]. Nevertheless, there are issues that should be considered when interpreting the data. One consideration is that maternal side perfusion may not fully represent utero-placental perfusion that occurs *in vivo* via the spiral arteries [77]. This may affect the efficiency of mixing within the intervillous space and thus the efficiency of transfer. Furthermore, when the transfer of a particular solute is studied, in general perfusion of only this single solute is performed. However, for example, the amino acid transfer is likely to be determined by the interaction between amino acids, and therefore experimentalists are continuously improving their perfusion techniques [78].

2.6 Review of placental modelling

In this section, the literature on previous placental modelling efforts is reviewed. From the early 70s, investigators have developed modelling interests in the placenta that ranged from the macroscopic to the microscopic scale. Modelling of the placenta has been mostly focussed on blood flows, gas and nutrient transfer. Nevertheless, other modelling approaches need to be mentioned (but not discussed further):

- Placental development and shape [79, 80].
- Mechanical properties of the placenta [81].
- Signalling pathways and placental biochemistry [82, 83].
- Risks of placental infections [84].

2.6.1 Placental geometry and blood flow

In the past, experimental methods of investigation that were based on radiography and casting techniques were used to graphically mimic the flow pattern in the branching villous structure of the

placenta [85]. Mathematical modelling was used to describe the two circulations as simple tubes to investigate the effect of different flow patterns. Briefly, one or a set of oxygenated tubes exchange solute (mostly gas) with one or a set of deoxygenated tubes. During the process, an exchange equilibrium is achieved. The two sets of tubes represent the two circulations (i.e. maternal and fetal) in the placental system. Five flow patterns were proposed: pool flow, double pool flow, counter-current flow, concurrent flow and cross-counter flow (Fig. 2.13). The cross-current pattern was found as the closest to the human placenta system, whilst the most efficient one was the counter-current pattern found in the pig's placenta [51, 86]. Albeit this description was very pragmatic, they oversimplified the dynamics of the placenta.

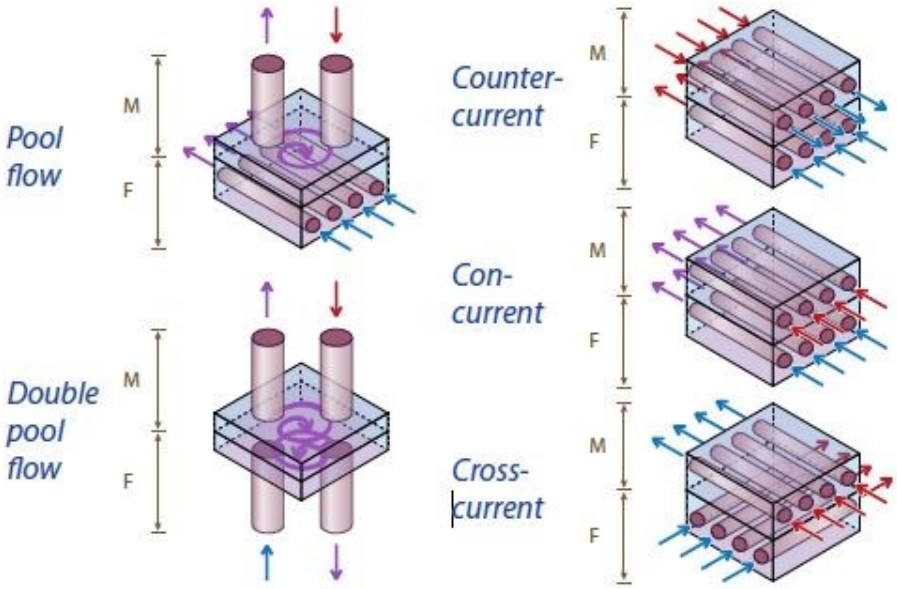

Figure 2.13. *Blood flow patterns used for placental modelling.*
The letters M and F mark the maternal and the fetal flows and the volume in-between represents the placenta, in which the solute is exchanged. The red arrows represent the oxygenated blood, while the blue ones the deoxygenated blood. The violet arrows depict an intermediated concentration of solute. When the fetal arterial blood (blue) flows through the tube (or tubes) there is an exchange of solute with the maternal arterial blood (red) until an equilibrium condition is achieved. Several conformations were proposed, although the counter-current and cross-current configuration were most commonly used for the placental system. Image modified from [11].

Due to the morphological and physiological complexity of the placenta, efforts in modelling the placenta have split into those that focus on modelling the maternal side with simplifying assumptions about the fetal side, and *vice-versa*. The maternal flow in the intervillous space around the villi branches has been modelled using Darcy's law for flow in porous media [87], as a uniform flow field [88, 89], or using Navier-Stokes equations in combination with images of the villous tree [90]. The work that employed porous media proposed a hemispherical geometry to represent a

cotyledon structure, the so-called *placentome* [87]. Building on the placentome idea, a stream-tube flow configuration was proposed to model the maternal flow between the villi (Fig. 2.14), which allowed predicting the maximum oxygen uptake as a function of maternal flow and villi density [88]. However, these studies were based on simplified macroscale geometries of the *placentome* therefore did not represent the characteristic villous shapes at the microscale. In fact, the specific 3D morphology of the placenta is highly likely to play a key role in the overall transfer, both locally at the microscale as well as at the macroscale and recent advances in imaging technology have allowed 3D image based models to be developed. For example, the maternal flow has been modelled to study the shear stress exerted by the maternal blood on the villous surface [90, 91] (Fig. 2.15). However, these studies did not include nutrient transport.

The effect of the placental microstructure on transfer has been simulated in realistic 2D sections [92] or 3D reconstructed geometries [93] (Fig. 2.16), yet in both cases, the capillaries were assumed as perfect sinks (*i.e.* concentration fixed at zero) and the maternal flow was neglected. Further studies have been performed to model the 3D fetal flow both at the microscale [94] and macroscale [95], however, this field is rather new and still needs a lot of work. Recent work has modelled the fetal blood flow as Stokes flow inside the capillary of a small reconstructed portion of the terminal villi[96], in order to assess vascular resistance and oxygen transfer efficiency. More extensive literature outside the direct scope of this thesis is available, with additional studies focussing specifically on spiral artery modelling [97, 98], villous tree structure and umbilical cord circulation [99-102], and water exchange [103, 104].

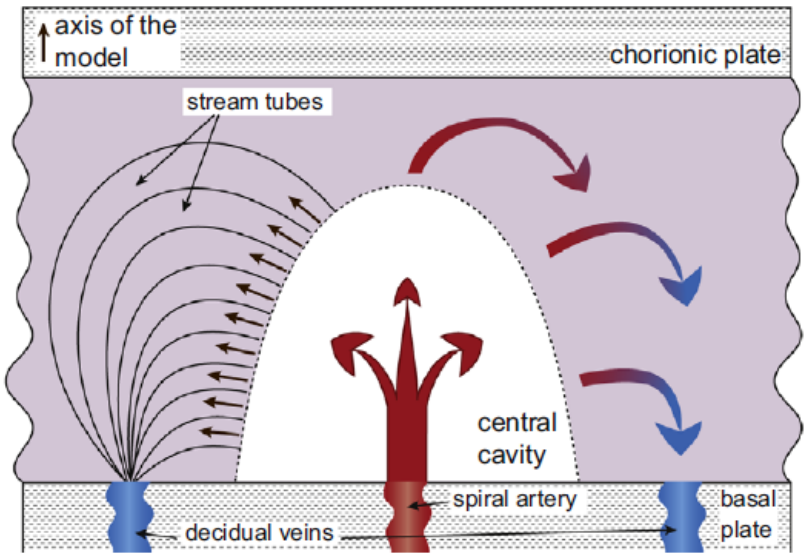

Figure 2.14. *A stream-tube model of oxygen exchange in the placentome. Curved arrows on the right show maternal blood losing oxygen while going from the central cavity to the decidual veins. Schematic curved lines on the left show stream-tubes of blood flow. Image adapted from* [88].

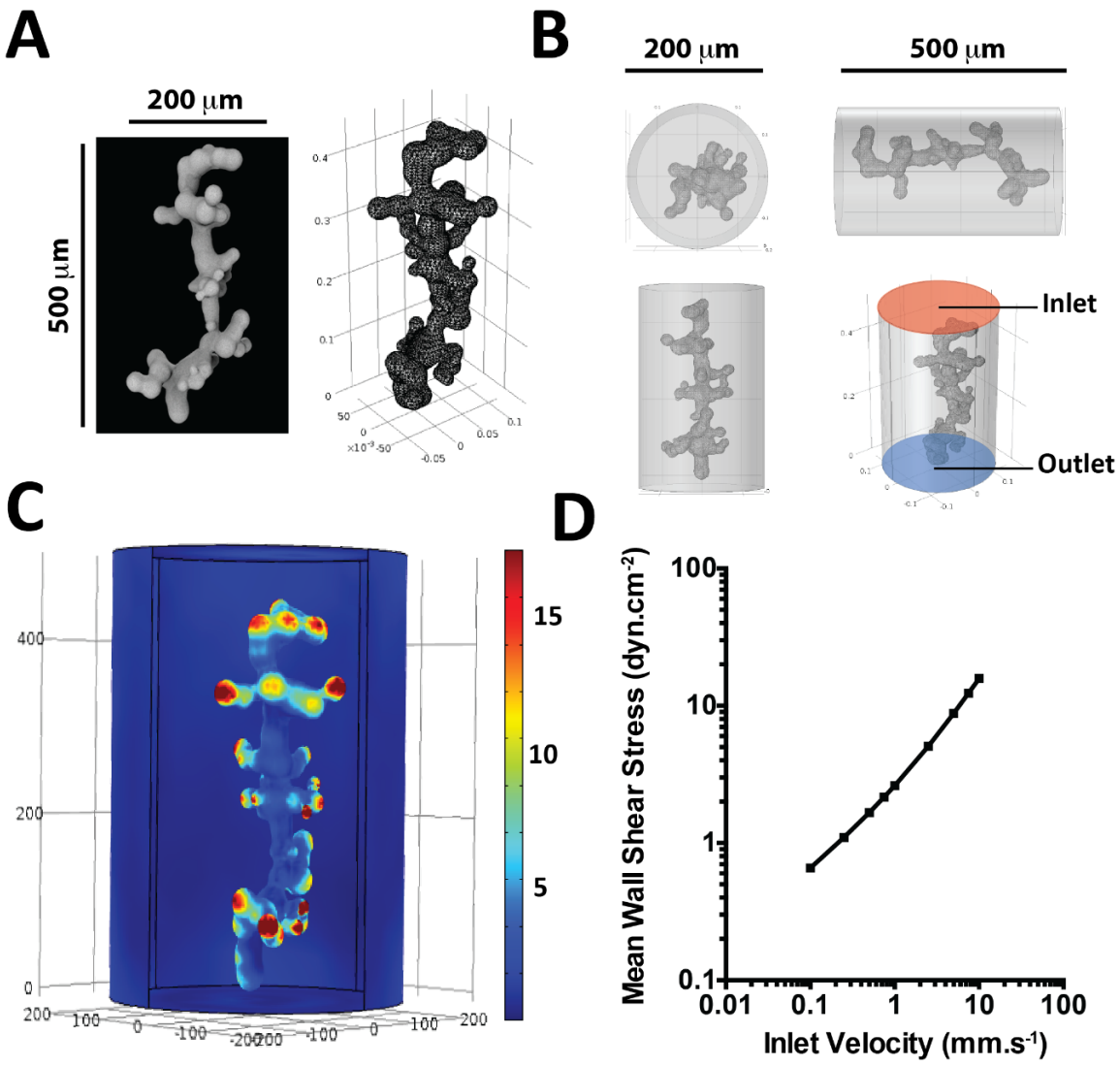

Figure 2.15. *Example of 3D reconstructed placental villi and simulated flow.*

(A) Reconstruction from imaging data of terminal villi. (B) The geometry of the simulation of the solid containing the villi. A laminar flow entered the solid on top (inlet rad solid face) and exited at the bottom of the solid (blue outlet face), mimicking the intervillous space and the maternal flow. (C) Simulation result where high levels of shear stresses were highlighted in red. (D) Simulation results of shear stresses as a function of flow velocity. Image adapted from [90].

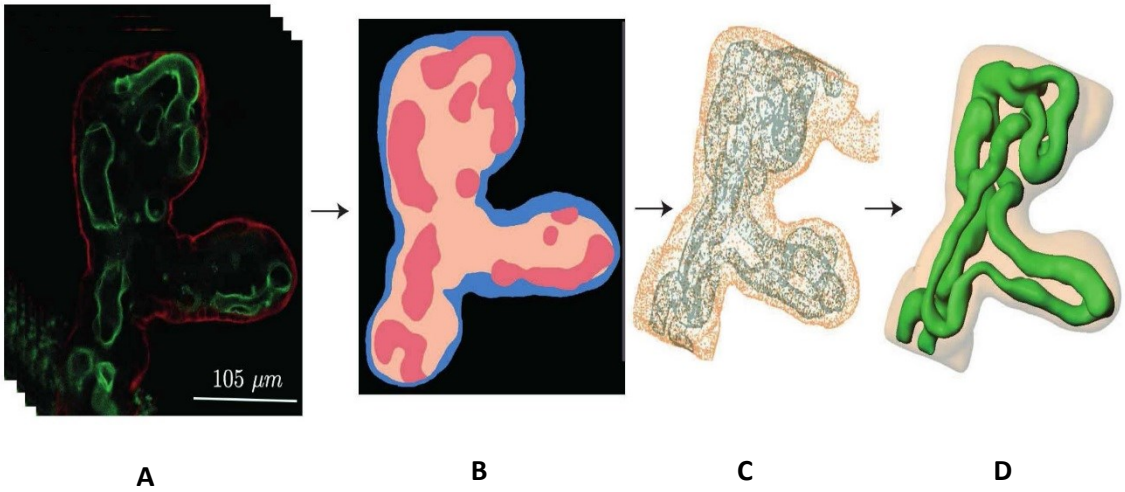

Figure 2.16: *Workflow of the 3D rendering of the placental blood capillaries. (**A**) Confocal microscopy stack of images of a terminal villous: red is the syncytiotrophoblast layer, green is fetal capillaries endothelium. (**B**) Segmentation and imaging elaboration: 2D map image of the different structures: blue syncytiotrophoblast layer, beige stroma, red capillary. (**C**) 3D meshing method as a point-cloud representation. (**D**) 3D rendering as a solid (using tetrahedra) of the point-cloud. Image modified from* [93].

2.6.2 Compartmental modelling

Compartmental modelling is a mechanistic approach based on the law of mass conservation and often used in the context of biological networks or systems. Each physical space is considered a compartment, where the solute is assumed well mixed within the invariable volume. In fact, geometrical dependence of the concentration with the volume is neglected and therefore the use of partial differential equations is no longer needed. This entails that the mathematical description has less parameters and boundary conditions, overall simplifying the system representation. Each compartment translates into one ODE per solute with the concentration of the solute as the state variable with respect to time. Within the system of ODEs, the equations for different solutes can be coupled by chemical reactions converting one solute into another. A general form follows:

$$\frac{dc(p,t)}{dt} = f\left[c(p,t), u(t), p\right] \quad c(t_0) = c_0 \tag{2.1}$$

where c is the n-dimensional concentration vector; u are the r-dimensional differentiable input functions; t is the time; p is the v-dimensional parameter vector as part of the model framework (including the compartment volume). Eq. 2.1 can generate non-linear or linear autonomous first order ODE depending on the system framework. For a discussion and methods of solving the ODE refer to [105]. For stability of these systems refer to [106]. Compartmental modelling has been used

for placental modelling purposes [107-110], which will be discussed in more detail in the sections below.

2.6.3 Placental fatty acid transfer modelling

The only model describing fatty acid transfer across the placenta dates back to 1976 by *Hummel et al* and is based on rat placenta [111]. They proposed a simple 3 compartments model using one tracer in order to investigate the rat placental fatty acid metabolism. They concluded that only 5% of the taken up fatty acids took part to the transfer, while the rest was accumulated in a dead end compartment. This was a very simple model based on the knowledge at the time.
Other relevant works have studied the fatty acid in other human tissues, such as the myocardium, showing that the influx of fatty acid in the tissue was saturable, as the fatty acid concentration increased in the circulating blood [112]. Another study showed the effect of albumin-fatty acid association-dissociation limited the uptake [34]. Other examples of modelling the fatty acids by compartmental models have been carried out in the blood (Fig. 2.17) [113, 114].

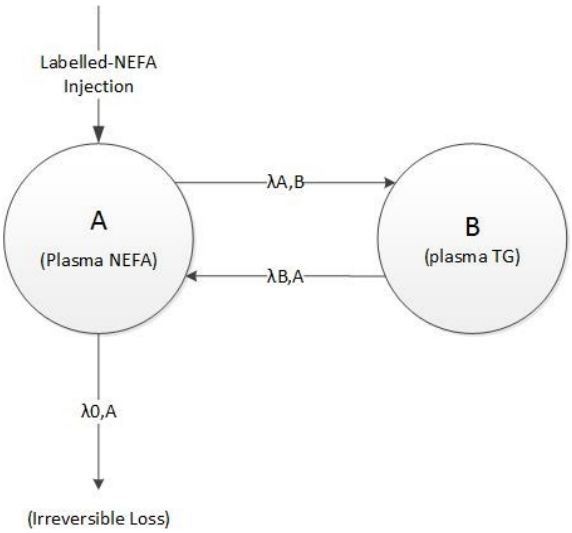

Figure 2.17: *Two-compartmental fatty acid model example.*
Example of fatty acid modelling and metabolism in the blood. Compartment A represents the plasma free fatty acids pool. Compartment B represents all the metabolic pools that receive fatty acids from the plasma free fatty acid pool and subsequently return them to the NEFA pool. λ are the rates. Image adpted from [114].

2.6.4 Placental amino acid transfer modelling

Amino acid uptake across cellular membranes is mediated through a combination of active and passive transporter processes. These mechanisms can be separated into accumulative, facilitated diffusion and exchanger transporters. Amino acid transporters can be further categorized into

distinct systems depending on characteristics such as substrate specificity and sodium dependence (e.g. System A [46]). It is worthwhile mentioning a compartmental modelling approach for the amino acid placental transport by *Sengers et al* [107]. In this model, maternal, syncytiotrophoblast layer and fetal capillaries volumes were distinguished in order to study the transport between compartments using facilitated transporters kinetics. Membrane nutrient transport experimentsare often carried out under the assumption that transport can be described as a Michaelis-Menten process due to the simplicity of this approach. Michaelis-Menten kinetics can operate in two limiting regimes, i.e. the linear and the saturated or constant regime. The linear regime can describe transporter behaviour at low substrate concentrations when the fluxes are proportional to concentration, while saturation occurs when the maximum transporter capacity is reached at high substrate concentrations. Note that in the linear regime the unidirectional uptake behaviour cannot be distinguished from simple diffusion.

Experimental studies usually employ a range of initial concentrations and then measure the initial rate of uptake to determine the Michaelis-Menten parameters. However, this approach masks the underlying carrier mechanisms, in particular for bidirectional transport and cases where intracellular concentrations vary. For example, an integration of compartmental modelling with more mechanistic carrier mediated membrane transporter models for amino acid exchange and facilitated transport was employed [47]. Here, the amino acid transporter *X* can bind either with substrate *A* or substrate *B* and subsequently the complex *AX* or *BX* can undergo a conformational change to expose the binding site to the other side of the membrane to enable transfer of the substrate across the membrane (Fig.2.18). For a detailed discussion see [47, 108].

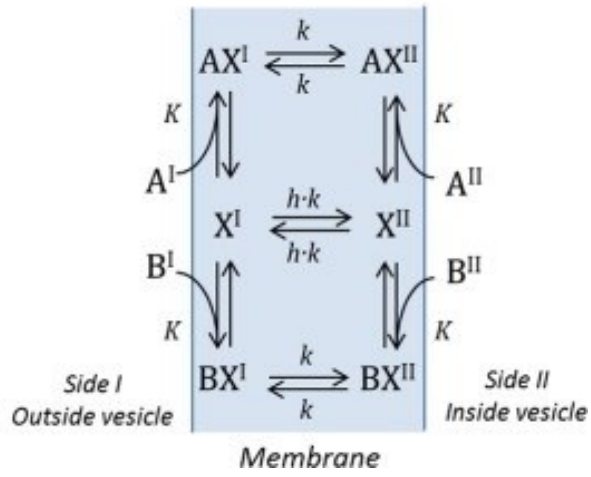

Figure 2.18: *States membrane carrier model used for modelling the transport of amino acids. The generic amino acid A and B bind with the carrier X either at the side I or II of a membrane. Carrier X can undergo a conformational change exposing its binding site to the other side of the membrane either with a substrate or on its own. K is a dissociation constant and k and h control the rate of*

translocation between the different transporter states in the models. Image taken with permission from [47].

2.7 Summary

Overall, the placenta plays a fundamental role in ensuring normal fetal development during pregnancy. However, there are still significant gaps in our knowledge of how the placenta actually functions, as it is not very accessible to study *in vivo* and due to limitations in the available experimental methods. Mathematical modelling approaches have been thus developed to provide additional insight, however, these have focussed mainly on flow and oxygen transfer, and often over-simplified the system. In the next Chapters of this thesis, we will propose novel modelling approaches to characterise the transfer of specific substances across the placenta, in comparison with experimental data.

Chapter 3: Modelling the transfer of fatty acids across the placenta

The following journal paper has been published based on the work presented in this chapter:

1. S. Perazzolo, B. Hirschmugl, C. Wadsack, G. Desoye, R.M. Lewis, B.G. Sengers, ***The influence of fetal metabolism on fatty acid transfer to the fetus***. *The Journal of Lipid Research*, V58-2 443-454, American Society for Biochemistry and Molecular Biology, 2016.

The following conference paper has been published based on the work presented in this chapter:

1. S Perazzolo, B Hirschmugl, C Wadsack, G Desoye, RM Lewis, BG Sengers. ***Computational modelling of fatty acid transport in the human placenta***. *Engineering in Medicine and Biology Society (EMBC),* 2015 37th Annual International Conference of the IEEE, 2015.

Main contributions:

1. Setting up a novel mathematical model for the transfer of fatty acids from the maternal to the fetal circulation and its possible implementations, applications and upgrading.
2. Testing and identification of the dominant rate limiting mechanisms involved in the fatty acid transfer.
3. Quantification of the transfer fluxes, such as placental uptake, placental tissue metabolism and delivery to the fetal circulation.
4. Setting out arguments in favour of the placental metabolism as a key limiting factor for the fatty acid transfer to the fetus.

The experiments and the extracted set of data conducted as part of this chapter were carried out by Dr Birgit Hirschmugl, Medical University of Graz, Austria.

3.1 Introduction

Long chain fatty acids are essential for the development of the fetal brain, visual system and as biosynthetic precursors for hormones [3]. Impaired placental delivery of fatty acids to the fetus may result in developmental changes with consequences for the life-long health of the offspring [62]. The mechanisms of fatty acid transfer to the fetus are not fully understood nor which of these mechanisms are likely to be rate determining. In this study, placental fatty acid transfer will be investigated using placental perfusion in combination with computational modelling.

The low solubility of fatty acids means that they are typically bound to carrier proteins e.g. lipoproteins, albumin in plasma and specific fatty acid binding proteins within the cytosol. Plasma albumin concentrations have been shown to be an important determinant of placental fatty acid transfer [115]. Within the cytosol, fatty acid binding proteins in the placenta include the heart type (H-FABP) and liver type (L-FABP) [43], to facilitate the cytosolic transfer [32]. Fatty acids transfer the human placenta following an overall concentration gradient with concentrations higher in maternal plasma than in the fetal capillaries [5].

Between the maternal and the fetal blood, the syncytiotrophoblast layer of the villous tree is considered the primary barrier to nutrients transfer through the human placenta [5, 19]. Membrane transport of fatty acids may occur by both simple [35] and facilitated diffusion [31]. The relative contribution of simple and facilitated diffusion of fatty acids is disputed but fatty acid transporters are found in the maternal-facing microvillous plasma membrane (MVM) of the syncytiotrophoblast and in the fetal-facing basal membrane (BM) [116]. These membrane transporters include members of the fatty acids transport protein (FATP) family, fatty acid binding protein plasma membrane (FABP-pm) and the fatty acid translocase FAT/CD36 [117].

Membrane transport of nutrients is widely believed to be a rate determining step in their transfer, but in the heart, it has been proposed that fatty acid uptake is determined by metabolic rate within the cell [118]. The first step in fatty acid metabolism is conversion to acyl-CoA. This is mediated by long chain fatty acid acyl-CoA synthetase in the cytosol or, for the FATP family of membrane transporters, directly associated with the membrane transport protein [119, 120]. Acyl-CoA can then be esterified into different lipid pools, triglycerides, phospholipids and cholesterol esters [121, 122], enter the β-oxidation pathway [123, 124] or be utilised for the biosynthesis of eicosanoids [125]. As most fatty acids are converted to Acyl-CoA in the cytosol the fatty acid concentration would be expected to be low. Placental metabolism poses a problem for fatty acid transfer, as the acyl-CoA and their products cannot easily be released to the fetal circulation. This is analogous to an unresolved problem with placental glucose transfer, as glucose is normally converted to glucose-6-phosphate as soon as it enters the cell trapping it there [126]. Glucose transferred to the placenta must somehow bypass this process as there is no placental glucose-6-phosphatese. However, the placenta does express genes for enzymes that can release fatty acids from acyl-CoA, triglyceride and phospholipid pools [124, 127]. It has been suggested that glucose and fatty acid transfer may occur preferentially in regions of vascular syncytial membrane where diffusion distance is low and metabolism may be limited [128].

Compartmental modelling has provided insight into the placental transfer of amino acids, in particular highlighting the role of amino acid metabolism [107, 108, 110]. Similarly, mathematical modelling could help interpret the factors that affect fatty acid transfer as it is currently not clear which of these will be rate determining. The aim of this study is to identify and evaluate the main

factors which determine fatty acid transfer across the placenta, by combining *ex vivo* placental perfusion experiments and computational modelling of the resulting data.

3.2 Methods

3.2.1 Placental *ex vivo* perfusion

Healthy women with uncomplicated pregnancies were asked to participate in this study prior to elective caesarean sections. All women provided written informed consent and the study was approved by the ethics committee of the Medical University of Graz (EK No. 24-529 ex 11/12).
For the 6 healthy placentas perfused in this study maternal BMI was (mean and SEM) 28.4 ± 10.6 kg/m^2, placental weight 665 ± 83 g and gestation length was 38.8 ± 0.4 weeks.
The perfusion method used in this study was previously described by Schneider et al. [129]. Briefly, within 20 min after delivery each placenta was examined in order to find a single intact cotyledon. The corresponding artery and vein pair, supplying the cotyledon, was cannulated and the cotyledon flushed immediately with pre-warmed perfusion medium. The perfusion medium consists of phenol red free DMEM of 1g/l glucose (Gibco, UK) and Earl´s buffer of 116.4 mmol/l NaCl, 5.4 mmol/l KCl, 1.2 mmol/l NaH_2PO_4, 0.8 mmol/l $MgSO_4 \bullet 7\ H_2O$, 1.8 mmol/l $CaCl_2$, 26.2 mmol/l $NaHCO_3$ mixed in a 3:1 ratio (Merck, Darmstadt, Germany), 250 mg/l amoxicillin (Sigma-Aldrich, Steinheim, Germany), 10 g/l dextran FP40 (Serva, Heidelberg, Germany), a total concentration of 11.1 mmol/l glucose (Merck, Darmstadt, Germany) and 5 g/l bovine serum albumin essentially fatty acid free (Sigma-Aldrich, Seinheim, Germany).
The cannulated cotyledon was placed in the pre-heated (37°C) perfusion chamber and the fetal circulation flow rate (Q_F) was set to 4 ml/min. Thereafter, the maternal circulation was established at a flow rate (Q_M) of 8.4 ml/min and both circulations were kept in the open circuit mode for 30 min. The maternal reservoir was changed to 200 ml perfusion medium containing 0.5% essential fatty acid free bovine serum albumin (BSA, Sigma-Aldrich, Schnelldorf, Germany) and ^{13}C-fatty acid (37.2 µM 16:0, 40.5 µM 18:1, 1.6 µM 18:2 n6, Sigma-Aldrich, Schnelldorf, Germany) and unlabelled fatty acids (0.78 µM 20:4 n6, 0.2 µM 20:5 n3, Sigma-Aldrich, Schnelldorf, Germany). The fetal circulation contained 0.5% BSA as an acceptor for fatty acids and was kept in open circuit mode throughout the experiment. The maternal perfusate was recirculated for 180 min. Samples were taken from maternal artery and vein and from the fetal vein at 0, 10, 20, 30, 60, 90, 120, 150 and 180 min. Adjacent, the maternal reservoir was changed to perfusion medium containing 0.5% BSA and both circulations were kept open during this washout phase. Sample collection was performed at 0, 10, 20 and 30 min during the washout phase. After removal of red blood cells, the samples were stored at -80°C until analysis.

3.2.2 Fatty acid analysis by GC-MS

Lipid extracts from samples collected during the perfusion experiment were extracted according to the method previously described by Matyash et al. [130]. Non-esterified fatty acids were determined by Trace-DSQ Gas Chromatography-Mass Spectrograph (GC-MS, Thermo Scientific, Waltham, USA) on electron impact MS mode, as previously published by Fuchs et al. [28]. Briefly, the sample solution is injected into the GC inlet where it is vaporized and swept onto a chromatographic column by the carrier gas (helium). The sample flows through the column and the compounds comprising the mixture of interest are separated by virtue of their relative interaction with the coating of the column and the carrier gas. The latter part of the column passes through a heated transfer line and ends at the entrance to ion source where compounds eluting from the column are converted to ions. A mass analyser, which separates the positively charged ions according to various mass related properties. After the ions are separated, they enter a detector the output from which is amplified to boost the signal. The detector sends information to a computer that records all of the data produced, converts the electrical impulses into visual displays and hard copy displays.

The model development, parameter sensitivity and analysis of transfer mechanisms was first performed using data from an initial experiment with 90 min of ^{13}C-fatty acid infusion, followed by a 30 min washout. Once the computational model was derived for this case, the same modelling methodology was applied to estimate the model parameters based on the data from the 180 min ^{13}C-fatty acid infusion + 30 min washout experiments (N = 6).

3.2.3 Uptake and delivery mass balance

Mass balance calculations for the placental system were carried out using the experimental concentration data. Thus for ^{13}C-fatty acids:

$$u = \int_0^{T_{perf}} (c_{ma} - c_{mv}) Q_M \, dt, \tag{3.1}$$

$$d = \int_0^{T_{perf}} c_{fv} Q_F \, dt, \tag{3.2}$$

u (µmol) was the uptake by the placenta from the maternal circulation and d (µmol) was the amount of fatty acid delivered to the fetal circulation (fetal delivery). c (µmol/l) was the measured concentration: the subscript *ma*, *mv* and *fv* referred to the experimental maternal artery, maternal vein and the fetal vein measurements sampled over time. T_{perf} = 180 min was the experimental ^{13}C-fatty acid perfusion time for N = 6. The mass balance for ^{13}C-fatty acid was $b_{tra} = u - d$. If $b = 0$ the entire amount of ^{13}C-fatty acid taken up by the placenta was delivered to the fetal circulation. For $b > 0$ a certain amount of ^{13}C-fatty acid was taken up by the placenta but not delivered to the fetal

circulation and thus had to be retained by the placenta. For the endogenous fatty acids the net release from the tissue was estimated as the sum of the amount of fatty acids recovered in the maternal reservoir and the amount of fatty acids recovered in the fetal efflux: $b_{endo} = d - u$. Thus, when $b > 0$ a certain amount of endogenous fatty acid was released by the placental tissue.

3.2.4 Mathematical modelling

Based on the placental physiology and experimental setup, the main compartments involved in fatty acid transfer included in the model were (in order from maternal to fetal circulation): the experimental maternal reservoir *R*, the maternal intervillous space *M*, the syncytiotrophoblast fatty acid pool *S* (i.e. those intracellular fatty acids available for transport) and the feto-placental capillaries *F*. Connected to *S*, an additional compartment *P* was added in order to account for the placental metabolism (Fig. 3.1). The placental metabolism represented all metabolic pathways that may occur in the placental tissue including reversible and irreversible processes. We will refer to *P* and the placental metabolism as described here as the "metabolic pool". This pool represents the sum of fatty acids that have been subject to metabolic processes including esterification (into triglyceride, phospholipid and cholesteryl-ester pools) and irreversible loss such as biosynthesis of eicosanoid or β-oxidation. The model configuration was based on current understanding of maternal to fetal transfer of fatty acids [131]. The volume of each compartment was assumed constant and well-mixed. Concentrations in the model were defined in accordance with the measured data, representing both unbound fatty acids and those bound to carriers. The placental metabolism was assumed to occur in the syncytiotrophoblast cytosol. The resulting model is described by the following set of governing equations:

$$\frac{dC_R}{dt} = \frac{1}{V_R}(-Q_M C_R + Q_M C_M), \tag{3.3}$$

$$\frac{dC_M}{dt} = \frac{1}{V_M}(Q_M C_R - Q_M C_M - J_{MVM}), \tag{3.4}$$

$$\frac{dC_S}{dt} = \frac{1}{V_S}(J_{MVM} - J_{BM} - J_{acc} + J_{rel}), \tag{3.5}$$

$$\frac{dC_P}{dt} = \frac{1}{V_P}(J_{acc} - J_{rel}), \tag{3.6}$$

$$\frac{dC_F}{dt} = \frac{1}{V_F}(-Q_F C_F + Q_F C_{F,inp} + J_{BM}). \tag{3.7}$$

Concentrations $C=C(t)$ (µmol/l) and volumes V(l) of the compartments were indicated with the relevant subscripts (with $V_P = V_S$). $C_{F,inp}$ was the fetal umbilical artery input concentration, which was zero in the experiments. Q_M(l/min) was the maternal circulation flow. Q_F(l/min) was the fetal circulation flow. J_{MVM}(µmol/min) and J_{BM}(µmol/min) were respectively the net fluxes across the MVM and BM. J_{acc}(µmol/min) and J_{rel}(µmol/min) were respectively the fluxes of fatty acids from

the pool S to the metabolic pool (accumulation pathway) and from the metabolic pool back to pool S (release pathway).

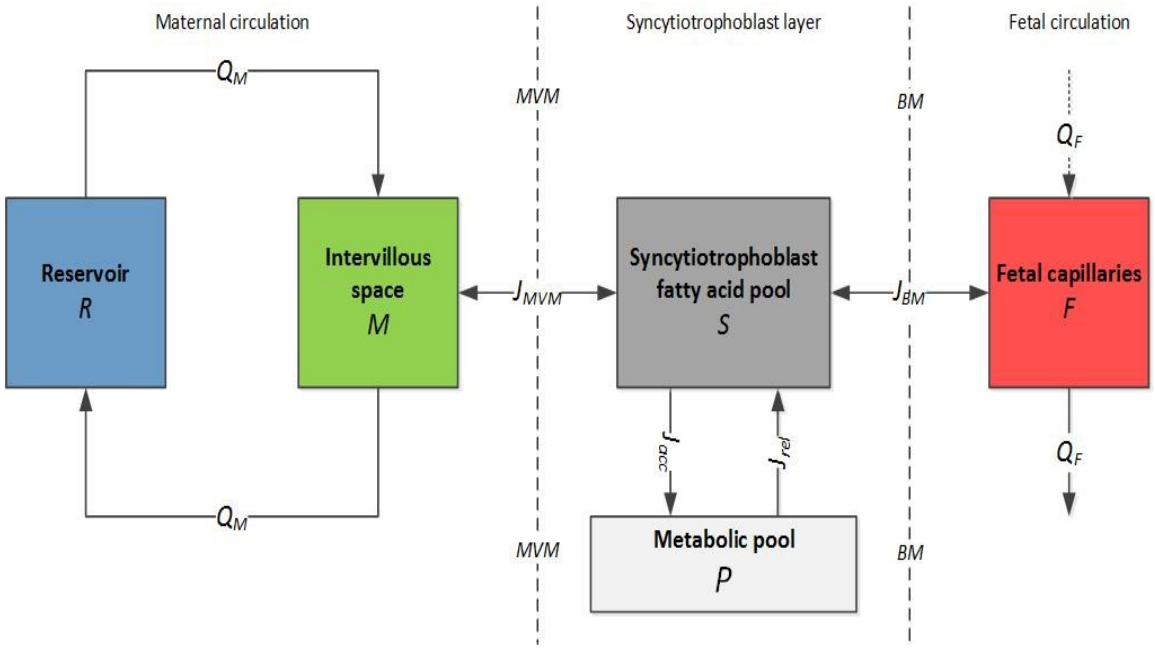

Figure 3.1. *Compartmental model schematic for fatty acid transfer across the placenta. R was the maternal reservoir; M was the maternal intervillous space; S was the syncytiotrophoblast fatty acid pool (intracellular fatty acids available for transport) and P the metabolic pool, both contained in the syncytiotrophoblast volume; F was the fetal compartment of the placenta, representing the fetal capillary volume. The maternal circulation was perfused in closed circuit with flow* Q_M *= 8.4 ml/min.* J_{MVM} *and* J_{BM} *(µmol/min) were the net fluxes across the placental membranes MVM and BM, respectively.* J_{acc} *and* J_{rel} *(µmol/min) were the metabolic fluxes representing the accumulation and release due to placental metabolism. The fetal circulation was perfused in an open circuit with flow* Q_F *= 4 ml/min.*

3.2.4.1 Membrane transport model

The membrane fluxes J_{MVM} and J_{BM} were modelled to represent a saturable bidirectional process. All different transport mechanisms, including dissociation and binding steps, were lumped together in a single "apparent" transport process. For the sake of simplicity, each fatty acid was considered independently, i.e. without an explicit model of competition. The same functional form was assumed on both MVM and BM, as follows [47]:

$$J_{MVM} = v_{MVM}\left(\frac{C_M}{K_{MVM}+C_M} - \frac{C_S}{K_{MVM}+C_S}\right), \quad (3.8)$$

$$J_{BM} = v_{BM}\left(\frac{C_S}{K_{BM}+C_S} - \frac{C_F}{K_{BM}+C_F}\right). \quad (3.9)$$

The parameters v_{MVM} and v_{BM} (µmol/min) represented the maximum flux capacity of the respective membrane. K_{MVM} and K_{BM} (µmol/l) were the fatty acid dissociation constants for each membrane, with $K_{MVM} = K_{BM} = K$. Note that for $K >> C$ this function reduces to a simple diffusive process. Thus, the fluxes are consistent with the concentration gradient: when $J_{MVM} > 0$ the net flux goes from *M* to *S*; when $J_{BM} > 0$ the net flux goes from *S* to *F*.

3.2.4.2 Metabolic pool model

The metabolism fluxes J_{acc} and J_{rel} representing an enzymatic cascade, were approximated as a single "apparent" metabolic process with Michaelis-Menten kinetics. Thus:

$$J_{acc} = \frac{V_{max,acc}C_S}{K_{m,acc}+C_S}, \quad (3.10)$$

$$J_{rel} = \frac{V_{max,rel}C_P}{K_{m,rel}+C_P}. \quad (3.11)$$

V_{max} and K_m were the Michaelis-Menten parameters. V_{max} represents the maximum conversion rate achievable by the "apparent" enzyme. K_m is the fatty acid concentration at which the conversion rate is equal to $V_{max}/2$, and it represents the inverse of the affinity of the fatty acid to the conversion. For the sake of simplicity, $K_{m,acc} = K_{m,rel} = K_m$, assuming that accumulation into the metabolic pool and release from the metabolic pool had the same apparent kinetics. An estimate for K_m was 435 µmol/l [132, 133].

3.2.4.3 ^{13}C-fatty acid modelling simulations

The model initial conditions were $C_R(0) = c_{ma}(0)$, with c_{ma} the maternal artery measurements (corresponding to the concentration in the reservoir *R*), while the initial ^{13}C-fatty acid

concentrations in all other compartments were set at zero. The ^{13}C-fatty acid amount used in the experiments were much lower than the metabolic K_m. Thus, Eq. 3.8-9 simplified:

$$J_{acc} = \frac{V_{max,acc}C_S}{K_{m,acc}+C_S} \simeq \frac{V_{max,acc}C_S}{K_m} = k_{a,trac}C_S, \text{ for } K_m >> C_S; \quad (3.12)$$

$$J_{rel} = \frac{V_{max,rel}C_P}{K_{m,rel}+C_P} \simeq \frac{V_{max,rel}C_P}{K_m} = k_{r,trac}C_P, \text{ for } K_m >> C_P. \quad (3.13)$$

$k_{a,trac}$ (min^{-1}) and $k_{r,trac}$ (min^{-1}) were linear rate parameters, where the former represented the accumulation and the latter the release metabolic pathway.

3.2.4.4 Endogenous (unlabelled) fatty acids modelling simulations

The model initial conditions for the maternal and fetal compartment were $C_M(0) = c_{mv}(0)$ and $C_F(0) = c_{fv}(0)$ respectively, with c_{mv} the maternal vein measurements (representing the intervillous space *M*) and c_{fv} the fetal vein measurements (representing the fetal capillaries volume *F*). The initial concentration in the reservoir *R* was set to zero for most of the endogenous fatty acids, except for those that had been added in together with the ^{13}C-fatty acid in the experiment at time zero (see methods). The initial syncytiotrophoblast concentration $C_S(0) = (c_{mv}(0) + c_{fv}(0))/2$, as an estimated value according to the overall gradient expected at time 0. In addition, it was assumed that the endogenous pool was large with $C_P(0) >> K_m$ [134] and $C_P(0) >> C_S(0)$. Thus, Eq. 3.8-9 simplified as:

$$J_{acc} = \frac{V_{max,acc}C_S}{K_{m,acc}+C_S} \simeq \frac{V_{max,acc}C_S}{K_m} = k_{a,endo}C_S, \text{ for } K_m >> C_S; \quad (3.14)$$

$$J_{rel} = \frac{V_{max,rel}C_P}{K_{m,rel}+C_P} \simeq \frac{V_{max,rel}C_P}{C_P} = k_{r0,endo}, \text{ for } C_P >> K_m. \quad (3.15)$$

$k_{a,endo}$ (min^{-1}) represented the accumulation metabolic pathway as a linear rate.
$k_{r0,endo}$ (µmol l^{-1}min^{-1}) represented the endogenous metabolic release pathway as a constant rate.

3.2.5 Parameter estimation

The model parameter values were reported in Tab. 1, with mass (kg) of the perfused cotyledon equated to the approximate total volume V_{coty} in litres [107]. Volumes of *M*, *S* and *F* compartments were calculated based on volume fractions of 34%, 15% and 7.5% of V_{coty} [107]. Moreover, the membrane dissociation constant *K* (Eq. 3.8-3.9) for different fatty acids were based on representative values from the literature (Tab. 3.1). The set of parameters to estimate was given by $\boldsymbol{p_{tra}} = [V_{MVM}, V_{BM}, k_{a,tra}, k_{r,tra}]$ for the ^{13}C-fatty acid, while $\boldsymbol{p_{endo}} = [V_{MVM}, V_{BM}, k_{a,endo}, k_{r0,endo}]$ for the endogenous fatty acids. Considering the measurement $c_{k,i}$ for the *k*-th compartment and the *i*-th

time-point, and $y_{k,i}$ as the model concentrations for the k-th compartment made at time i, the estimation of $\boldsymbol{p}$ was about resolving a least square problem of the residual sum of squares. Follows:

$$\boldsymbol{p_x} = \underbrace{\arg min}_{p} \sum_{k=1}^{h} \left[\sum_{i=1}^{m} \left(c_{k,i} - y_{k,i} \right)^2 \right], x = [tra, endo], \quad (3.16)$$

With h = 3 compartments and m the total number of time-points. Simulations and parameter estimations were implemented in MATLAB2015a (The MathWorks, Inc., Natick, USA).

The governing model equations were numerically solved with *Runge-Kutta 4* (MATLAB: *Ode45*). *Runge-Kutta* is a family of iterative methods used for solving first order ODE by discretization of time (t_n) and approximation of the solution (y_n). When the initial conditions and the initial time are set, at each temporal step (h), the algorithm computes: $t_{n+1} = t_n + h$; $y_{n+1} = y_n + h \sum_{i=1}^{s} b_i k_i$. Where k_i represent predictive increment functions (see [135] for further details), b_i are coefficients and s is the order of the method. Normally a very good estimation occurs at the 4th order (s=4) in which the global truncation error is $O(h^4)$ and the local truncation error is $O(h^5)$.

The non-linear least square problem (non-linear data fitting) as in Eq. 3.16, was carried out using the *Trust-Region-Reflective* algorithm (MATLAB: *lsqnonlin*). The basic idea is to approximate a residual sum of squares function f with a simpler function q, which reasonably reflects the behaviour of function f in a neighbourhood N around the point p_0. The neighbourhood N is the trust region. A trial step s is computed by minimizing (or approximately minimizing) over N. The point p_0 is the initial choice of $\boldsymbol{p}$ and it will be iterated in order to find that p that satisfies f. This is the trust-region sub-problem. For each region a quadratic approximation q is defined by the first two terms of the Taylor approximation; the neighbourhood N is usually spherical or ellipsoidal in shape. The current point p is updated to be $p + s$ if $f(p + s) < f(p)$; otherwise, the current point remains unchanged and N, the region of trust, is shrunk and the trial step computation is repeated. For discussion on convergence, choice of s and further discussion refer to [136, 137].

The integrals of Eq. 3.1 and 3.2 were solved using the trapezoidal numerical integration (MATLAB: *trapz*) [138].

A summary of the model parameters was reported in Table 3.1. Although these values could be enough representative in this context, a sensitivity analsysis will have to be carried out in order to assess possible effects of such assumptions.

Table 3.1. Summary of the fatty acid transfer model parameter values.

Parameter	Value	Unit	Description
V_R	0.20	l	Maternal reservoir volume
V_M	$0.34V_{coty}$	l	Intervillous space volume
$V_S = V_P$	$0.15V_{coty}$	l	Syncytiotrophoblast volume
V_F	$0.075V_{coty}$	l	Fetal capillaries volume
Q_M	0.0084	l/min	Maternal circulation flow
Q_F	0.0040	l/min	Fetal circulation flow
K	0.22	µmol/l	Dissociation constant for saturated fatty acid [139-141].
K	0.18	µmol/l	Dissociation constant for mono-unsaturated fatty acid [139, 141-145].
K	0.15	µmol/l	Dissociation constant for poly-unsaturated fatty acid (C<20) [38, 139, 141].
K	0.06	µmol/l	Dissociation constant for very long-chain poly-unsaturated (C≥20) [141].
K_m	435	µmol/l	Metabolic pool accumulation and release affinity constant [132, 133].

3.2.6 Non-saturable transport test

The impact of simple diffusion as opposed to a saturable transport process on the overall transfer of fatty acid across the placental membranes was evaluated by modifying the membrane fluxes from a saturable to a non-saturated simple diffusive process. Thus:

$$J_{MVM} = q_{MVM}(C_M - C_S), \quad (3.17)$$

$$J_{BM} = q_{BM}(C_M - C_S). \quad (3.18)$$

q_{MVM} and q_{BM} were the diffusion rate capacities of the membranes (l/min). In addition, a model was tested using the saturable form for J_{MVM} (Eq. 3.8) and simple diffusion for J_{BM} (Eq. 3.11).

3.2.7 Sensitivity analysis

The sensitivity analysis of the model was carried out, in which each parameter was varied in turn, while all others were kept fixed at their reference values (either best-fit estimates or as given in Table 3.1), evaluating the impact on the uptake and delivery for ^{13}C-fatty acid, and the maternal and fetal recovery for endogenous fatty acids. An analysis of the controlling effects of the parameters and mechanisms affecting uptake and transfer in the system was carried out, in which the MVM maximum rate v_{MVM} was varied over three orders of magnitude and for each fixed value of v_{MVM} the other parameters were fitted according to the criterion in Eq. 3.14 to determine the impact on the quality of fit of different combinations of parameters.

3.2.8 Statistics

Statistical comparisons between two groups were performed using the unpaired t-test. Statistical analysis of comparison among multiple fatty acids was performed using One-Way-ANOVA (MATLAB: *multicompare*) with Turkey-Kramer *post-hoc* correction. Statistical significance was assumed with when $p \leq 0.05$. Data are presented as mean values and SEM.

3.3 Results

After an initial phase of approximately 10 min the fetal vein concentrations reached a steady state, while maternal vein and reservoir concentrations gradually decreased for ^{13}C-fatty acid and increased for endogenous fatty acids over time (Fig. 3.2A). In addition, the washout phase showed a quick drop followed by another steady state both in maternal and fetal vein concentrations, in particular for the endogenous fatty acids (Fig. 3.2B).

The proportion of ^{13}C-fatty acid fatty acid in the maternal reservoir taken up by the placenta was on average 61 ± 10% with no significant difference between fatty acids (Fig. 3.3A). The placental ^{13}C-fatty acid mass balance *b* was greater than zero and it was estimated that on average 93.8 ± 0.8 % of the ^{13}C-fatty acid taken up from the maternal circulation was retained in the placenta while the remaining 6.2 ± 0.8 % was delivered to the fetal circulation (Fig. 3.3B), with no statistical differences between fatty acids.

The endogenous fatty acids mass balance *b* was greater than zero, demonstrating that a substantial net amount of fatty acid was released by the placenta into the circulations. On average, and summing both circulations, the measured amount of palmitic acid (C16:0) was the highest (39 ± 8% of the total, $p < 0.05$), followed by linoleic (C18:6n2) (26 ± 8%), oleic (C18:1) (14 ± 4%) and arachidonic acid (C20:4n6) (10 ± 5%) (Fig. 3.4A). Excluding arachidonic acid and eicosapentaenoic acid, which had been added in the experiment, the average amount of endogenous fatty acid released from the placental tissue and recovered in the maternal circulation was 78 ± 5% of the total, while the remaining 22 ± 5% was found in the fetal circulation. This is reflected in the recovery of different endogenous fatty acids (Fig. 3.4B).

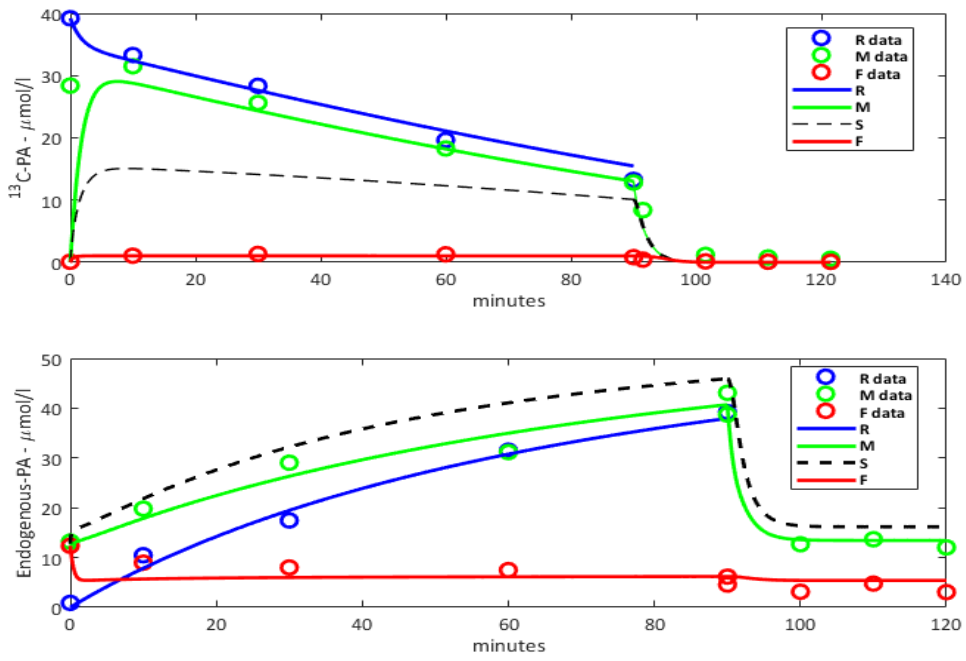

Figure 3.2. *Experimental data vs. model results for palmitic acid.*

***(A)** For the ^{13}C-palmitic acid (^{13}C-PA) added to the maternal reservoir. (**B**) For the endogenous palmitic acid (C16:0) released from placental tissue. The experimental data were represented as hollow circles and the model best fit by solid line. The syncytiotrophoblast prediction was represented by a dashed line due to the lack of measurements available to compare with the model. Similar results for other subjects and fatty acids.*

A **B**

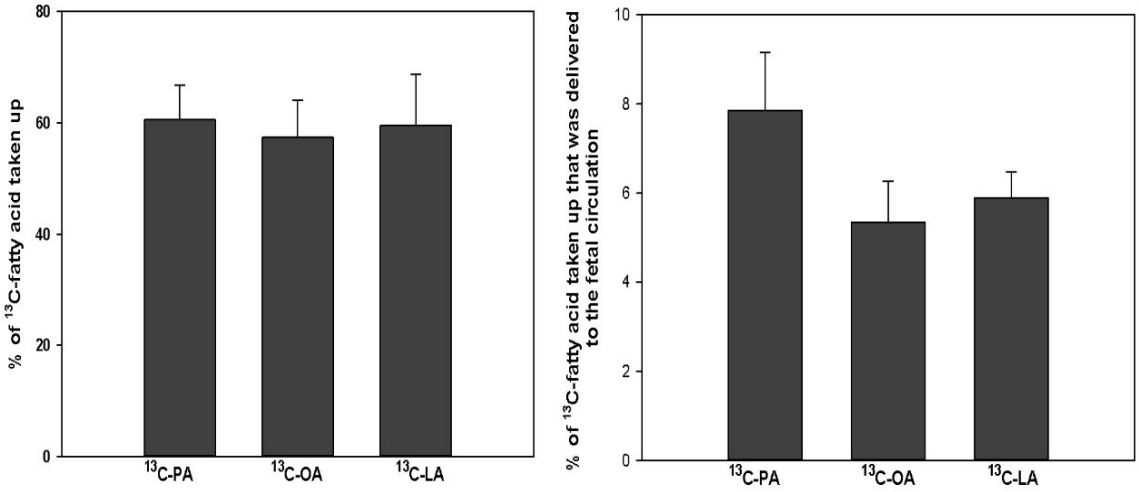

Figure 3.3. *Comparison of 13C-fatty acid uptake and transfer in the perfused placenta. (**A**) ^{13}C-fatty acid taken up by the placenta from the maternal circulation as a percentage of the amount initially present in the reservoir. (**B**) ^{13}C-fatty acid delivered to the fetal circulation as a percentage of the amount taken up by the placenta. ^{13}C-PA: labelled palmitic acid; ^{13}C-OA: labelled oleic acid; ^{13}C-LA: labelled linoleic acid; No statistical differences were found. Data is expressed as mean ± SEM (N = 6).*

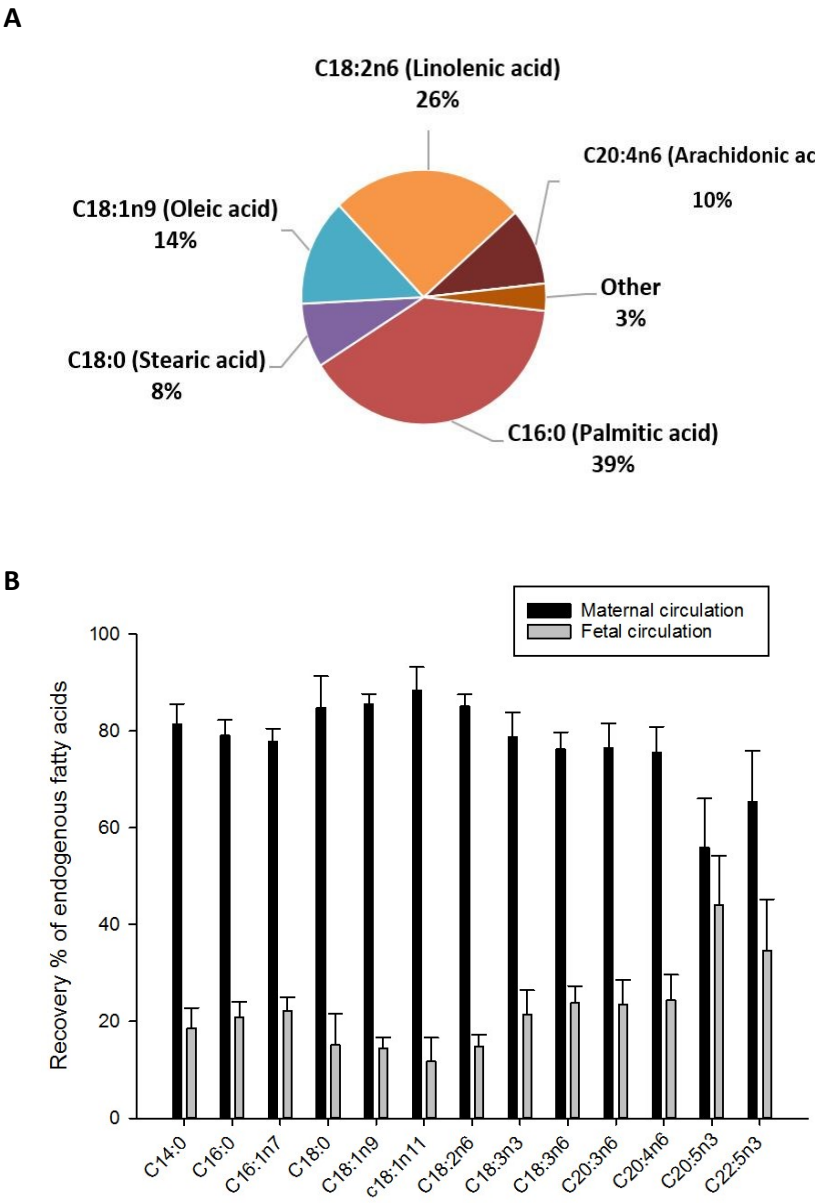

Figure 3.4. *The release of endogenous fatty acids from the perfused placenta: mass balance results (t = 0-180 min).*

(A) *Endogenous fatty acid release by the placenta.* ***(B)*** *Percentages of the fatty acid release recovered in the maternal circulation and in the fetal circulation as part of the total released. Maternal recovery was significantly higher than fetal recovery for all fatty acids except C20:5n3 *p < 0.01. All values in expressed as means ± SEM (N = 6).*

3.3.1 Modelling results

The model concentrations were found to correspond well to the experimental data ($R^2 > 0.8$, Fig. 3.2). The model could not fit the experimental data without the metabolic pool, as the absence of metabolism would result in a 15 fold over-prediction of the fetal delivery of ^{13}C-fatty acids.
The parameter estimation results are summarised in Fig. 3.5 A (N = 6). For the ^{13}C-fatty acid, the MVM rate capacity v_{MVM} was found to be much larger than v_{BM} on the BM by more than two orders of magnitude. The accumulation rate $k_{a,tra}$ was found similar among ^{13}C-fatty acid with an average value of 0.9 ± 0.1 min^{-1} (results not shown). The release rate for ^{13}C-fatty acid $k_{r,tra}$ was found to be 0 for all ^{13}C-FA. The results for the endogenous fatty acids are summarised in Fig. 3.5B (N = 6), where the MVM maximum rate capacity was two orders of magnitude larger than that of the BM. The v_{MVM} was higher for the palmitic acid (C16:0) and linoleic acid (C18:2n6) compared to the rest, except the oleic acid and arachidonic acid (C20:4n6) ($p<0.01$). v_{BM} was higher for the palmitic acid with respect to the rest ($p<0.01$). The accumulation pathway rate constant $k_{a,endo}$ for the metabolic pool was higher for the α-linolenic acid (C18:3n3) compared to the rest except dihomo-γ-linolenic acid (C20:3n6) and eicosapentaenoic acid (C20:5n3) ($p<0.01$) (Fig. 3.6A). The release pathway rate constant $k_{r0,endo}$ was the highest for the palmitic acid (C16:0) ($p<0.01$), while oleic acid (C18:1), linoleic acid (C18:2n6) and arachidonic acid (C20:4n6) were larger with respect to rest of the fatty acids ($p<0.01$) (Fig. 3.6B).

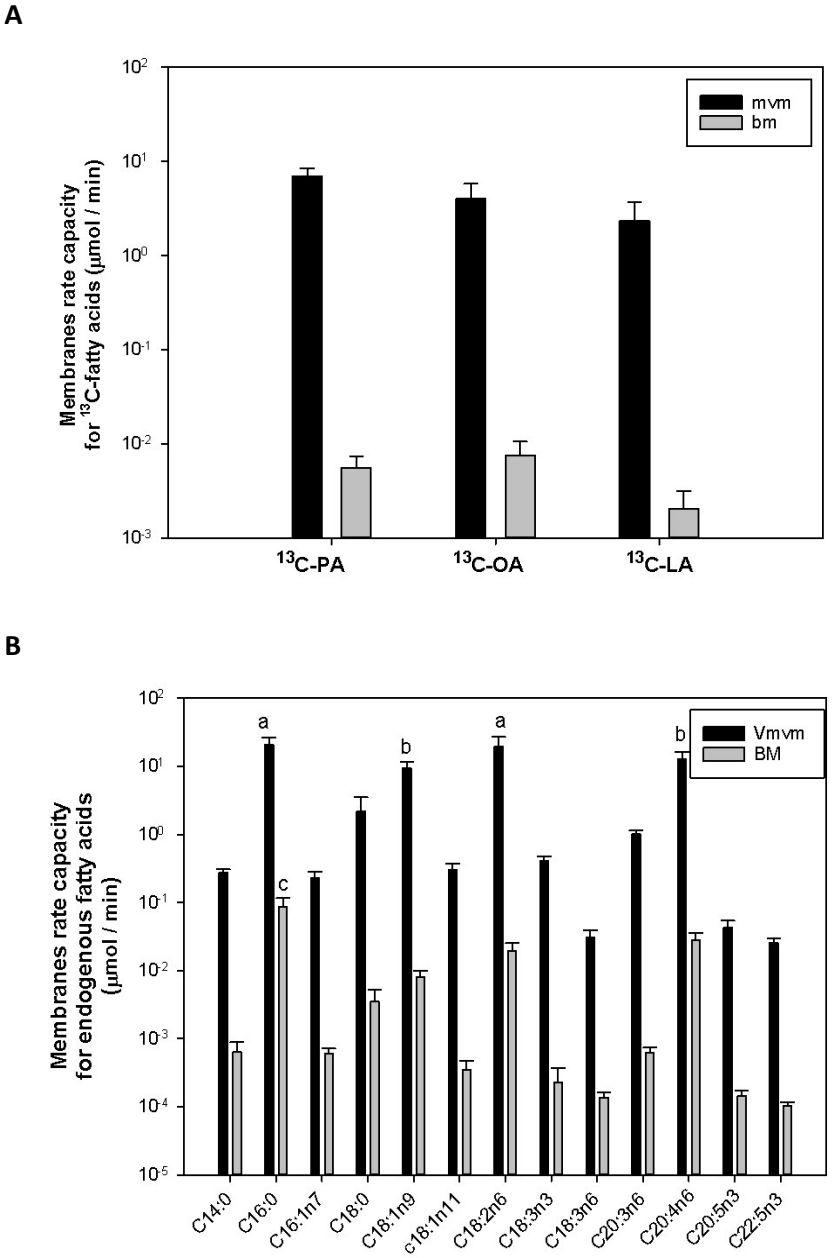

Figure 3.5. *Maximum transport rate model parameters for MVM and BM.* ***(A)*** *^{13}C-PA: palmitic acid labelled fatty acid; ^{13}C-OA: oleic acid labelled fatty acid; ^{13}C-LA: linoleic acid labelled fatty acid.* ***(B)*** *Endogenous fatty acids membrane rate capacities ^{a} differed from the rest of the endogenous fatty acids except those marked with ^{b} ($p < 0.01$); ^{b} were not different with the rest of the substrates ($p < 0.05$). ^{c} differed from the rest of the endogenous fatty acids ($p < 0.05$). All values expressed as mean ± SEM ($N = 6$).*

A **B**

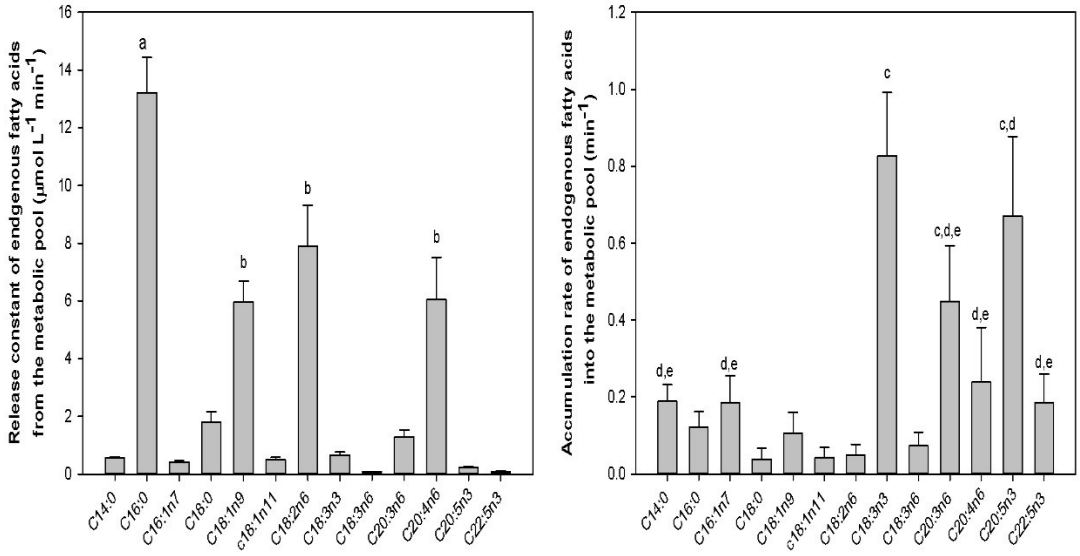

Figure 3.6. *Endogenous fatty acid model parameter estimation for the metabolic pool pathway. Metabolic pool release pathway rate constant ($k_{r0,endo}$, µmol l^{-1} min^{-1}). The substrates labelled [a] differed from the rest of the endogenous fatty acids (p<0.01); the substrates. (**B**) Metabolic pool accumulation pathway constant (k_a, min^{-1}). [a] differed from the rest of the endogenous fatty acids. [b] differed from the rest of the endogenous fatty acids but not within the same group (p<0.01). [c, d, e] differed from the rest of the endogenous fatty acids but not within the same group (p<0.01). All values expressed as mean ± SEM (N = 6).*

3.3.2 Non saturable membrane transport

The modified model with both the MVM and BM membrane fluxes implemented as simple diffusive processes (using Eq. 3.17-3.18 instead of Eq. 3.8-3.9), could represent the experimental ^{13}C-fatty acid data, but failed to do so for the endogenous fatty acids. In particular, for the endogenous simulations, the "diffusive" model could not follow the fetal vein steady state and the washout phase (results not shown). Another 'mixed' version of the model was evaluated in which the MVM flux was kept as a saturable mechanism (Eq. 3.8) and the BM as a simple diffusive process (Eq. 3.18). Again, this model could not fit the endogenous fetal vein steady state (results not shown). Therefore, when simple diffusion was implemented as the sole mechanism in either membrane this led to a worse fit of the data.

3.3.3 Parameter sensitivity analysis and fitting procedure

The model sensitivity analysis in Fig. 3.7A suggested that the uptake was sensitive to the metabolic pool accumulation rate $k_{a,\,tra}$ for the ^{13}C-FA. Delivery to the fetus was sensitive to changes in the

fetal flow Q_F, the BM rate capacity v_{BM} and the membrane parameter K. For the endogenous fatty acids in Fig. 3.7B, the sensitivity analysis showed that the parameters that produced the largest effects on the absolute amount of fatty acid released to the maternal circulation were the metabolic incorporation and release parameters, $k_{a,\,endo}$, $k_{r0,\,endo}$, and the reservoir volume V_R. The fetal delivery instead reported sensitivity for the v_{BM}, the metabolic accumulation rate $k_{a,\,endo}$, K and $Q_{F.}$ Similar results were found for the other ^{13}C-fatty acid (results not shown).

The ability of the model to explain the experimental data was investigated further by studying the interactions between different combinations of parameters (Fig. 3.8). v_{MVM} was varied, while the other parameters were fitted according to Eq. 3.16, and the goodness of the fit of either the maternal or fetal data were reported as R^2 (red and orange lines). The maternal-side data represented the uptake process, the fetal-side data represented the delivery. To the left of the vertical dashed line, the uptake could not be fitted since the membrane transport capacity v_{MVM} was too low to follow the experimental decrease in maternal concentrations over time observed in Fig. 3.2A (i.e. even for the maximum possible gradient across the MVM with syncytiotrophoblast concentrations C_s equal to zero). To the right, the uptake was fitted well irrespectively of the increasing values of v_{MVM}, as this was compensated by an increase in syncytiotrophoblast concentrations C_s (lowering the MVM gradient), via a reduction in the metabolic accumulation rate parameter $k_{a,tra}$. Once the MVM uptake capacity was large enough, it was not limiting anymore and uptake was determined by the metabolic accumulation rate, which approached a constant value. The fetal delivery became well fitted towards the right when v_{BM} fluctuations stabilised once sufficiently high syncytiotrophoblast concentrations C_s were available for BM transport, while further increases were irrelevant. The best fit (vertical dotted line) was found on the right side in this stable region. Thus, also considering that only 6.2% of the total tracer taken up by the placenta was delivered to the fetal circulation, fatty acid uptake was primarily controlled by the rate of incorporation into the metabolic pool, while the delivery was controlled by the combination of metabolic pool and BM rate capacity.

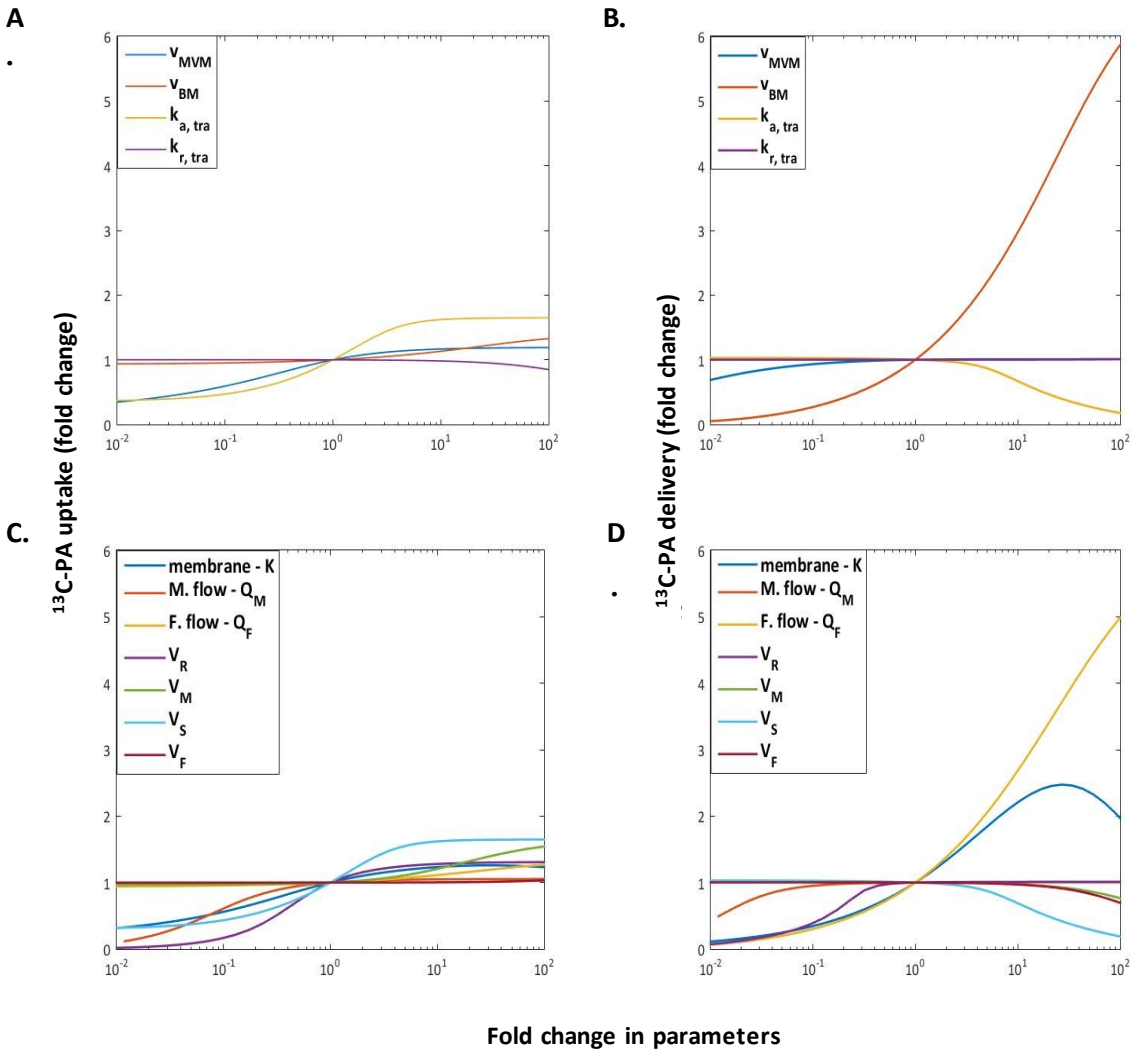

Figure 3.7. *Sensitivity analysis for the model parameters with respect to the total uptake and delivery of (13C-PA).*

*The x-axis represents the fold change in parameters compared to the reference values. The y-axis represents the change in the amount of either uptake or delivery of ^{13}C-PA. (**A**) Analysis for the estimated parameters with respect to the uptake. (**B**) Analysis for the estimated parameters with respect to the delivery. (**C**) Analysis for the model parameters with respect to the uptake. (**D**) Analysis for the model parameters with respect to the delivery. Similar results for other subjects and other fatty acids.*

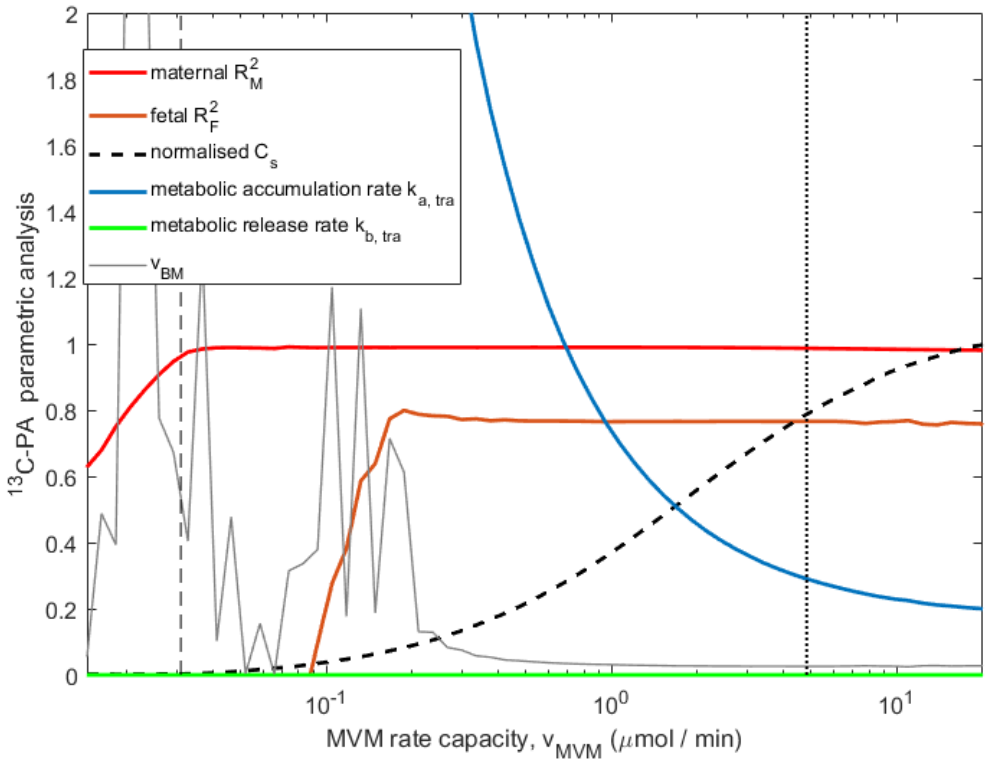

Figure 3.8. *Experimental data can be represented over a wide range of MVM transport capacities*

The MVM rate capacity v_{MVM} (x-axis) was varied over a range of fixed values, while the other unknown parameters were fitted again for each value of v_{MVM} to best represent the data. The red and orange lines indicate the R^2 for the maternal-side concentrations and fetal-side concentrations after the initial phase (t≥10 min). The left vertical line (dashed) is the minimum value of v_{MVM} below which the experimental uptake could not be represented (see text). The right vertical black line (dotted) indicates the best fit found previously. Higher values of v_{MVM} tend to equalise the maternal and syncytiotrophoblast fatty acid concentrations in the model (C_s normalised by the maternal vein measurement at 90 min of perfusion). This implies that for high v_{MVM} uptake is only determined by k_a, which approaches a constant value. Similar results for other subjects and other fatty acids.

3.4 Discussion

This study presents a mathematical model that is able to represent the experimental data for uptake and release of both perfused exogenous ^{13}C-fatty acids and the unlabelled endogenous fatty acids. A key finding of the model was that when modelling membrane transport alone the model could not fit the experimental data, as fetal delivery would be over-predicted by a factor 15. In order for the model to work, it was necessary to model a separate metabolic pool representing all metabolic processes (incorporation of fatty acids into other lipid pools as well catabolism). The

model supported higher permeability of the maternal side of the placenta to fatty acids compared to the fetal side. The model suggested that on the MVM the rates of the metabolic processes are dominant in determining fatty acid uptake, while both metabolic processes and basal membrane transport processes are rate determining for placental fatty acid transfer to the fetus.

3.4.1 Transport across placental membranes

The microvillous membrane (MVM) was found to have a greater flux capacity than the BM based on both the experimental data and model simulations. This was supported by the observation that 78% of all endogenous fatty acids recovered were found in the maternal reservoir even though this operated in closed circuit (which would reduce net transfer due to re-uptake). The inequality between the MVM and BM membrane capacities could be due to differences in transport across the membrane, for instance due to differences in transporter activity. However, it may also be due to other factors, which are not explicitly included in the model but are bundled in the model parameter *v*, such as exchange area, diffusion across the stroma and endothelial permeability. Similarly, the dissociation constant *K* used to represent the saturation process could implicitly account for the competition among fatty acids (apparent K_m is higher in the presence of competitive substrates). Increasing the flows in the maternal and fetal circulation was not predicted to influence placental fatty acid uptake, while fatty acid delivery to the fetus was predicted to be sensitive to the fetal blood flow (Fig. 3.7B). However, this modelling prediction needs to be tested by future experiments.

There were a number of assumptions within the model that are relevant to our understanding of underlying physiological processes. Membrane transport of fatty acids was implemented within the model as a saturable process, without excluding the potential contribution of simple diffusion (which cannot be distinguished from facilitated transport in the linear regime). While we could not distinguish between simple and facilitated diffusion for the ^{13}C-fatty acid, the quality of fit was reduced when models based on pure simple diffusion were attempted for the endogenous fatty acids. The model did not distinguish between membrane transport kinetics and the kinetics of disassociation of insoluble fatty acids from binding proteins in the plasma or cytosol. Depending on the physiological or experimental system, the effects of albumin association and dissociation on FA transfer may need to be taken into account explicitly [31, 34, 118, 146]. Furthermore, we need to be aware that other transport processes may exist, including active and selective transport systems (e.g. the recently discovered DHA transporter [147]) and endocytotic uptake of lipoproteins [148].

3.4.2 Placental metabolism determines uptake of maternal fatty acids

Our initial assumption was the membrane transport would be the rate determining factor for placental fatty acid uptake by the placenta. However, modelling of the experimental data suggests that fatty acid metabolism and not membrane transport will be the main rate determining factor. This is because when membrane transport has a high capacity, the transmembrane gradient becomes small and metabolism becomes the rate determining driver of uptake. A similar conclusion about the role of metabolism was reached in a study of fatty acid uptake into cardiac myocytes [118].

3.4.3 Placental metabolism may buffer the supply of fatty acids to the fetal circulation

In contrast to the maternal side of the placenta, on the fetal side the model predicts that both metabolism and membrane transport will influence the supply of fatty acids to the fetus. This is because the placental-fetal transport capacity is lower than for maternal-placental transport. While transport capacity is more important on the fetal side of the placenta, the driving force for fatty acid transport is still the transmembrane fatty acid gradient that is determined by incorporation and release of fatty acids by the metabolic pool. We suggest that the metabolic pool may buffer the transfer of fatty acids to the fetal circulation. This is supported by our observations of a relatively constant steady state of the fetal vein fatty acid concentrations irrespective of variations in the maternal concentrations.

The washout phase of the experiment provides important support for the role of the metabolic pool, in particular, the results for the endogenous fatty acids. When switched to open circuit perfusion, the maternal vein concentration dropped quickly and stabilised at the same level as at the start of the experiment, when the maternal arterial input concentration from the reservoir was zero. This rapid drop, followed by a new equilibrium in output, is only possible if the intracellular concentration that is readily available for transport represents only a very small fraction of the total fatty acid in the tissue (whether free or incorporated within more complex lipid classes). This is in accordance with a previous study in rat placenta, which estimated that during maternal to fetal transfer, fatty acids pass through a small placental compartment that accounts for only 5% of the total placental free fatty acid [111].

In addition, the fetal response during washout is illustrative as it displays a similar drop and new equilibrium, whereas the only external change is the switch to open circuit perfusion on the maternal side. The explanation provided by the model is that the concentration of fatty acids available for transport in the syncytiotrophoblast drops rapidly due to the increased transport to the maternal side (most fatty acids diffuse out the maternal side as it is the route of least resistance), reducing the gradients driving BM transport. According to our model scheme, the

internal concentrations available for transport are then sustained at a constant lower level by release from the metabolic pool and this concentration determines the transport across the BM. The model assumes the metabolic pool is located within the syncytiotrophoblast because this is in direct contact with the maternal plasma. However, we cannot exclude a role for other placental cell types and a recent study has suggested a role for the cytotrophoblast in lipid metabolism [149]. In the current study, we obtained an initial estimation of the metabolic activity in the placental tissue. Importantly, future studies are needed to determine specifically which lipid pools the fatty acids taken up by the placenta are incorporated into and the rate of beta-oxidation of these fatty acids. This may be of clinical relevance as placental lipid metabolism is reported to be altered in diabetic pregnancy [150, 151]. While the perfused placenta is a highly useful model, it must be remembered that there will be many differences *in vivo* including the concentrations of maternal and fetal substrates and hormones which may both influence placental metabolism and transport. Furthermore, in the perfusion model, the total availability of fatty acids to the placenta will have been lower than *in vivo* as we only perfused with a limited number of fatty acids and there will not be any release of fatty acids from lipoproteins. Lower fatty acid availability could potentially have influenced the proportion of fatty acids entering the metabolic pool and the metabolic capacity of this pool needs to be investigated further.

3.4.4 Differences between fatty acids

There is preferential transfer of specific LCPUFA across the placenta referred to as biomagnification [152]. It has been assumed that this is due to preferential transport of LCPUFA, but it may be that differential metabolism underlies this process. The estimated endogenous MVM and BM membrane transport capacities and metabolic rate parameters in the model displayed considerable variation between fatty acids. The accumulation rate parameters in the model displayed the highest values for α-linolenic acid (C18:3n3) and eicosapentaenoic acid (C20:5n3), which in combination with release could indicate a tighter metabolic control of their syncytiotrophoblast concentrations for these omega-3 fatty acids. This is in accordance with results of a recent cohort study where the portions of linoleic acid and α-linolenic acid as long-chain precursors were lower in fetal than in maternal plasma [153] supporting our idea that the metabolic pool may buffer the transfer of specific fatty acids to the fetal circulation. These estimated parameters clearly indicate biological variation in the underlying processes but should not be over-interpreted as they incorporate a range of factors not explicitly captured within the model.

3.5 Conclusion

In summary, a combined computational-experimental approach was adopted highlighting the importance of the metabolic pool in the placental transfer of fatty acid. We propose that fatty acid uptake is regulated by metabolism rather than microvillous membrane transport and that delivery of fatty acids to the fetus is determined by both metabolism and basal membrane transfer. The modelling framework can be extended further in the future as new data becomes available to describe in more detail the metabolic pathways and transport mechanisms involved, including interactions and competition between fatty acids, which were presently not included. In particular, this should be informed by more detailed experimental analysis of metabolic sub-compartments in placental tissue.

Chapter 4: Modelling transfer of DHA in obese mothers

Main contributions:

1. Application of the previously presented model (Chapter 3) to a similar experiment, but now focussed on comparing lean and obese mothers.
2. Model assessment of differences in kinetic parameters for ^{13}C-DHA in obese subjects
3. Model evaluation of a series of different ^{13}C-DHA dosages in a lean subject to further characterize the particular transfer behaviour of DHA and to assess the ability of the model to make predictions outside of the concentration range originally fitted.

The experiments conducted as part of this chapter were carried out by Dr Birgit Hirschmugl, Medical University of Graz, Austria.

4.1 Introduction

In this chapter, the model presented in Chapter 3 was applied for a comparison study between lean mothers and obese mothers for a particular fatty acid, docosahexaenoic acid (DHA).
Worldwide, the incidence of obesity in mothers is increasing at an alarming rate (one-third of women in the USA), and the number of children with obesity is a particular concern [154]. Obese mothers are defined as BMI > 30 kg/m^2. Although it has been established that there is a correspondence between high BMI and fetal overgrowth [155, 156], there is still debate about the underlying causes for that correlation [157]. What is established though, is that maternal obesity can also affect the infant's health by increasing fetal adiposity [62], inducing early onset of metabolic disorders such as type 2 diabetes [158], and increasing the risk of birth defects [159]. In particular, the transfer of docosahexaenoic acid (DHA) may be altered in obese mothers [160], with likely consequences for a correct fetal development [6]. Therefore this chapter will focus primarily on modelling the transfer of DHA to evaluate any differences between lean and obese populations.

4.2 Methods

Placentas were obtained from women between 18 and 29 years old, with uncomplicated pregnancies after overnight fasting and elective caesarean sections. The study population was divided into two groups. Placentas from women, with a body mass index (BMI) before pregnancy below 25 kg/m² were included in the lean group (N = 8) whereas, placentas from women, with a BMI above 30 kg/m² were included the obese group (N = 7). All women provided written informed consent and the study was approved by the ethics committee of the Medical University of Graz (EK

No. 24-529 ex 11/12). Data were extracted from the dual *ex vivo* perfusion in a similar experimental setup reported in Chapter 3.3.1. Measurements were carried out as described in Chapter 3.3. The difference with the previous protocol was that the maternal vein concentration was collected only at t = 90 min. An additional experiment was carried out in a single lean subject, where ^{13}C-DHA was added two times, first at a physiological concentration of 0.3 µmol/l at t = 0, and then an additional dose of 1.5 µmol/l (5 fold higher) at t = 120 min, to test the ability of the model kinetics to predict the response for different dosages of DHA outside of the range that was originally fitted. All data reported mean ± SEM.

4.2.1 Mathematical modelling

The model described in Chapter 3.3 was applied to this experiment and fitted to the dataset described in the previous paragraph using the same methodology as described previously. Model parameters (those not to be estimated from the data) for obese were summarised in Table A.1 (Appendix A). Analysis of statistical differences in the parameters was carried out as described in Chapter 3.3.8. For the experiment in which ^{13}C-DHA was added twice at different concentrations the same models were set up in series but with different initial conditions according to the different dosages. In this case, the model was only fitted to the data for the lower dose during the first 120 min of the experiment, and the same set of kinetic parameters was then used to predict the response to the second higher dose from 120 min onwards.

4.3 Results

Data analysis revealed that the uptake of fatty acid did not differ significantly between the lean and obese groups, with values of respectively 29 ± 9% and 29 ± 11% of the initial amount given (Fig. 4.1A). Similarly, no statistical difference was found in the overall combined delivery of all labelled fatty acids to the fetal circulation, which was respectively 7.7 ± 3.2% of the total taken up by the placenta for the lean group and 11.3 ± 4.0% for the obese group (Fig. 4.1B). Looking more closely at the different species of fatty acids, delivery of DHA appeared to be higher in the obese group, however, this was not statistically significant. Overall no statistical differences were found in uptake and delivery between the lean and obese groups and between different fatty acids within the same group.

A

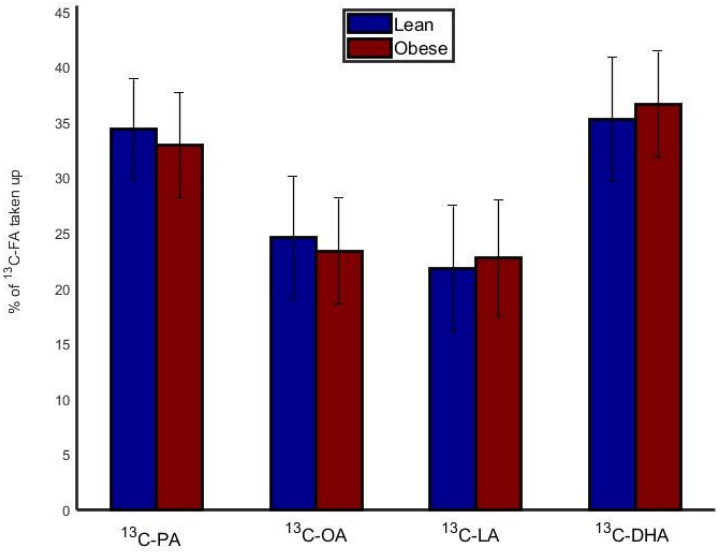

B

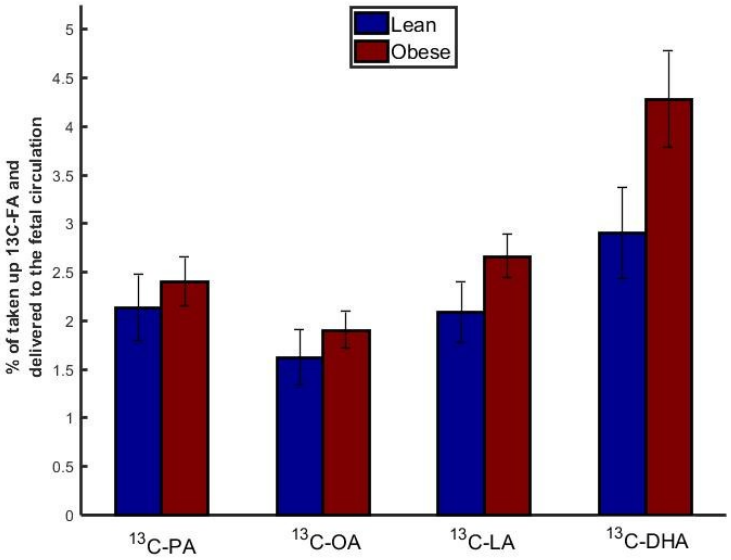

Figure 4.1. *Mass balance results of the uptake and delivery of ^{13}C-FA from the lean and obese study.*

*(**A**) Labelled fatty acid taken up by the placenta from the maternal circulation as a percentage of the amount initially present in the reservoir. (**B**) Labelled fatty acid delivered to the fetal circulation as a percentage of the amount taken up by the placenta. ^{13}C-PA: labelled palmitic acid; ^{13}C-OA: labelled oleic acid; ^{13}C-LA: labelled linoleic acid; ^{13}C-DHA: labelled docosahexaenoic acid. No statistical differences were found between the lean and obese group. Data is expressed as mean ± SEM.*

4.3.1 Parameters of the model for ^{13}C-DHA

The model concentrations were able to effectively match the experimental data (Fig. 4.2). The kinetic model parameters estimated for ^{13}C-DHA are presented in Fig. 4.3. Within each group, the v_{MVM} was significantly higher than the v_{BM} by around 3 orders of magnitude. Comparing the control and obese group there was a trend for a difference in the metabolism parameter k_{acc}, but this was not significant ($p = 0.08$). The estimated parameter k_{rel} for metabolic release of ^{13}C-DHA during the experiment was zero in both cases.

Fig. 4.4 displays the results for the additional test experiment in which the perfusion was continued with a second higher dose at t = 120 min. This demonstrated that the model could predict reasonably well perfusion experiments for different ^{13}C-DHA input conditions based on the kinetics estimated previously. Note that due to the experimental variation in this particular case the initial concentrations values used for the model were based on the initial dose administered, rather than the first concentrations measured.

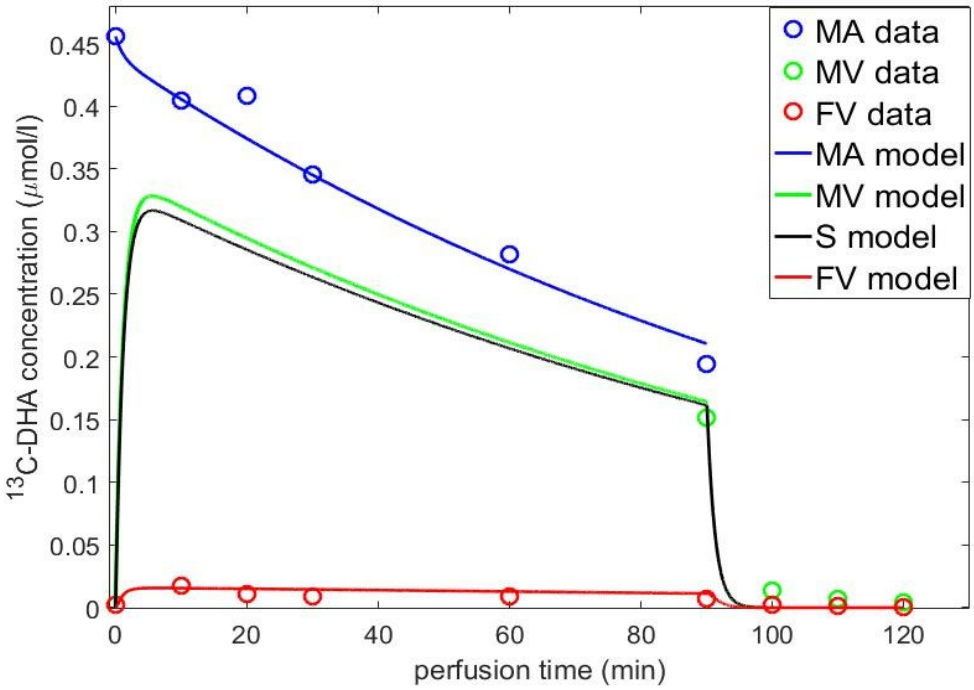

Figure 4.2. *Example of the model fitting the perfusion data for the ^{13}C-DHA of one obese subject. Circles represent the experimental data, solid lines the model best fits. Blue represented the maternal artery (MA); green the maternal vein (MV); black the syncytiotrophoblast compartment (S); red the fetal vein (FV). Note that maternal vein concentrations were measured only at t = 90 min, whilst no experimental data was available for the syncytiotrophoblast concentrations.*

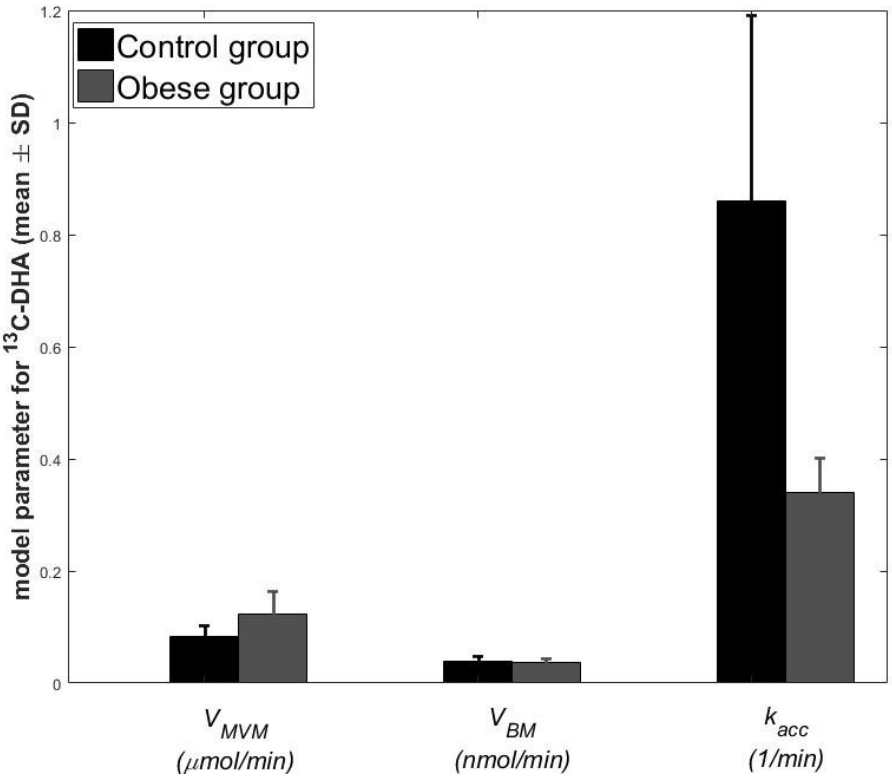

Figure 4.3. *Model parameters for ^{13}C-DHA. Lean vs. Obese*.

Estimated model parameters for ^{13}C-DHA. Black bars indicate the control group; gray bars the obese group. V_{MVM} was the maximum uptake flux parameter for the MVM (µmol/min); V_{BM} was the maximum flux parameter for the BM (nmol/min); k_{acc} was the metabolic accumulation rate constant (1/min). The rate constant k_{rel} for metabolic release of labelled fatty acid from the placental tissue was equal to zero and not reported in the graph. All bars are shown as mean ± SEM. There were no statistically significant differences between control and obese groups but there was a trend for a difference in k_{acc} ($p = 0.08$).

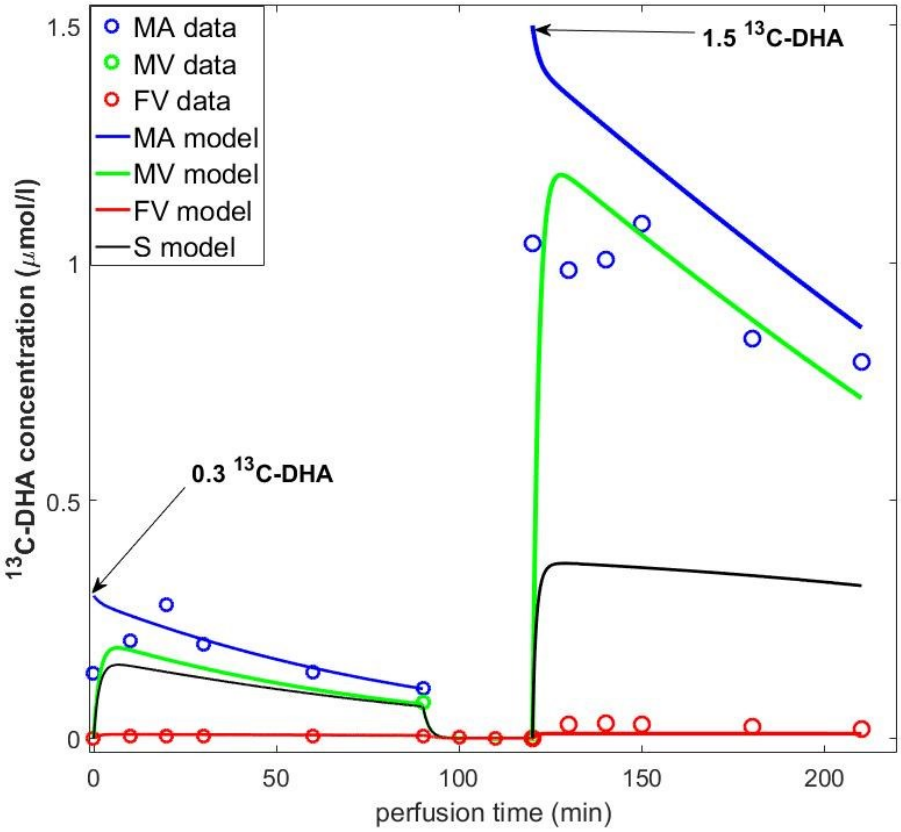

Figure 4.4. *Model results and prediction when two doses of ^{13}C-DHA were given at different times. Model best fit result when 0.3 µmol/l of ^{13}C-DHA was added at time zero, followed by the prediction when 1.5 µmol/l of ^{13}C-DHA was given at t = 120 min. The total perfusion time was 210 min. Circles represent the experimental data, solid lines for the model concentrations and predictions. Blue represented the maternal artery (MA); green the maternal vein (MV, t = 90 min only); black the syncytiotrophoblast compartment (S, no experimental data available); red the fetal vein (FV). The model parameters were estimated solely based on the data from the first phase of the perfusion experiment (0-120 min) and then applied to predict the second phase of the experiment (120-210 min). Note that initial concentrations values used for the model were based on the initial dose administered*.

4.4 Discussion and future work

In this chapter, the application of the model from Chapter 3 was carried out for comparison of two groups, lean mothers and obese mothers. The methodology, experimental data and results were similar to those discussed in Chapter 3. No statistical differences were found both in the experimental data and in the estimated model parameters between the two groups for each fatty acid. However, previous studies have indicated that maternal obesity may influence pregnancy lipid transfer mechanisms [157], and other obesity-related factors, such as a larger fetus or higher circulation flow rates need to be accounted for. Among the fatty acids studied, docosahexaenoic acid DHA (an essential fatty acid) is thought to play a crucial role in normal fetal growth [6]. Modelling the transfer of DHA in this study showed a trend towards higher placental metabolism for lean subjects compared to obese, however, this did not achieve statistical significance ($p = 0.08$). That metabolism plays a key role in controlling the transfer of fatty acids to the fetus in the placenta was found in the previous Chapter 3. Therefore, investigation of the DHA metabolic pathways should be the first priority to shed light on the DHA transfer mechanisms. Furthermore, to improve the assessment of DHA kinetics and as an initial study to test the predictive capabilities of the model, DHA was injected in series with different dosages (Fig. 4.4). The model was used to estimate the kinetic parameter based on the first phase of the experiment from 0 to 120 min and those parameters were then used to predict the behaviour during the second phase of the experiment from 120 to 210 min after the second dose had been administered. This demonstrated that, based on this initial set of parameters, the model could also reasonably well predict the behaviour for a much higher input dose (note that the nominal input concentration at $t = 120$ used in the model appeared to be higher than the actual measurements, offsetting the whole curve). From this the following observations can be made: (1) results provide initial support for the predictive power of the model; (2) Increasing the maternal DHA translates in increasing fetal levels of DHA; (3) no effects of saturation for the DHA transfer kinetics were observed.

In addition to placental transfer, future work should focus on other obesity-related factors such as specific flow rates and fetal metabolism influencing the fatty acid transfer in pregnancy *in vivo*. Furthermore, the additional DHA experiment should be expanded to test the model further using higher dosages and over longer time scales.

Chapter 5: Modelling fatty acid transfer *in vivo*

Main contributions:

1. Adaptation of the fatty acid model presented in Chapter 3 to an *in vivo* experiment
2. Application of the model to test which classes of lipid are taken up by the placenta
3. Modelling assessment of differences in kinetics between fatty acids types
4. Model prediction of the total net amount of fatty acid reaching the fetus from the maternal blood during the experiment.

The experiments conducted as part of this chapter were carried out by Dr. Antonio G. Gazquez, University of Murcia, Spain. The experiments were designed by a group led by Professor Elvira Larque as part of the Early Nutrition Project FP7-289346-EarlyNutrition.

5.1 Introduction

In this chapter, the model presented in Chapter 3 was modified to represent an *in vivo* experiment. Orally absorbed fatty acids are taken up by the intestinal epithelium and synthesised into triglyceride (TG) before being released into the circulation as triglyceride within membrane bound lipoproteins (chylomicrons). These will deliver fatty acids to peripheral maternal tissues (adipose, muscle) and to the liver. The appearance of labelled free fatty acid, phospholipid (PL) and cholesteryl ester (CE) in the circulation represents the release of free fatty acids from these tissues and the release of lipoproteins containing the esterified forms (TG, PL, CE). The placenta is able to take up free fatty acids (NEFA) from maternal plasma and expresses enzymes that can release the fatty acids within plasma triglycerides. The fatty acids within maternal plasma phospholipids and cholesteryl esters are less readily available to the placenta [157].

Overall, the behaviour of fatty acids in the body is very complex and our current knowledge of lipid kinetics from ingestion to incorporation into the fetus is limited. Since this thesis focusses on the placenta, we will not consider modelling of the pregnant mother's body (see for whole-body modelling examples [161, 162]). Instead, the modelling approach will consider the maternal plasma lipid profile as input and the plasma umbilical cord values as the output of the placental system. Using the model will allow to predict the total amount of fatty acids transferred to the fetus during the experiment, which cannot be measured experimentally.

5.2 Methods

An eligible group of 10 pregnant women was chosen with BMI < 25 kg/m^2 (lean), age between 18 and 35 years, non-smoking. An additional group of 10 obese women BMI > 25 kg/m^2 were also considered for comparison with the lean group, however, due to the similarity of the results, these will be presented as an appendix (Appendix A – *In vivo* fatty acid modelling transfer in obese mothers). All women provided written informed consent and the study was approved by the ethics committee of the University of Murcia, Spain. Five fatty acid isotopic tracers were administered orally at different times before birth by planned caesarean section, in the form of NEFA: ^{13}C-OA (^{13}C-18:1, oleic acid tracer), ^{13}C-LA (^{13}C-18:2 n-6, linoleic acid tracer) and ^{13}C-DHA (^{13}C-22:6 n3, docosahexaenoic acid tracer) at -12h, ^{13}C-PA (^{13}C-16:0, palmitic acid tracer) at -8h and ^{13}C-SA (^{13}C-C18:0, stearic acid tracer) at -4h (Fig. 5.1). All the tracers were administered orally to the mothers at 0.5 mg/kg body weight, except for ^{13}C-DHA, which was given at 0.1 mg/kg body weight. Tracers concentrations were measured in maternal plasma collected at different times before birth (time -8 h, -4 h and at 0 h (delivery)) (Fig. 5.1). Measurements at birth (time zero) were collected also for placental tissue, umbilical cord vein plasma and umbilical cord artery plasma. Each measurement was used to determine the fractions of the different lipid classes, NEFA, TG, PL and CE.

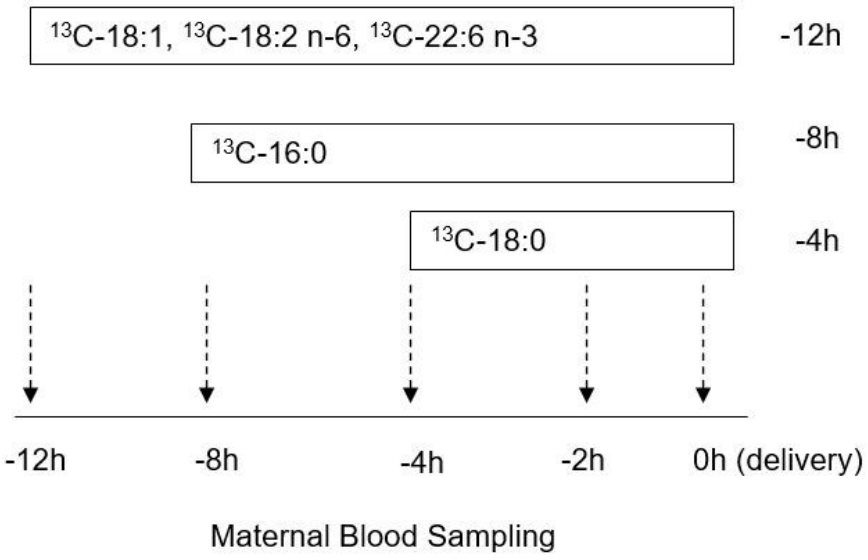

Figure 5.1. *In vivo tracer study intake protocol.*

Tracers were administered orally to the mothers at different times before birth (delivery/time zero). ^{13}C-OA (oleic acid tracer), ^{13}C-LA (linoleic acid tracer) and ^{13}C-DHA (docosahexaenoic acid tracer) at -12h, ^{13}C-PA (palmitic acid tracer) at -8h and ^{13}C-SA (stearic acid tracer) at -4h. Samples to determine the maternal plasma lipid concentrations were collected at the times indicated by the vertical dashed arrows.

5.2.1 Computational modelling

Four physical spaces were identified (Fig.5.2). The first is the maternal plasma in which the lipid concentrations were measured. From the maternal plasma, the uptake flux transfers a net amount of lipids to the placenta compartment. The placenta compartment represented the whole organ with no metabolic pools attached. From the placenta, there is a net flux towards the fetal plasma compartment representing the delivery to the fetus. The concentrations in the fetal plasma compartment are considered to correspond to the fetal umbilical artery plasma lipid concentrations measured. From the fetal plasma compartment, a net flux was defined, representing the lipid deposition rate into the fetal tissue as the final destination of the lipids.

The model input was considered to consist of the measured maternal plasma concentrations, effectively prescribing the concentrations in the maternal plasma compartment. Although the NEFA are considered the only lipid class able to move across membranes, the system transforming the TG, PL and CE to transportable NEFA at the local level near the membrane is unclear. Therefore, we tested two input hypotheses, which we will subsequently refer to as case 1 and case 2. In Case 1, the uptake into the placenta is a function of the sum of the maternal plasma lipid classes, NEFA + TG + PL + CE. In Case 2, the uptake into the placenta is a function of the sum of just two lipid classes, NEFA + TG. Case 2 considers the fatty acids NEFA and TG as the classes more readily available to the placenta [157].

The fluxes between compartments were modelled using linear kinetics, i.e. the flux leaving the compartment is proportional to the compartmental concentration. This is supported by the fact that tracer concentration was much lower than those for endogenous fatty acids were [163]. Only uni-directional fluxes were assumed to represent the *in vivo* net fluxes based on the overall concentration gradients from mother to fetus.

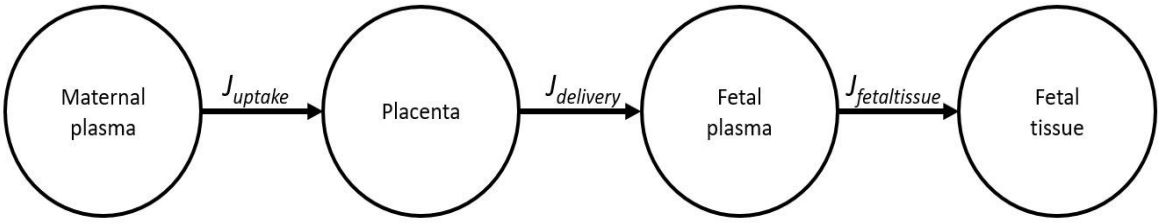

Figure 5.2. *In vivo modelling schematic.*

The four components shown represented (from left to right): the tracer concentration in the maternal blood plasma; the tracer in the placental tissue; the tracer concentration in the umbilical artery blood plasma; and the concentration of tracer in the fetal tissue as the final destination of the fatty acids. Compartments are connected by unidirectional fluxes, representing the net transfer occurring from mother to the fetus. J_{uptake} is the placental uptake flux, $J_{delivery}$ is the release flux of fatty acid from the placenta to the umbilical cord, $J_{fetaltissue}$ is the flux of fatty acid taken up by the fetal tissue (fetal metabolism flux).

Model equations for the concentrations C(µmol/l) are:

$$\frac{dC_P}{dt} = \frac{1}{V_P}\left(J_{uptake} - J_{delivery}\right), \quad (5.1)$$

$$\frac{dC_F}{dt} = \frac{1}{V_F}\left(J_{delivery} - J_{fetaltissue}\right), \quad (5.2)$$

The equations for the fluxes *J* (µmol/min) were:

$$J_{uptake} = k_{uptake}\, C_M, \quad (5.3)$$

$$J_{delivery} = k_{delivery}\, C_P, \quad (5.4)$$

$$J_{fetaltissue} = k_{fetaltissue}\, C_F. \quad (5.5)$$

C_M (µmol/l) was the maternal plasma input concentration; C_P and C_F (µmol/l) were the placental and fetal plasma compartmental concentrations. Volumes followed the same subscript nomenclature. *k* (l/min) were the flux rate constants for each compartment. Note that the concentration in the fetal tissue itself is not modelled, as only the total output based on $J_{fetaltissue}$ is of interest. The parameters to estimate were thus the values of *k* that determine the lipid fluxes. It was assumed that OA, PA and SA have similar kinetics [5, 39], therefore ^{13}C-OA, ^{13}C-PA and ^{13}C-SA were fitted together using a single set of kinetic parameters for the three tracers. Similarly, since ^{13}C-LA and ^{13}C-DHA are both very-long chain fatty acids, these were assumed to have the same kinetics in the first instance [37]. The fitting procedure used for the estimation of the *k* parameters is defined by:

$$\boldsymbol{k} = \underbrace{\arg min}_{k} \sum_{j=1}^{h} \left[\sum_{i=1}^{m} \frac{1}{c_{j,i}} \left(c_{j,i} - y_{j,i} \right)^2 \right] \quad (5.6)$$

The set of parameters to estimate was given by $\boldsymbol{k} = [k_{uptake}, k_{delivery}, k_{fetaltissue}]$ for each group of ^{13}C-fatty acids. Considering the measurement $c_{j,i}$ for the *j*-th compartment and the *i*-th time-point, and $y_{j,i}$ as the model concentrations for the *j*-th compartment made at time *i*. Eq. 5.6 is similar to Eq. 3.16 in Section 3.3.5, but divided by *c* to give a relative measurement, thus equalising the weight of each measurement in the search of the minimum. This choice was due to the different magnitudes between the tissue and fetal measurements, where the use of an absolute residual sum of squares would only have weighted the tissue, neglecting the contribution of the fetal points.

Parameters values used in the model and for data calculations are provided in Table 5.1. As a first approach, we averaged the clinical parameters (N = 10, Table 5.2). For example, the placental weight used in the model was the mean of the placental weights of the 10 subjects. Sample lipid concentrations were also averaged for each time-point (N = 10) and the model was fitted to this "average subject".

Table 5.1. Parameter used for modelling *in vivo*.

N = 10 subjects. Values as mean ± SD.

Parameter	Value
Maternal weight	74.6 ± 6.3 kg
NEFA oral intake	0.5 or 0.1 mg/kg body weight
Maternal haematocrit	0.331 ± 0.3
Uterine artery blood flow	541 ml/min [161]
Uterine artery plasma flow	362 ml/min
Placenta weight	0.61 ± 0.12 kg
Fetal weight	3.24 ± 0.4 Kg
Fetal haematocrit	0.48 ± 0.03
Umbilical vein blood flow	347 [164]
Umbilical vein plasma flow	180 ml/min
Fetal blood volume	0.34 l
Fetal plasma volume	0.18 l [165]

Note that: maternal weight, fetal weight, placental weight, oral intake, maternal haematocrit and fetal haematocrit were collected clinically; uterine blood flow, umbilical blood flowand fetal plasma volume were found in literature; uterine plasma blood flow, umbilical plasma blood flow and fetal blood volume were inferred from relationships between clinical and literature values.

5.3 Results

Experimental measurements at birth are reported in Fig. 5.3. The maternal lipid profile was characterized by large fractions of TG and PL, in different amounts for each fatty acid. The placental tissue was characterized mainly by PL, while the fetal lipid profile in turn was again characterized mainly by TG and PL.

The following presentation of the modelling results is divided into two sections: Case 1 was the case when maternal input C_M was the sum of all the maternal plasma lipid classes (NEFA + PL + TG + CE), while for Case 2 C_M was NEFA + TG.

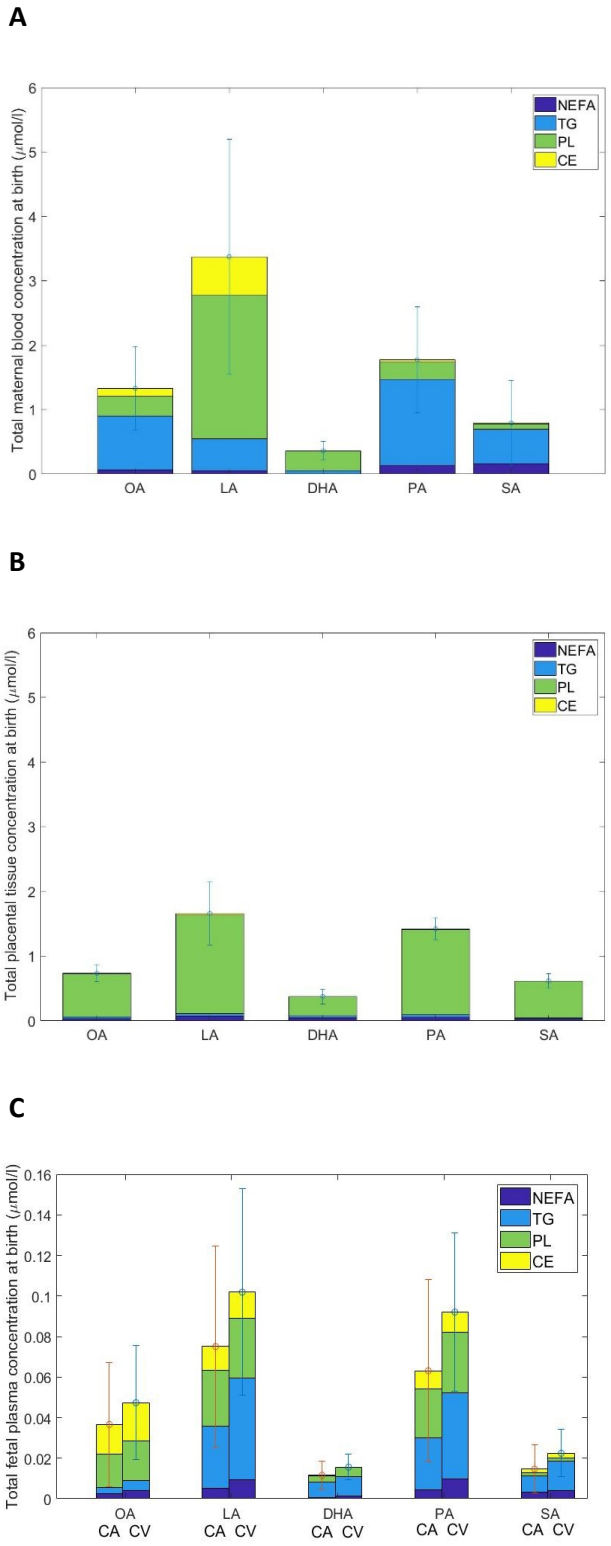

Figure 5.3. *In vivo dataset at t = 0 (at birth). Results presented as mean ± SEM. Each bar is the sum of the NEFA (blue), TG (azure), PL (green), and CE (yellow) for each of the tracers. OA = Oleic acid, LA = Linoleic acid, DHA = Docosahexaenoic acid, PA = Palmitic acid, SA = Stearic acid.(A) Maternal plasma concentrations. (B) Placental tissue concentration. (C) Fetal plasma concentration. CV was the cord vein; CA was the cord artery.*

5.3.1 Case 1: Placental uptake of maternal TG + NEFA + PL + CE

Fitting the ^{13}C-OA, ^{13}C-PA and ^{13}C-SA data with a single set of parameters *k* resulted in an overall satisfactory fit (Fig. 5.4A). In addition, looking closer, the modelled fetal concentrations showed an overall good fit for most of the small fetal plasma values (Fig. 5.4B). In contrast, fitting the ^{13}C-LA and ^{13}C-DHA data with a single set of parameters *k* did not produce a satisfactory fit (Fig. 5.5), in particular for the placental tissue concentrations of DHA. The values of the estimated parameters were reported in Table 5.2.

A

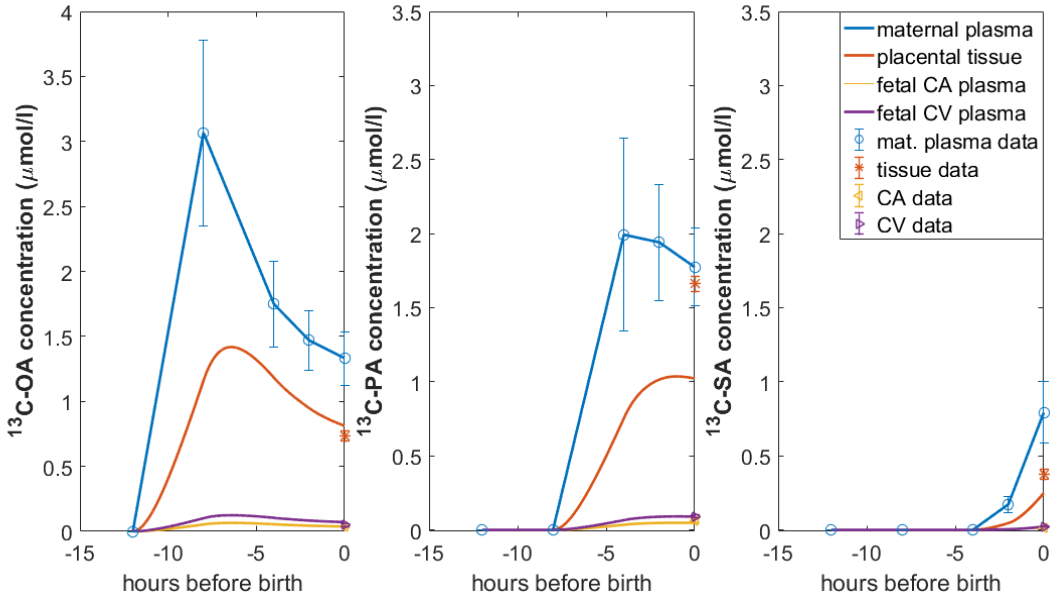

B

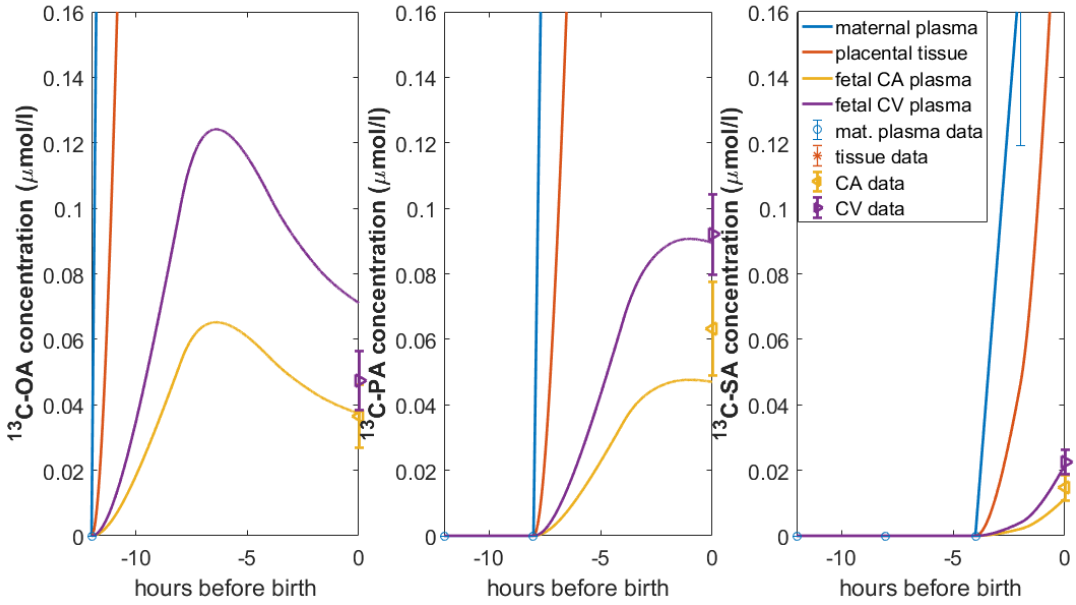

Figure 5.4. *^{13}C-OA, ^{13}C-PA and ^{13}C-SA fit results for the case in which the input was the sum of all lipid classes (TG + NEFA + PL + CE).*

Model prediction (solid lines) vs. experimental data (circles, asterisks, triangles) at time 0. Blue for the maternal plasma, orange for the tissue content, purple for the cord vein plasma, yellow for cord artery plasma. From left to right, results for ^{13}C-OA, ^{13}C-PA and ^{13}C-SA, respectively given at -12h, -8h and -4h. All data reported as mean ± SEM. (A) model predictions. (B) Close up of model predictions for the fetal side.

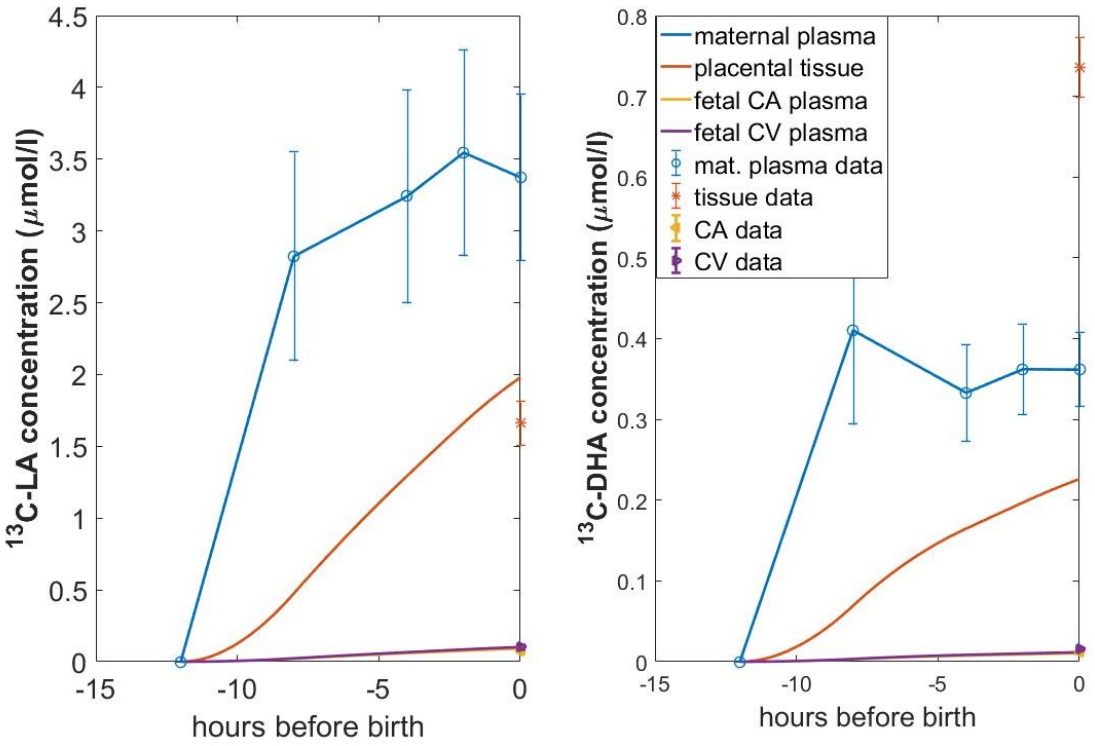

Figure 5.5. *^{13}C-LA and ^{13}C-DHA fit results for the case in which input was the sum of all lipid classes (TG + NEFA + PL + CE).*

Model prediction (solid lines) vs. experimental data (circles, asterisks, triangles). Blue for the maternal plasma, orange for the tissue content, purple for the cord vein plasma, yellow for cord artery plasma. Left panel for ^{13}C-LA, right panel for ^{13}C-DHA, both given at -12h. All data as mean ± SEM.

Table 5.2. Model parameter fitting results for Case 1 (input as TG + NEFA + PL + CE).

Model parameters	**OA**	**PA**	**SA**	**LA**	**DHA**
k_{uptake} (ml/min)	4.2	4.2	4.2	0.97	0.97
$k_{delivery}$ (ml/min)	7.5	7.5	7.5	0.95	0.95
$k_{fetaltissue}$ (ml/min)	163	163	163	20.5	20.5
Predicted total fetal tissue metabolism-accumulation (output)	4.96 µmol	2.28 µmol	0.13 µmol	0.61 µmol	0.08 µmol
Experimental amounts*	**OA**	**PA**	**SA**	**LA**	**DHA**
given to mother	132 µmol	145 µmol	131 µmol	133 µmol	23 µmol
Total maternal delivery to the placenta (input)	473 µmol	253 µmol	25 µmol	684 µmol	81 µmol
in placental tissue at birth	0.45 µmol	0.87 µmol	0.38 µmol	0.74 µmol	1.42 µmol
in fetal plasma at birth	0.0065 µmol	0.0112 µmol	0.0026 µmol	0.0135 µmol	0.0021 µmol
estimated placental transfer[$]	**1.05%**	**0.91%**	**0.53%**	**0.089%**	**0.095%**

*Calculated from data and using assumptions outlined in Table 5.1 (e.g. fetal plasma volume).

[$] Output/Input: Predicted fetal tissue metabolism-accumulation as a fraction of total maternal delivery to the placenta.

5.3.2 Case 2: Placental uptake of maternal TG+NEFA

Fitting the ^{13}C-OA, ^{13}C-PA and ^{13}C-SA data with one set of parameters *k* resulted in a satisfactory fit (Fig. 5.6A). The close up of the fetal concentrations showed good fits for most of the small fetal plasma values (Fig. 5.6B). Fitting the ^{13}C-LA and ^{13}C-DHA data with a single set of parameters *k* was again not able to represent the experimental results satisfactorily (Fig. 5.7). Estimated parameter values were reported in Table 5.3. Case 2 did not produce relevant differences compared with Case 1

A

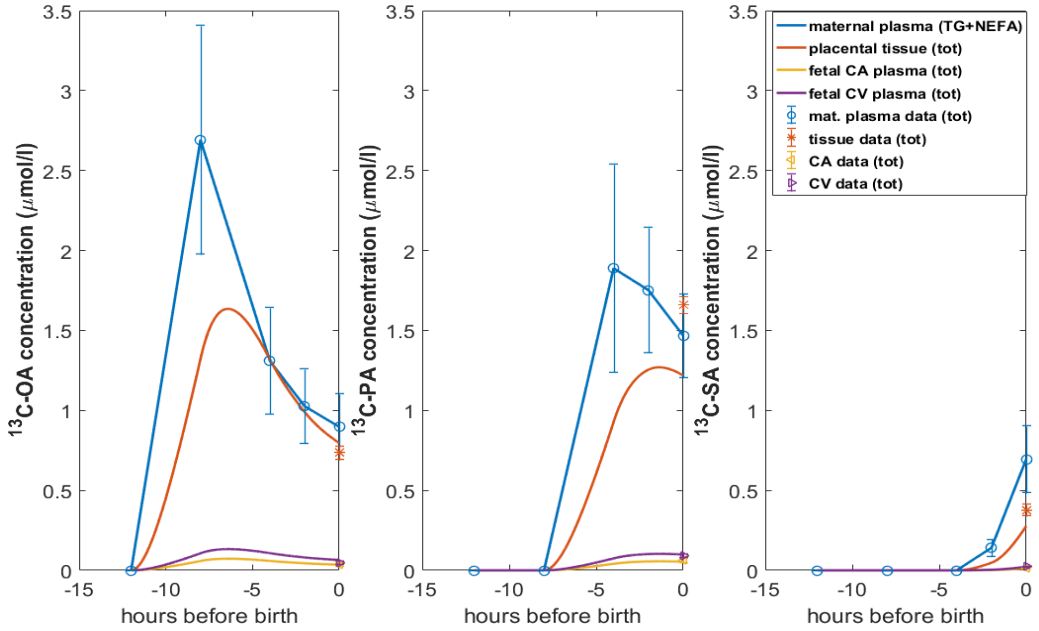

B

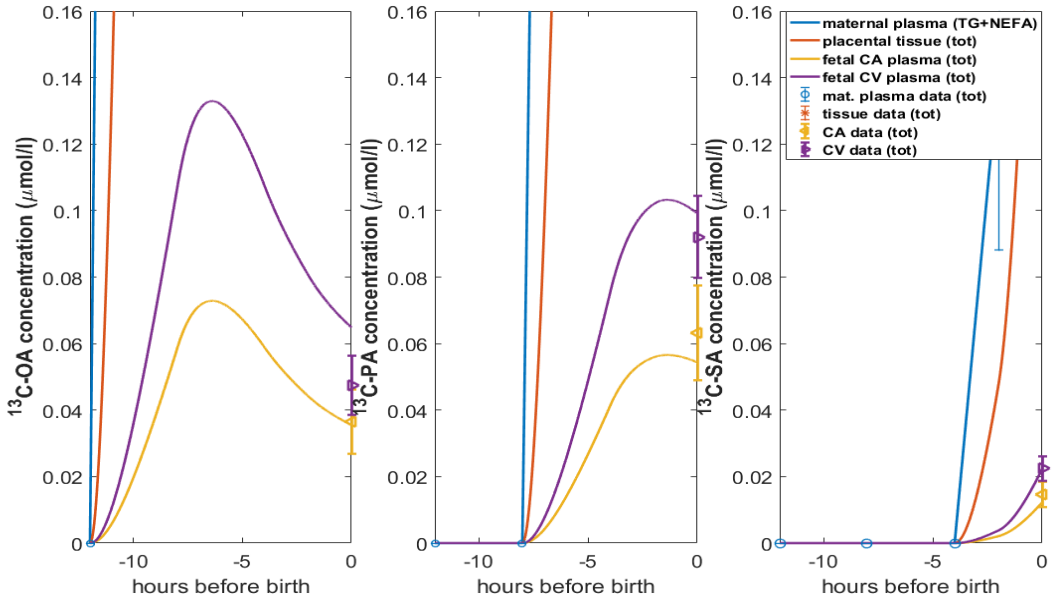

Figure 5.6. *^{13}C-OA, ^{13}C-PA and ^{13}C-SA fit results for the case in which input was the sum of TG+NEFA.*

Model prediction (solid lines) vs. experimental data (circles, asterisks, triangles). Blue for the maternal plasma (NEFA + PL), orange for the tissue content, purple for the cord vein plasma, and yellow for cord artery plasma. (tot) = PL + TG + NEFA + CE. From left to right, results for ^{13}C-OA, ^{13}C-PA and ^{13}C-SA, respectively given at -12h, -8h and -4h. All data reported as mean ± SEM. (A) model predictions. (B) Close up of model predictions for the fetal side.

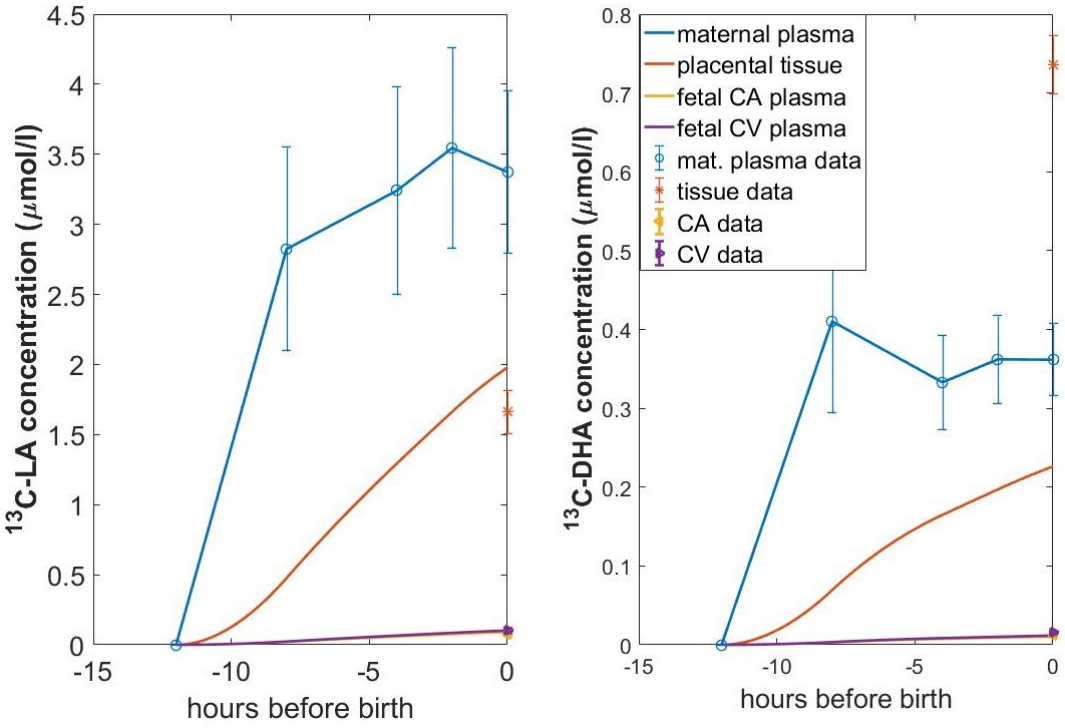

Figure 5.7. *^{13}C-LA and ^{13}C-DHA fit results for the case in which input was the sum of TG+NEFA. Model prediction (solid lines) vs. experimental data (circles, asterisks, triangles). Blue for the maternal plasma, orange for the tissue content, purple for the cord vein plasma, yellow for cord artery plasma. Left panel for ^{13}C-LA, right panel for ^{13}C-DHA, both given at -12h. All data as mean ± SEM.*

Table 5.3. Model parameter fitting results for Case 2 (input as TG+NEFA).

Model parameters	**OA**	**PA**	**SA**	**LA**	**DHA**
k_{uptake} (ml/min)	5.1	5.1	5.1 n	3.1	3.1
$k_{delivery}$ (ml/min)	6.6	6.6	6.6	0.60	0.60
$k_{fetaltissue}$ (ml/min)	149	149	149	14.2	14.2
Predicted total fetal tissue metabolism-accumulation (output)	4.88 µmol	2.48 µmol	0.13 µmol	0.45 µmol	0.08 µmol
Experimental amounts*	**OA**	**PA**	**SA**	**LA**	**DHA**
given to mother	132 µmol	145 µmol	131 µmol	133 µmol	23 µmol
Total maternal delivery to the placenta (input)	383 µmol	231 µmol	21 µmol	200 µmol	34 µmol
in placental tissue at birth	0.45 µmol	0.87 µmol	0.38 µmol	0.74 µmol	1.42 µmol
in fetal plasma at birth	0.0065 µmol	0.0112 µmol	0.0026 µmol	0.0135 µmol	0.0021 µmol
estimated placental transfer[$]	**1.3%**	**1.1%**	**0.6%**	**0.22%**	**0.25%**

*Calculated from data and using assumptions outlined in Table 5.1 (e.g. fetal plasma volume).

[$]Output/Input: Predicted fetal tissue metabolism-accumulation as a fraction of total maternal delivery to the placenta.

5.4 Discussion

A modelling approach for the transfer of fatty acid from maternal plasma to fetal plasma based on *in vivo* measurements was presented. Such modelling provided flux estimates for the uptake, delivery and fetal deposition during the 12 hours of the experiment. Each flux can be calculated by multiplying the corresponding estimated parameter *k* with the concentration at given time points. Although in Chapter 3 metabolism was shown to be very important for the uptake from the maternal circulation, here it was not included in first instance and therefore the estimated fluxes represent the minimum fluxes necessary to match the measured data. In reality, higher fluxes can occur for the uptake from the maternal circulation if the loss due to placental metabolism is included; however estimating this is currently not possible due to the lack of direct measurements of the maternal arterial-venous difference *in vivo*. In addition, preliminary tests including placental oxidation (as linear kinetics) in the model did not produce significantly different results (results not shown).

A main result of the modelling was that when comparing the different lipid input classes Case 1 and Case 2 did not show a different fit quality (Fig. 5.4 *vs.* Fig. 5.6) and parameter values (Table 5.2 *vs.* Table 5.3), therefore we found that the system converting the plasma lipids into a transportable form is fast enough in both cases to match the fetal need. What is interesting is that for Case 2, i.e. when the input is only TG and NEFA, the total maternal delivery to placenta is similar compared to Case 1 for OA, PA and SA (e.g. PA 253 µmol vs 231 µmol) but significantly decreased for LA and DHA (e.g. LA 658 µmol vs. 200 µmol). Thus, it is possible that LA and DHA rely also on PL as source of placental input, although actual uptake cannot be directly verified *in vivo*.

Data for OA, SA and PA could be fitted reasonably well with a single set of parameters. Using information from different time points of fatty acid administration allowed to predict the overall time course with more confidence rather than fitting each tracer alone based on a single end point, which would give a better individual fit but less certainty about the time course. In particular, a coherent picture of fatty acid transfer emerged, with initial high rates of uptake following administration leading to a peak, which then subsided as maternal input concentrations decreased over time (Fig. 5.4).

While OA, PA and SA could be represented reasonably well by the same kinetics, LA and DHA could not. In fact, DHA had on average a relatively high placental tissue concentration that could not be fitted with the current model as it was inconsistent with the measured concentration gradient between compartments. The fact that DHA may have a unique behaviour, in terms of transport and metabolism in the placental system has been proposed previously [6, 65, 166]. In addition, LA and DHA were given at the same time (-12 h) and therefore there was less confidence in the time course prediction, potentially missing out the appearance of a peak in the tissue after administration and

therefore leading to under-prediction of the transfer. Thus, for OA, PA and SA the predicted fetal tissue metabolism/accumulation and therefore the estimated placental transfer was considered more reliable (note that for PA and SA the values of fetal tissue accumulation reported in Table 5.2 and Table 5.3 were lower as these fatty acids were administered at later time points). In addition, the model results can be related back to the initial dose administered. For example, around 4% of the given oral dosage of OA can be predicted to be incorporated into the fetal tissue after 12 h of *in vivo* experiment.

5.5 Future work

Future work must focus on filling the gaps in data in terms of tissue content and umbilical plasma concentrations in-between -12 h and 0. This would strengthen the OA, PA and SA prediction, and may resolve the LA and DHA prediction. An example of such a dataset was provided although just a rudimentary one (See next section). In addition, LA and DHA should be studied separately due to the particular importance and potentially distinct behaviour of DHA.

Application of the model for comparison between lean and obese mothers was also carried out (Appendix A). It was found that the parameters for the obese group were very similar to those from the lean group, which would indicate that any changes in transfer in obesity might be explained by other obesity-related factors (e.g. clinical parameters such as a bigger placenta and higher flow rates). It has to be noted that only averaged patient results were modelled and at this point and no statistical comparison between the lean and obese groups could be performed, as individual patients in the obese group displayed considerable variation within some cases, where umbilical artery concentrations were higher than in the vein, implying uptake from the fetus. Therefore, this warrants further investigation in the future.

5.5.1 Example of additional time course dataset

The previous experiment combined data from different fatty acids given at different time points, assuming the same kinetics. Interestingly, an additional preliminary experiment had been performed where the same fatty acid was administered to different patients either 12 h or 4 h before birth. In both cases, maternal plasma samples were collected at birth and at 3, 2 and 1 h before birth. Tissue and fetal plasma were collected also at birth. Data at birth were reported as bar graphs in Fig. 5.9. Combining the data of these 12 h and 4 h experiments in a single timeline allowed assembling a “more” complete set of time course information (Fig. 5.10).

Comparing the measurements for administration 4 h before birth with those for administration 12 h before birth, it is clear that lipid compartmentalization is different: maternal plasma was characterized by TG, placental tissue by PL and fetal cord plasma by TG and PL (Fig. 5.9).

When LA and DHA were fitted separately, but now with this new more detailed time course information, a better fit was achieved than previously observed (Fig. 5.10), providing thus a suggestion to improve the experimental design for modelling purposes. In addition, the different maternal input scenarios Case 1 (TG + NEFA + PL) and Case 2 (NEFA + TG) were also tested for this application (note CE was not measured for the 4 h experiment). When using only maternal NEFA + TG as input (case 2), there was an under-prediction of placental tissue values, possibly due to a sharper drop in maternal concentrations over time (results case 2 not shown). Again, this points to the question whether for LA and DHA the phospholipids PL may take part in the uptake process.

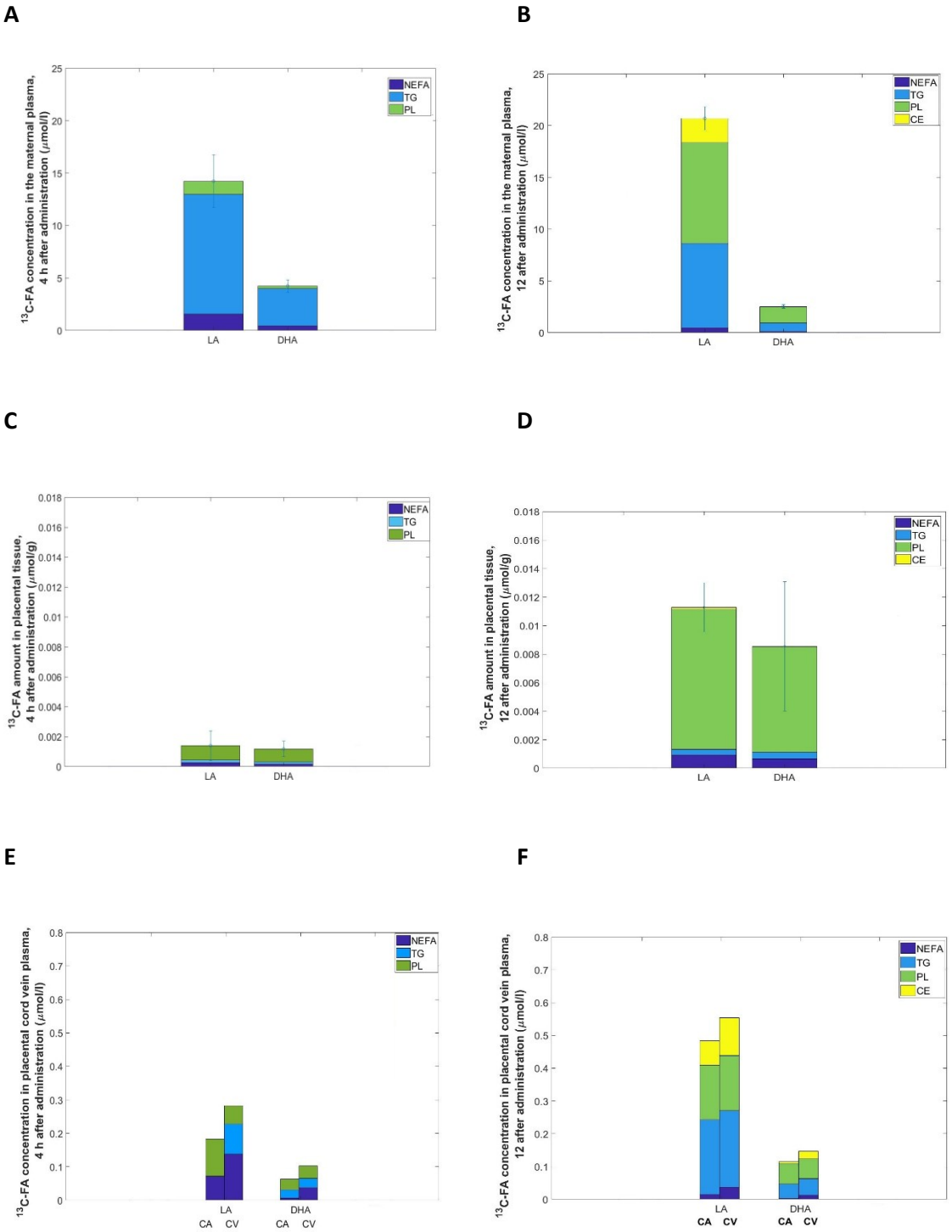

Figure 5.9. *Lipid distributions in the maternal plasma, placental tissue and fetal plasma either 4 h after administration (left column) or 12 h after administration (right column) in the experiment. (**A**) Maternal plasma lipid distributions of tracers 4 h after administration. (**B**) Maternal plasma lipid distributions of tracers 12 h after administration. (**C**) Placental tissue lipid distributions of tracers 4 h after administration. (**D**) Placental tissue lipid distributions of tracers 12 h after administration. (**E**) Fetal plasma lipid distributions of tracers 4 h after administration. (**F**) Fetal plasma lipid distributions of tracers 12 h after administration. Note that measurements for the 4 h experiment did not include CE. All data presented as mean ± SEM.*

A

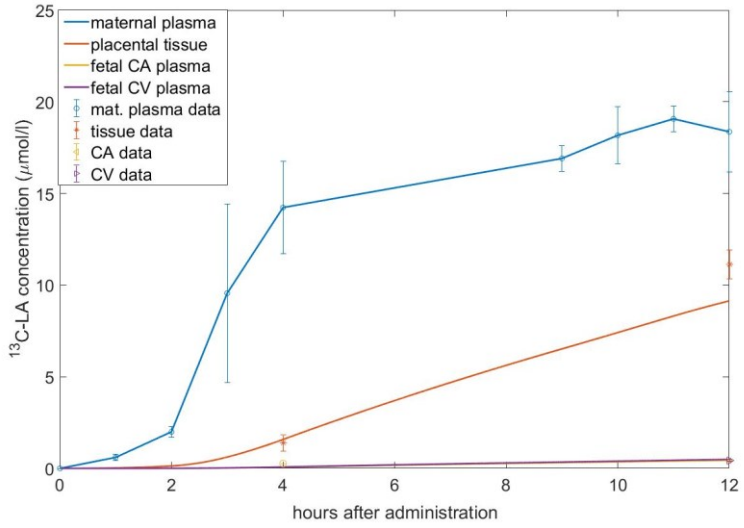

B

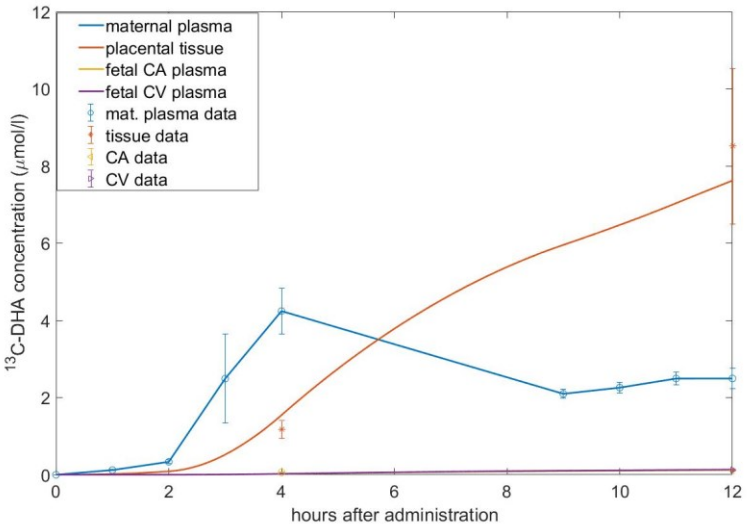

Figure *5.10. Example of modelling prediction and fit for LA and DHA for Case 1 (input as NEFA + TG + PL).*

*(**A**) Results for ^{13}C-LA. (**B**) Results for ^{13}C-DHA. Model prediction (solid lines) vs. experimental data (circles) for the hypothesis of Case 1* (maternal input as NEFA + TG + PL). *Blue for the maternal plasma, orange for the tissue content, purple for the cord vein plasma, yellow for cord artery plasma. Note, the maternal plasma, placental tissue and fetal cord values shown combine the data from the 4 h and 12 h experiment in a single time line, i.e. the 4 h experiment provides data on the initial phase after administration (1 to 4 h), while the 12 h experiment provides the long term data (9 h to 12 h). All data presented as mean ± SEM.*

Chapter 6: Modelling phenylalanine transfer across the isolated perfused human placenta

The following journal paper has been published based on the work presented in this chapter:

Lofthouse EM, Perazzolo S, Brooks S, Crocker IP, Glazier JD, Johnstone ED, Panitchob N, Sibley CP, Widdows KL, Sengers BG, Lewis RM***, Phenylalanine transfer across the isolated perfused human placenta: an experimental and modelling investigation.*** American Journal of Physiology-RICP, V310-9 R828-R836, 2015.

My main contributions:

1. I adapted an existing generic amino acid transport model to be applicable to the experimental design for this study, including relevant substrates and different flow rates.
2. I modelled placental transfer data for the amino acid phenylalanine and used the model to analyse the underlying physiological processes by comparing different potential transfer mechanisms.
3. In light of these results I adapted the model to include metabolism and reran the simulations, which revealed the influence of amino acid metabolism on transfer.

The experiments conducted as part of this chapter were carried out by Dr Emma Lofthouse, Faculty of Medicine, University of Southampton, UK.

6.1 Introduction

Amino acid transfer is a key placental function required for fetal growth, which is reduced in growth-restricted pregnancies [167]. To understand why placental amino acid transfer becomes restricted in these pregnancies, we need to define the factors that may be limiting to this process. It is clear that net placental amino acid flux to the fetus is dependent upon membrane transport proteins localised to the microvillous (MVM) and basal plasma membranes (BM) of the syncytiotrophoblast [168]. However, other variables, such as blood flow or metabolism could be equally limiting to net placental amino acid transfer [78].

Amino acid transfer across the placenta is an active process that occurs against a concentration gradient, and it is mediated by exchanger and facilitated transporters. In particular, exchangers are expressed in both the MVM and BM, while facilitated transporters are only expressed in the BM [169]. Also, paracellular diffusion could be present but is generally thought to be of less importance. Placental amino acid transfer has not generally been considered to be flow-limited [168, 170].

Nevertheless, previous modelling of the placental amino acid transfer has suggested that flow may be an important determinant [107, 108], however those results lacked experimental validation. Thus, in the present study, we set out to investigate the question of what are the main mechanisms and factors influencing the transfer of amino acid across the placenta. Although experimental and modelling approaches were carried out for this study, in this text we will focus on the latter.

6.2 Methods

Human placentas were collected from daytime term vaginal deliveries from uncomplicated pregnancies at the Princess Anne Hospital in Southampton, in accordance with the ethical approval from the Southampton and Southwest Hampshire Regional Ethics Committee (REC approval number 11/sc/0323). Placentas were perfused using the methodology established in the group of Prof. Lewis at Southampton General Hospital, i.e. similar as described in Section 2.5 (to note maternal open loop here), but using open loop perfusion for both maternal and fetal circulations.

6.2.1 Experimental methodology

Phenylalanine was chosen as the candidate amino acid as it is a substrate for both exchangers and facilitated transporters [171]. It is also not catabolised (i.e. phenylalanine hydroxylase is not expressed) within the human placenta [172]. The maternal circulation was perfused with 2.7 nmol/l ^{14}C-phenylalanine. Initial baseline maternal and fetal flow rates were 14 and 6 ml/min respectively for 30 min. As outlined in Fig. 6.1, maternal flow rate was then changed from 14 ml/min to 10 ml/min, back to 14 ml/min and then 18 ml/min, for an hour each. During each hour, fetal flow rates were changed to 3, 6 and 9 ml/min for 20 min each. In each 20 min block, sampling of the maternal and fetal venous exudate was performed at 5, 10, 15 and 18 min, respectively. Finally, both circulations were perfused with buffer that did not contain ^{14}C-phenylalanine for 15 min to wash out the tissue. Following the perfusion protocol of 220 min in total, the cotyledon was analysed to determine the amounts of intracellular amino acids in the tissue.

Experimental measurement of the placental uptake (mol/min) was calculated from the difference in concentration (mol/l) between maternal arterial and maternal venous outflow, multiplied by maternal flow rate (l/min). Placental transfer (mol/min) was calculated from fetal vein concentrations (mol/l) multiplied by fetal flow rate (l/min).

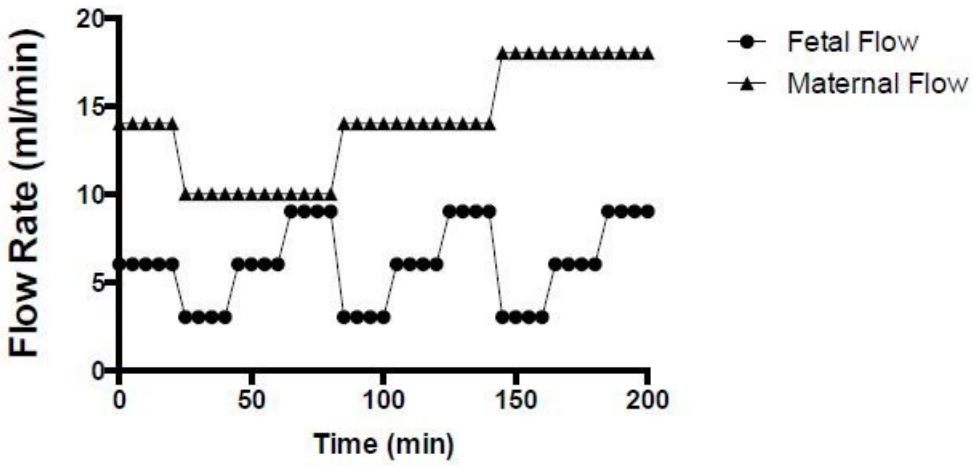

Figure 6.1. *^{14}C-phenylalanine experimental design of the flows.*

Stepwise changes in maternal and fetal perfusion flow rates from the beginning of ^{14}C-phe tracer infusion. Following an initial 20 min equilibration period, flow rates were varied every 20 min and maternal and fetal venous outflow samples collected at 15 and 18 min to determine uptake and transfer, respectively. Image modified from [110].

6.2.2 Computational modelling

A compartmental model was constructed to represent the intervillous space, syncytiotrophoblast and fetal capillaries (Fig. 6.2A) and using relative volume fractions from the literature [107]. The model implemented the labelled phenylalanine (^{14}C-phe) as the amino acid of interest for the transfer. Intracellular (endogenous) unlabelled amino acids were grouped in two classes: those that can be transported by facilitated and exchange transporters, and those that can be transported only by exchanger transporters. In addition, simple diffusion was included (paracellular route). Transport of amino acids across the placenta will be studied as (i) purely by simple paracellular diffusion, (ii) transporter mediated and (iii) simple diffusion plus transporter mediated. For the transporter mediated case simulations were carried out with or without metabolism. An additional modelling simulation was carried out for physiological maternal input concentrations for the case of transporter mediated transfer, including metabolism. Modelling results will be compared to experimental results. Flow rates were based on the experimental protocol outlined in Fig. 6.1. Fluxes between compartments were modelled by assuming that the relevant transporters could be grouped together in generic exchange and facilitated transporters as outlined in Fig. 6.2B. The model was built and solved in MATLAB 2014b.

A **B**

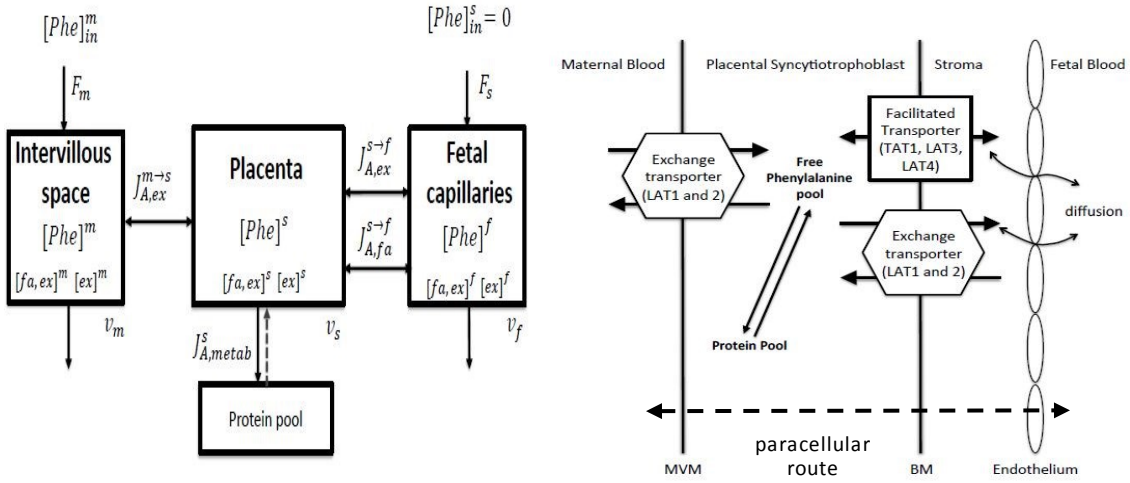

Figure 6.2. *Phenylalanine conceptual and modelling outlines.*

*(**A**) Compartmental modelling schematic with nomenclature used in the equations. (**B**) Conceptual outline of phenylalanine transport across the human placenta showing the transporters in the MVM and BM. Images taken from* [110].

6.2.2.1 Compartmental modelling

A compartmental modelling approach was adopted based on previous work [107], but with the inclusion of metabolism. Briefly, the placenta was represented as three separate volumes, corresponding to the maternal intervillous space, syncytiotrophoblast, and fetal capillaries, respectively. All compartments were assumed well mixed. The transfer of amino acids between the compartments was modelled as fluxes mediated by the exchange transporters in the MVM and facilitative and exchange transporters in the BM:

Intervillous space:

$$\frac{d[A]^m}{dt} = \frac{1}{v_m}\left(J^m_{A,flow} - J^{m\to s}_{A,ex} - J^{m\to f}_{A,dif}\right) \quad (6.1)$$

Syncytiotrophoblast:

$$\frac{d[A]^s}{dt} = \frac{1}{v_s}\left(J^{m\to s}_{A,ex} - J^{s\to f}_{A,ex} - J^{s\to f}_{A,fa} - J^s_{A,metab}\right) \quad (6.2)$$

Fetal capillaries:

$$\frac{d[A]^f}{dt} = \frac{1}{v_f}\left(J^f_{A,flow} + J^{s\to f}_{A,ex} + J^{s\to f}_{A,fa} + J^{m\to f}_{A,dif}\right) \quad (6.3)$$

where $[A]^i$ is the concentration (mol/l) of ^{14}C-phe in compartment *i*, and v_i is the volume of compartment *i* (l). $J_{A,x}^{i\to j}$ represents the net molecular flux (mol/min) of ^{14}C-phe from compartment *i* to *j* mediated by transporter *x*. Here, *i,j* = [*m*, *s*, *f*], where *m* stands for the maternal, *s* for syncytiotrophoblast, and *f* for fetal compartments. *x* = [*ex*, *fa*], denote the exchange and facilitative transporters, respectively. $J_{A,flow}^{k}$ is the net molecular flux of ^{14}C-phe due to blood flow, with k = [*m*, *f*], being *m* and *f* the maternal and fetal circulation flows, respectively. $J_{A,metab}^{S}$ is the consumption of ^{14}C-phe *A* by metabolic processes (for phenylalanine primarily protein synthesis) and $J_{A,dif}^{m\to f}$ the flux due to simple diffusion (paracellular route). Note that simulations were carried out either for transporters alone or for diffusive transfer alone by omitting the relevant terms in the compartmental model equations.

6.2.2.2 Transport modelling

A carrier-based model was used to represent the transporters involved in the amino acid transport across the placenta as mentioned in Section 2.6.4 and depicted in Fig. 2.18. For further reading refer to [169]. For the exchanger (*ex*) model, the net flux $J_A^{I\to II}$ (mol/min) of ^{14}C-phe from compartment *I* to compartment *II* is given by:

$$J_{A,ex}^{I\to II} = V_{ex}\frac{[A]^I[R]_{ex}^{II}-[A]^{II}[R]_{ex}^{I}}{K_{ex}([Tot]_{ex}^{I}+[Tot]_{ex}^{II})/2+[Tot]_{ex}^{I}[Tot]_{ex}^{II}} \tag{6.4}$$

and for the facilitated transporter (*fa*):

$$J_{A,fa}^{I\to II} = V_{fa}\left(\frac{[A]^I}{K_{fa}+[Tot]_{fa}^{I}}-\frac{[A]^{II}}{K_{fa}+[Tot]_{fa}^{II}}\right) \tag{6.5}$$

where $[A]^i$ is the concentration (mol/l) of ^{14}C-phe in compartment *i* and $[Tot]^i$ is the total sum of all substrates of either the exchanger or facilitative transporter in compartment *i*, while $[R]_{ex}^{i}$ is the sum of all exchanger substrates, excluding ^{14}C-phe. *K* is the dissociation constant (mol/l) for the exchanger (K_{ex}) or facilitated transporter (K_{fa}), and the maximum transport rate V_{max} for the exchanger is V_{ex} (mol/min) or for the facilitated transporter V_{fa} (mol/min).

Intracellular unlabelled amino acids in the model were represented by two generic amino acids to differentiate between substrates that are transported by both exchange and facilitated transporters, and substrates transported by exchange transporters only. For the first generic amino acid, i.e. substrates transported by facilitated transporters and exchangers, an intracellular concentration was applied of 3132 µmol/l [173, 174], which is the sum of the intracellular concentrations available in the literature for the following amino acids: alanine, isoleucine, leucine, methionine, unlabelled phenylalanine, tyrosine, tryptophan and valine. For the second generic amino acid, i.e. those amino acids transported by exchangers, but not facilitated transporters, an

intracellular concentration of 4491 µmol/l was applied [173, 174], which is the sum of the intracellular concentrations available in the literature for the following amino acids: asparagine, cysteine, glutamine, glycine, histidine, serine and threonine. Previous data indicate that in perfused human placentas, there were few significant decreases in intracellular amino acid concentrations over the course of an experiment [175]. As such, the intracellular concentrations of the two generic classes of amino acids described here were kept constant within the model throughout the simulations.

MVM and BM exchangers were assumed to be symmetric with the same dissociation constants on either side of the membrane in MVM and BM (K_{ex} = 200 µmol/l; K_{fa} = 1000 µmol/l) [176]. The maximum transport rates V_{max} were fitted by manually adjusting the parameters so that the model matched the average of the experimental steady state placental uptake and transfer values over all flow conditions. In the first instance, the BM exchanger and facilitated transporter were assumed to have the same V_{max} to reduce the number of parameters required for the model.

The simulation using maternal physiological concentrations of unlabelled amino acids in the maternal input was carried out, where amino acids were grouped by transport mechanisms (as done intracellularly) with maternal inlet values found in literature [174]. For exchange and facilitated substrates, this was 615 µmol/l, and for the exchanger only substrates, this was 915 µmol/l.

6.2.2.3 Transfer as result of flow

Blood flow in and out of the maternal and fetal compartments results in a net flux $J^i_{A,flow}$ (mol/min) as follows:

$$J^i_{A,flow} = F_i\left([A]^i_{in} - [A]^i\right) \tag{6.6}$$

where $[A]^i_{in}$ is the inlet concentration (mol/l) of ^{14}C-phe in compartment i and $[A]^i$ is the concentration in the compartment. F_i is the constant flow rate in and out of compartment i (l/min).

6.2.2.4 Metabolic modelling

Metabolism of amino acids was represented by linear kinetics assuming an unsaturated process with rate constant k_{metab}.

$$J^s_{A,metab} = k_{metab}[A]^s \tag{6.7}$$

where $J^s_{A,metab}$ is the metabolic rate (mol/min), $[A]^s$ is concentration (mol/l) of ^{14}C-phe in the syncytiotrophoblast, and k_{metab} is the rate constant (l/min). This represents metabolic removal of phenylalanine, and as there is no phenylalanine hydroxylase activity, this is likely to represent

primarily protein synthesis incorporation. k_{metab} was fitted by manually adjusting the parameter so that the model matched the average of the experimental steady state placental uptake and transfer values over all flow conditions.

6.2.2.5 Diffusion modelling

To determine if paracellular diffusion could explain the transfer of phenylalanine, the effective diffusive permeability was fitted by manually adjusting this parameter so that the model matched the experimental average steady state placental uptake. The following equation was used to model the flux due to simple diffusion:

$$J_{A,dif}^{m\to f} = V_{dif}\left([A]^m - [A]^f\right), \tag{6.8}$$

where V_{dif} is the effective diffusive permeability constant (l/min).

6.3 Results

6.3.1 Experimental data and results

The average cotyledon weight was 42.0 ± 9.7 g (N = 5 placentas). Based on the steady state measurements over the course of the experiment, ^{14}C-phenylalanine uptake per cotyledon was 4.6 ± 0.7 nmol, 15% of which 0.7 ± 0.02 nmol was transferred to the fetal circulation, leaving 3.9 ± 0.01 nmol retained within the perfused cotyledon (N = 5). The concentration of free ^{14}C-phenylalanine in the tissue was 1.0 ± 0.7 nmol/cotyledon and that incorporated into protein was 1.2 ± 0.5 nmol/cotyledon. Total recovery of ^{14}C-phenylalanine was thus 2.2 ± 0.8 nmol/cotyledon, which equates to 56 % of the tracer retained in the tissue (N = 5).

Experimental uptake of ^{14}C-phenylalanine increased with increasing maternal flow (N = 5 placentas, p = 0.011) but was not related to fetal flow (Fig. 6.4A). There were no significant interactions between maternal and fetal flow.

Net flux of ^{14}C-phenylalanine (mol/min) to the fetus was unaffected by varying fetal (p = 0.89) or maternal (p = 0.94) flow rates, nor was there an interaction between maternal and fetal flows (p = 0.95, N = 5, Fig. 6.4A). As such, the increase in placental uptake with increasing maternal flow did not translate into an increased transfer to the fetal circulation. A more detailed overview of the experimental results is reported in the published paper [110].

6.3.2 Placental uptake of ^{14}C-phenylalanine, modelling results

An overview of the model predictions as a function of time input levels (Fig. 6.3A) is presented in Fig. 6.3B for the model based on exchange and facilitated transporters, including metabolism. The overall modelling results reported in Fig. 6.4B, C showed that transfer via membrane transporters (MVM exchange, BM facilitated transport and exchange), resulted in the best match for the experimental results for uptake from the maternal circulation.

More specifically, modelling results fitted the experimental data better with uptake by transporter (R^2 = 0.77, Fig. 6.4C) rather than simple diffusion (R^2 = 0.02, Fig. 6.4B). For the former, the predicted total uptake was 3.9 nmol, which is of the same order as the experimental value of 4.6 ± 0.7 nmol. The modelled uptake trends for transporter mediated uptake (Fig. 6.4C) followed the experimental findings, i.e. uptake increased when maternal flow was increased, but was relatively insensitive to changes in fetal flow. This in contrast to the case of paracellular diffusion where a clear dependency on fetal flow could be observed (Fig. 6.4C). A simulation was also conducted in the presence of physiological maternal concentrations of amino acids. In this case, there was only a marginal effect of flow on phenylalanine uptake (Fig. 6.4D).

Although for the transporter model the predicted uptake from the maternal circulation was essentially identical if modelled with or without placental metabolism, metabolism was included in Fig.6.3, 6.4C and 6.4D because this will prove to be fundamental later to match the transfer to fetal circulation. The combined paracellular diffusion plus transporter model could only provide a good match for uptake if diffusion was very low and therefore it was not pursued further.

A

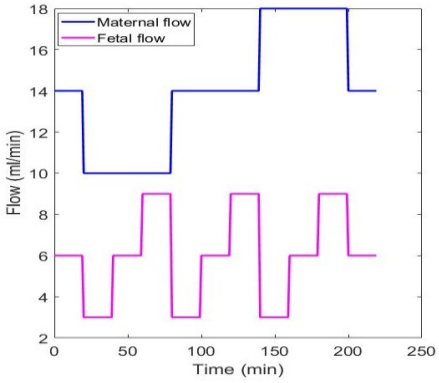

B

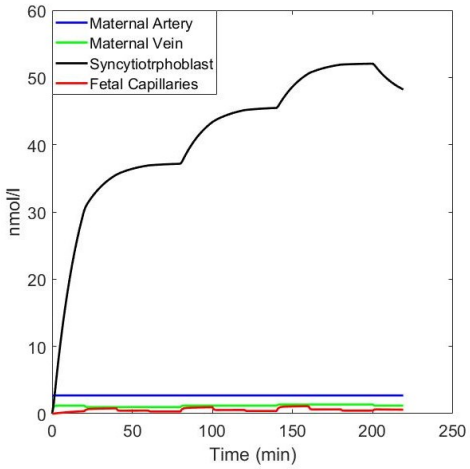

C

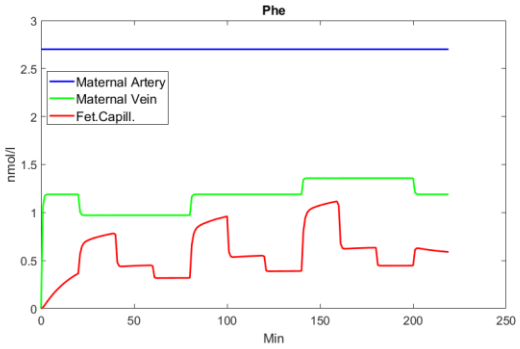

Figure 6.3. *Placental ^{14}C-phe model predictions as a function of time for the transporter-based model including metabolism*.

*(**A**) Maternal and fetal circulation flow inputs for the model corresponding to the experimental protocol in Fig. 6.1. (**B**) Model predictions of the concentrations in the compartments, where blue represents the maternal artery, green the maternal vein, black the syncytiotrophoblast and red the fetal capillaries. Parameters were manually adjusted to match the experimental uptake and delivery, V_{ex} = 3000 nmol/min on the MVM, $V_{ex} = V_{fa}$ = 1000 nmol/min on the BM and k_{metab} = 0.1 l/min.* (**C**) *Close-up of the lower intensity model concentrations of figure **B***

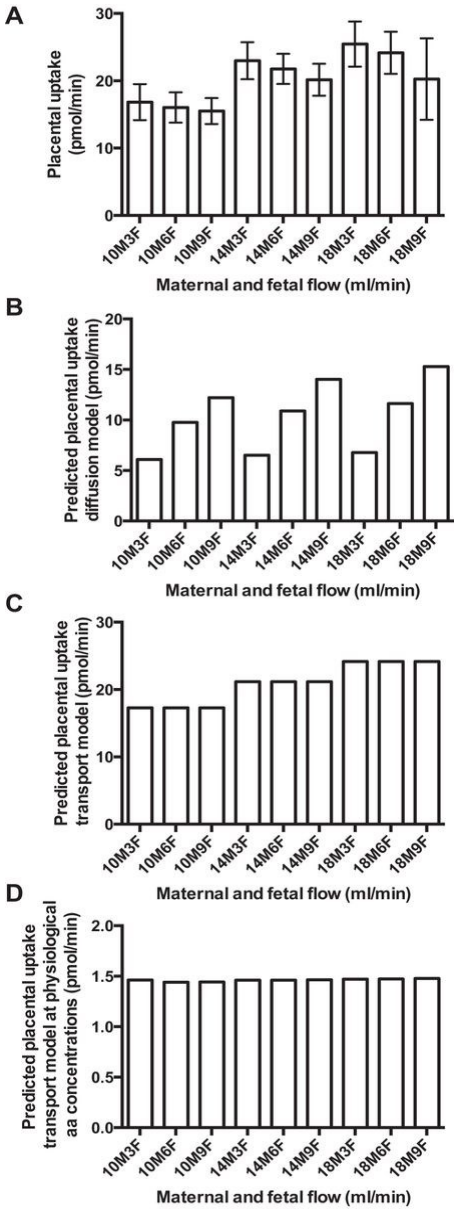

Figure 6.4. *Placental phenylalanine uptake data and modelling.*

*(**A**) **Experimental uptake** of ^{14}C-phenylalanine across the perfused placental lobule. Uptake of ^{14}C-phenylalanine from the maternal circulation was associated with maternal ($p = 0.011$) but not fetal flow rates ($p = 0.41$). There were no significant interactions between maternal and fetal flow ($p = 0.96$). Data presented as mean ± SEM, N = 5 placentas. (**B**) Predicted uptake of phenylalanine if transfer is mediated by **simple diffusion**. Note, maternal uptake levels could not be matched and there was no fit between predicted uptake and experimental data ($R^2 = 0.02$) (**C**) Predicted uptake of phenylalanine if transfer is mediated by **facilitated** and **exchange transporters**. There was good fit between predicted uptake and experiential data ($R^2 = 0.77$) (**D**) Predicted uptake of phenylalanine tracer at **physiological** maternal arterial amino acid levels if transfer is mediated by transporters and assuming intracellular metabolism. In this case, because amino acid concentrations within the perfusate are much higher, delivery is no longer rate limiting and maternal flow does not determine uptake. Image taken from* [110].

6.3.3 Placental transfer of ^{14}C-phenylalanine, modelling results

The computational model was used to predict placental transfer assuming simple diffusion (Fig. 6.5B) and transport (MVM exchange, BM facilitated and exchange), firstly in the absence of metabolism (Fig. 6.5C), and secondly with metabolism assumed (Fig. 6.5D). The model assuming syncytiotrophoblast metabolism (Fig. 6.3), provided the best overall qualitative representation of the experimental data, as observed from Fig. 6.5D. Nonetheless, there was still a progressive increase in phenylalanine transfer associated with increasing maternal flow and the quantitative fit was poor (R^2 = 0.14). This model estimated a total placental transfer of 0.8 nmol, which was close to the experimental value of 0.7 ± 0.02, and combined with the uptake amount, the amount left in the placental tissue was predicted to be 3.4 nmol, which again was close to the experimental value of 3.9 ± 0.01 nmol.

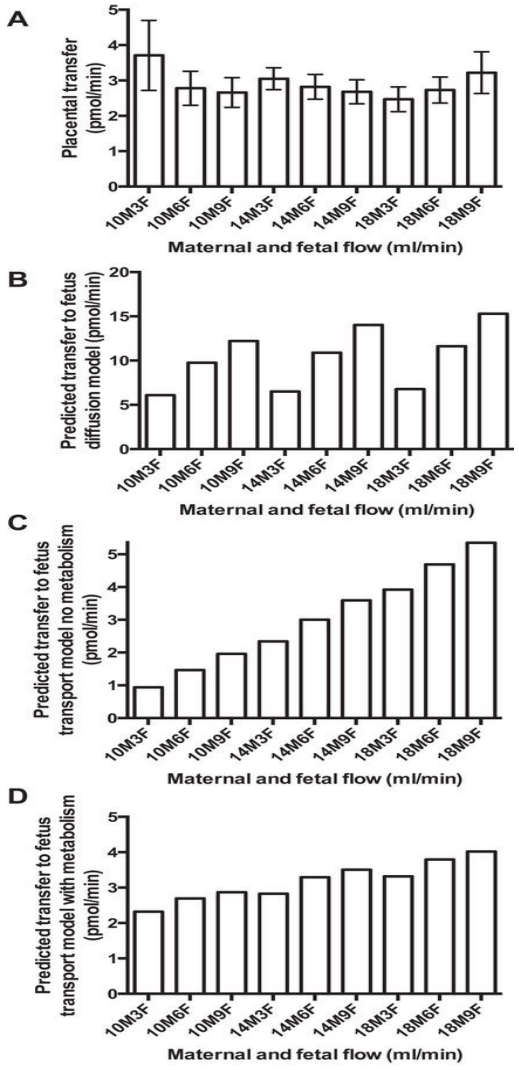

Figure 6.5. *Placental phenylalanine transfer showing experimental data and predicted transfer under certain assumptions.*

*(**A**) **Experimental** transfer of ^{14}C-phenylalanine across the perfused placental lobule. The transfer of phenylalanine to the fetal circulation was not related to maternal (p = 0.89) or fetal (p = 0.94) flow rates and there were no interactions between maternal or fetal flow (p = 0.95). Data are presented as mean ± SEM, N = 5 placentas. (**B**) Predicted transfer of phe if transfer is mediated by **simple diffusion**. In this case uptake and transfer are equal and fetal flow has the predominant effect on transfer. (**C**) Predicted transfer of phenylalanine if transfer is mediated by **transporters** and assuming **no** intracellular **metabolism**. Because uptake is greater than transfer, intracellular phenylalanine concentrations rise over time driving a progressive increase in transfer across the course of the experiment. This scenario does not reflect the experimental data. (**D**) Predicted transfer of phenylalanine if transfer is mediated by transporters and assuming intracellular **metabolism**. While transport with metabolism demonstrates the closest agreement to the experimental data (R^2 = 0.14), none of the model outputs showed enough good fit, indicating that other factors are required to fully account for the mechanisms underlying transfer of phenylalanine. Image taken from* [110].

6.3.4 Sensitivity analysis for the transporter model, including metabolism

Parameter variation was undertaken in the transport model with metabolism included, in which the effect of a 5-fold increase and decrease in model parameter on the uptake/transfer of phenylalanine was considered. The sensitivity analysis for uptake indicated that V_{max} and K for the exchanger on the MVM are the major determinants of transfer (Fig. 6.6). The sensitivity analysis for transfer indicated that the V_{max} of the facilitated transporter on the BM, followed by the V_{max} of the exchanger on the MVM, are major determinants of transfer, when metabolic rate is applied as a major limiting factor. Sensitivity analysis showed that uptake under experimental conditions was dependent on the ratio between K and V_{max} in the linear regime (Fig. 6.6A). As regards to the BM, transfer was highly sensitive to rate of metabolism and V_{max} of the facilitated transporter (Fig. 6.6B). However, when sensitivity analysis was performed including physiological amino acid concentrations, distinct differences were observed, particularly in regard to uptake where metabolism, and to a lesser degree facilitated transporter V_{max}, now affected the model (Fig 6.6C, Fig. 6.6D).

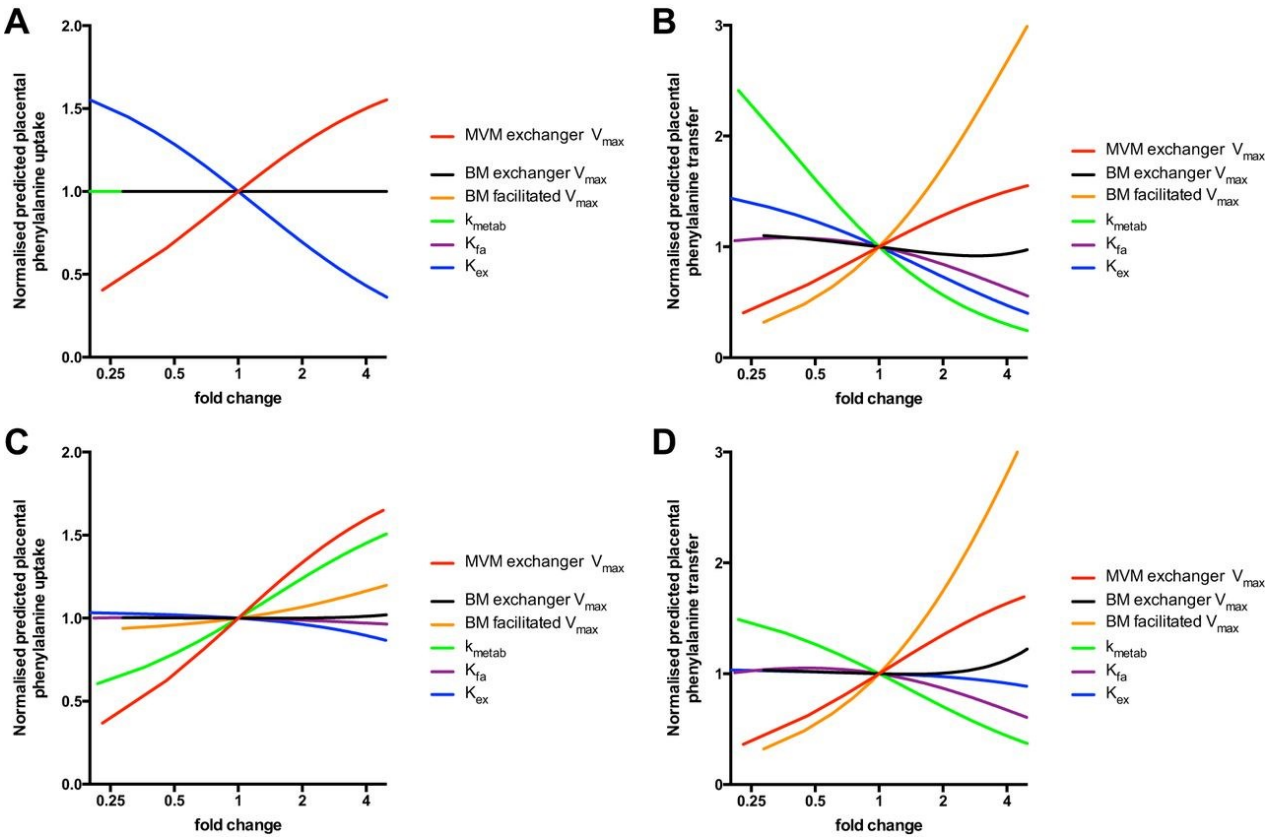

Figure 6.6. *Parameter variation of the amino acid model.*

*(**A**) Sensitivity analysis for placental **uptake** indicated that it was dependent on the ratio between K and V_{max} in the linear transport regime. (**B**) Sensitivity analysis for placental **transfer** indicated that it was highly sensitive to metabolic rate and V_{max} of the BM facilitated transporter. Note that this sensitivity analysis is based on the low uterine arterial phenylalanine concentration used in in the experimental model. Parameter variation showing the predicted effect of a 5-fold increase and decrease respectively in model parameter on uptake or transfer of phenylalanine using conditions assumed for the physiological modelling. (**C**) Sensitivity analysis for placental **uptake** using conditions assumed for the **physiological** modelling indicated that it was dependent on MVM exchanger V_{max} and metabolic rate. There is a marked difference between predicted sensitivities under experimental and physiological conditions. (**D**) Sensitivity analysis for placental **transfer** using conditions assumed for the **physiological** modelling indicated that it was sensitive to metabolic rate and V_{max} of the MVM transporters and BM facilitated transporter. Image taken from [110].*

6.4 Discussion

This study demonstrates that factors additional to transporter activity and flow determine placental transfer of phenylalanine to the fetal circulation. A possible mechanism was proposed in the form of the inclusion of a metabolic pathway mediating the transfer. Including metabolism resulted in the best predictions when compared to the experimental data.

Experimental results indicated that there were no significant interactions between maternal and fetal flow. As such, the increase in placental uptake with increasing maternal flow did not translate into an increased transfer to the fetal circulation. Model outcomes must mimic these results.

Two distinct mechanisms of placental transfer were explored using the model, in which the amino acid was transferred across the placenta either by simple diffusion or by transporters (or by a combination of the two mechanisms). Simple diffusion, which represents the paracellular route, could only match experimental transfer to the fetal circulation, but importantly could not be made to match the high level of uptake from the maternal circulation observed in the experiments. Even when massively increasing the diffusivity parameter, effectively equalising the concentrations in the maternal and fetal compartments, this was not enough to match uptake, as this became limited by the maternal and fetal flows. From this, it could be concluded that simple paracellular diffusion is unlikely to be the sole physiological route for placental transfer.

On the other hand, for the model based on the transporters a satisfactory fit for the uptake was achieved, and maternal flow dependency was achieved as observed in the experiment. However, note that for the simulation under physiological conditions, no flow dependency of uptake was found. In this case, because amino acid concentrations within the maternal input perfusate are much higher than the labelled phenylalanine, transporters are saturated and maternal flow does not further affect uptake.

Predicted uptake matched the experimental uptake with or without metabolism, however, transfer could be matched only when metabolism was included. In fact, for the model without metabolism, the intracellular concentration accumulated, increasing linearly over time, which implied a proportional increase in transfer (Fig. 6.5C), which was not observed in the experiment.

Within experimental variation the transfer observed in the experiment was surprisingly constant (Fig. 6.5A), independent of flow. This could also imply that the transporters were saturated; however this is unlikely as the tracer concentration is well below the K_m and in this range flux should increase proportionally with concentration (even if transfer of the unlabelled substrate were saturated).

While metabolism is likely to play a key role, nevertheless, the model could not fully reproduce the constant rate of phenylalanine transfer observed experimentally (Fig. 6.5D). The reason for this is that in the model linear kinetics were assumed for metabolism and every time maternal uptake is

increased this would directly lead to a higher equilibrium of intracellular amino acid concentration (Fig. 6.3, syncytiotrophoblast), thus increasing the concentration gradients that drive amino acid transport across the BM. Only if intracellular phenylalanine concentration was fixed, could the model provide a good representation of our experimental data. Therefore, for metabolism to fully explain the data there would need to be tight regulation of metabolism in order to maintain a constant free intracellular phenylalanine concentration at the BM interface. Previous work in the guinea pig has suggested an important role for protein metabolism in amino acid transfer [177], and phenylalanine catabolism or sequestration within intracellular organelles could regulate the free amino acid pool available for transport.

While all the factors modelled are necessary for transfer, it is important to identify those that are most likely to become rate limiting and thus have greatest clinical relevance. The model sensitivity analysis identifies those factors that, assuming the model is representative, have the biggest impact on phenylalanine transfer. It is important to note that the sensitivity analysis favoured different factors under experimental (low phenylalanine concentrations) and physiological amino acid concentrations. However, it appears that MVM exchanger activity, BM facilitated transporter activity and incorporation of amino acids into protein were predicted to be the primary determinants of placental transfer.

In conclusion, this experimental and modelling study suggests that transporter activity is a major determinant of phenylalanine transfer across the perfused human placenta, but flow is not. In addition, the modelling approach leads us to conclude that also other factors, such as metabolism within the placenta, play a previously underappreciated role.

Future work should focus on modelling the placental amino acid metabolism in a more sophisticated way, thus shedding light on specific metabolic sub-compartments and their contribution to the intercellular concentration, which may be instrumental in regulating transfer.

Chapter 7: Modelling cortisol transfer across the human placenta

Main contributions:

- First model of cortisol-cortisone transfer in the placenta
- Comparison of modelling results with previously published experimental data
- Model evaluation to determine the most important mechanisms involved

7.1 Introduction

Natural glucocorticoids, such as the stress hormone cortisol in humans belong to the group of steroid hormones that are secreted from the adrenal cortex in response to environmental or physiological stress [178]. Prenatal exposure to corticoids retards the fetal growth leading to low weight offspring that might lead to other health problems in future life [179]. In order to protect the fetus from this exposure, the placenta possesses an enzyme (11β-HDS), which converts the cortisol to cortisone, the inactive form of the cortisol. Therefore, this enzyme represents effectively a "barrier" mechanism preventing excessive quantities of cortisol reaching the fetal circulation [180, 181].

Little is known about the nature of the transmembrane transport of cortisol although this is likely to be a key process in the tissue-specific regulation of cortisol action. Currently, no specific transporter is known for cortisol; it is therefore still assumed that this hormone moves through the plasma membrane by passive simple diffusion. Its hydrophobic nature may permit this; however, there is new evidence of carrier mediated transport in the liver [182], where the transport may be a combination of simple and facilitated diffusion. The effect of the albumin and cortisol binding globulin on the placental transport is not clear [181]. Yet, some authors concluded that albumin had virtually no effect on transfer of cortisol into human placental trophoblast [183].

In this work we will model the system mediating transfer of cortisol from the mother to the fetus and investigate the role of the placenta as a "barrier" preventing maternal cortisol overexposure to the baby.

7.2 Methods

A compartmental model was built accounting for the experimental setup and the main physical spaces of the placenta (Fig 7.1). The experimental cortisol perfusion technique was presented by *Benediktsson et al* [181]. It consists of an *ex vivo* perfusion system (see Section 2.5) with maternal

and fetal open loops and with the continuous provision of cortisol over time from a reservoir. Three different cortisol input concentrations (mimicking lower, normal and higher than physiological cortisol levels in maternal blood) were used during the time course experiment and this was modelled using the step function for C_{input} (nmol/l) and depicted in Fig 7.2.

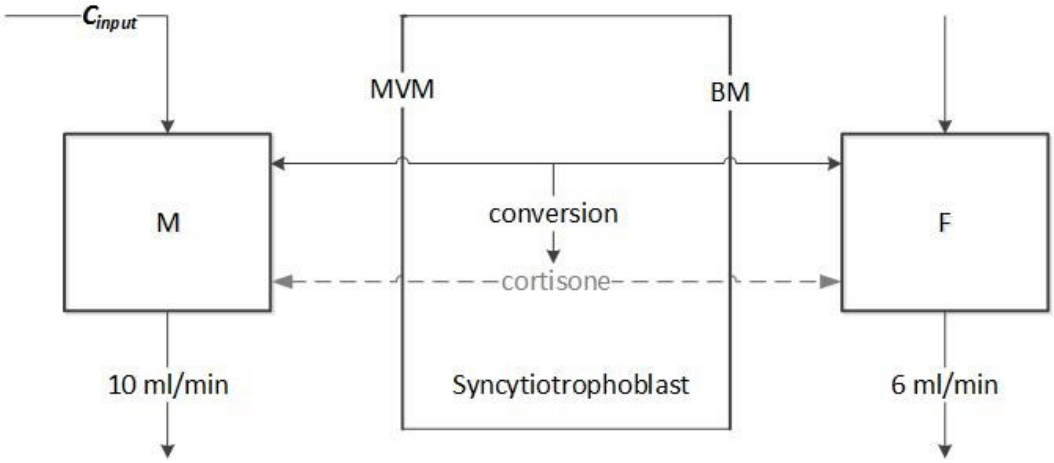

Figure 7.1. *Model schematic of the transport of cortisol in placenta (Cortisol study).*

The tracer is perfused in the maternal circulation (maternal artery) reaching the maternal part of the placenta (M). The MVM and BM membrane plus the Syncytiotrophoblast represents the placental barrier for transfer. In the Syncytiotrophoblast, the conversion of cortisol to cortisone occurs; F represents the fetal capillaries. The cortisone transport is represented by dashed gray lines.

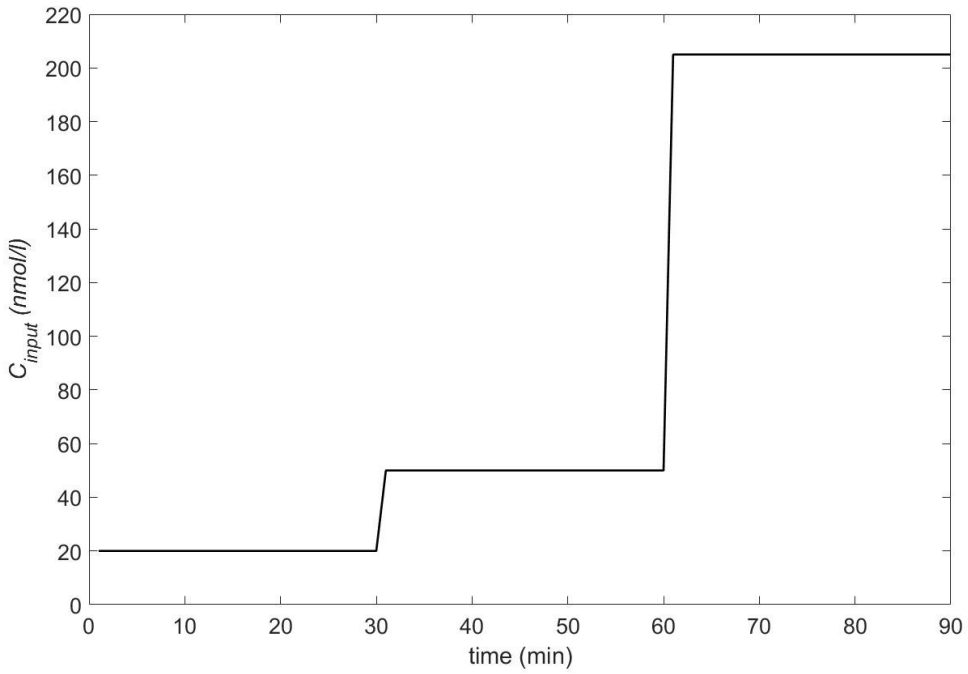

Figure 7.2. *Experimental infusion over time; modelling input function.*

The compartmental model had 3 compartments, the maternal intervillous space *M*, the syncytiotrophoblast, and the fetal capillaries *F* (Fig. 7.1). The maternal compartment, syncytiotrophoblast and fetal capillary volumes were derived from literature [107]. The set of parameters was entirely chosen from existing literature except for $V_{max}^{11ß-HDS}$(nmol/min), which was estimated by manually matching the data from *Benediktsson et al* [181].

The model is defined mathematically by the following set of equations:

$$\frac{dC_M}{dt} = \frac{1}{V_M}\left(-k_{MVM}C_M + k_{MVM}C_S - Q_M C_M + Q_M C_{input} \right), \quad (7.1)$$

$$\frac{dC_S}{dt} = \frac{1}{V_S}(+k_{MVM}C_M - k_{MVM}C_S - k_{BM}C_S + k_{BM}C_F - k_c C_S), \quad (7.2)$$

$$\frac{dC_F}{dt} = \frac{1}{V_F}(-k_{BM}C_S + k_{BM}C_F - Q_F C_F), \quad (7.3)$$

With the usual convention and nomenclature used in this thesis, *C* are the cortisol concentrations in each compartment, Q_M = 10 ml/min, Q_F = 6 ml/min, V_S = 6.6 ml and V_F = 3.3 ml. The transfer across each membrane was assumed to occur only by simple diffusion, for simplicity in first instance equal diffusive permeability was assumed $k_{MVM} = k_{BM}$ = 2.0 µl/min [184].
In particular, the conversion of cortisol to cortisone is assumed to occur inside the syncytiotrophoblast determined by a rate constant k_c (µl/min). Enzymatic reaction converting cortisol (active form) to cortisone (inactive form) is mediated by the 11ß-HDS enzyme and therefore modelled as Michaelis-Menten kinetics with $K_m^{11ß-HDS}$= 50 nmol/l [180]:

$$k_c = \frac{V_{max}^{11ß-HDS}}{K_m^{11ß-HDS} + C_S}. \quad (7.4)$$

7.2.1 Cortisone model

In parallel, cortisone can be modelled using the same approach as for cortisol (Eq. 7.1-7.3), with the exception that the maternal input is zero and the source term is positive. Cortisone originates from the conversion of cortisol following the rate determined by Eq. 7.4. Experimentally cortisone is found both in maternal and fetal circulation, in particular in the maternal output at higher concentrations than expected, therefore after conversion, a certain amount of cortisol is transferred back to the maternal circulation (*Benediktsson PhD Thesis, 1997* [181]), as indicated in Fig. 7.3. Based on the modelled concentrations of cortisol and its inactive form cortisone, the total steroid load could be predicted.

7.3 Results

Results showed that the model rapidly reached steady state after changing the input levels, with $V_{max}^{11ß-HDS}$ = 3000 nmol/min. (Fig 7.3A). The cortisone reaches the steady states with a small delay due to the enzymatic conversion process (Fig. 7.3B). The amount of cortisol and cortisol predicted with the current modelling assumptions was found to closely correspond to previously published experimental results (Fig. 7.4).

A **B**

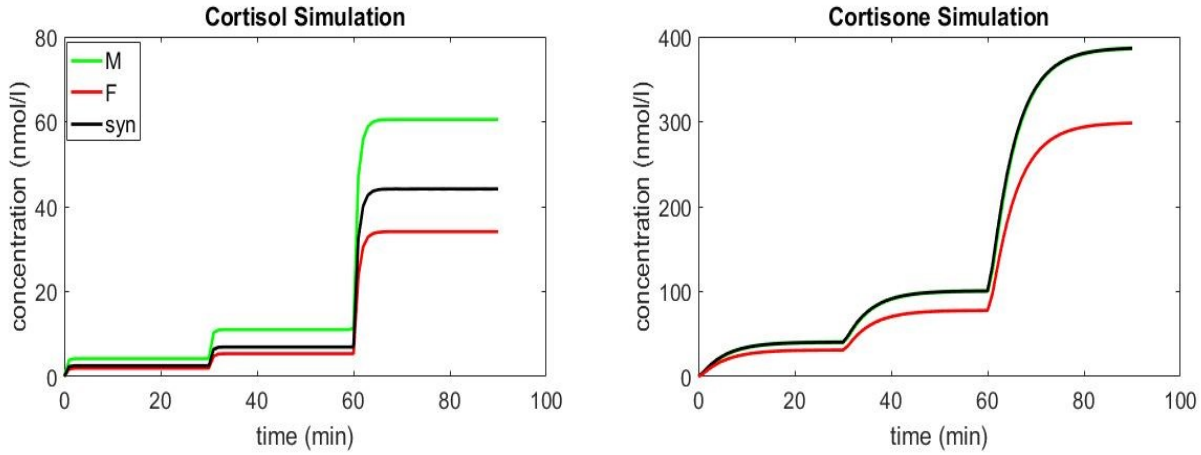

Figure 7.3. *Cortisol modelling prediction results.*

*(**A**) shows the cortisol concentrations in the simulation. (**B**) shows the cortisone concentrations; the syncytiotrophoblast (black line) and the maternal concentration (green line) overlap but there is a small difference with the sysncytiotrophoblast being slightly higher than the maternal concentration.*

A

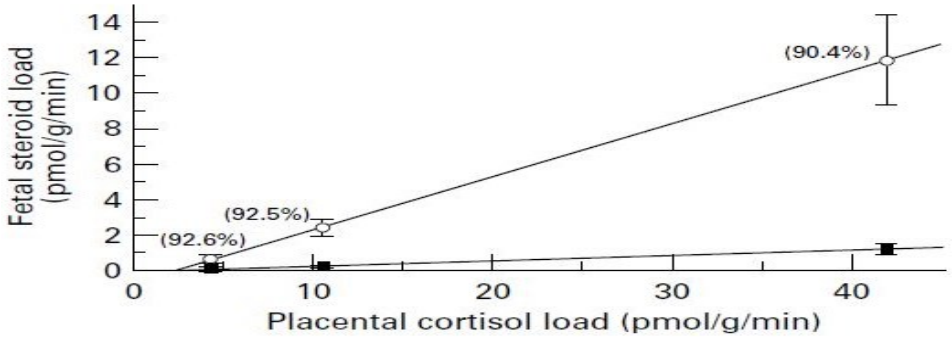

B

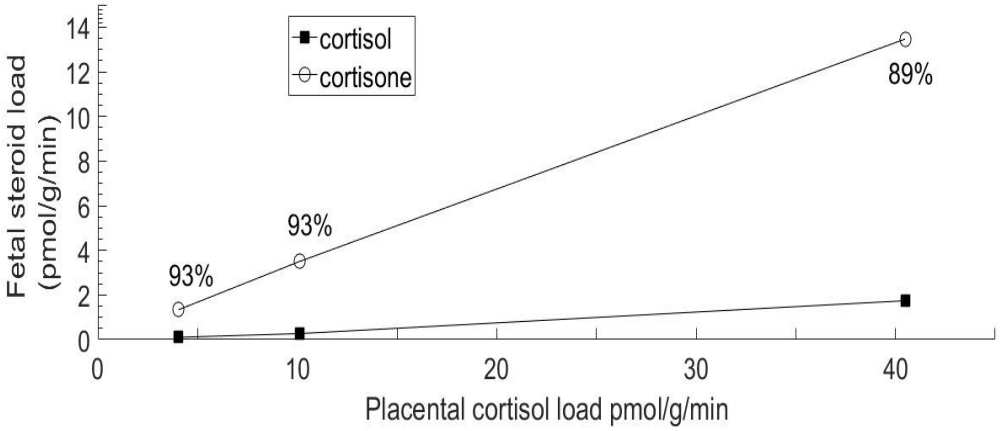

Figure 7.4 *Results of cortisol transfer data (experiment vs. model)*.

*Fetal steroid load (output) vs. the maternal infusion (input). The amounts are divided by the mean value of the cotyledon (38 g) and the experimental time (130 min). The black squares represent the cortisol (mean ± SD) as part of the total steroid load measured. The empty bullets represent the cortisone (mean ± SD) as part of the total steroid measured. Above the empty bullets is given the relative percentage of cortisone out of the total steroid load. (**A**) Experimental results published by Benediktsson et al* [181]. *Image taken from* [181]. *(**B**) Modelling results reported in the same format to allow comparison with those depicted in (**A**).*

7.4 Discussion

The model could simulate the cortisol and cortisone concentration to resemble the experimental results obtained by *Benediktsson et al.* [181]. Compared to other parameters in the model, the value of $V_{max}^{11ß-HDS}$= 3000 nmol/min suggests a large placental capacity of conversion which is not saturated even when the maternal cortisol concentration increases, emphasizing thus the key role of enzyme metabolism in the function of the placenta as a protective barrier. At current concentrations, simple diffusion across the membranes and metabolism/conversion operate in the linear regime, in particular for metabolism this is due to its $K_m^{11ß-HDS}$= 50 nmol/l. Hence, in future experiments we suggest to raise the cortisol concentration until saturation occurs. Saturation could be due to transport, metabolism, or both. In order to distinguish effects of transport and metabolism, we suggest including the use of specific inhibitors blocking the enzyme in the design of future perfusion experiments.

Although the model confirmed and contributed to the understanding of the biological problem, the current experimental data is limited. Additional time points are necessary to explore in detail the dynamics of the cortisol-cortisone transfer and conversion system, as at the moment solely the final experimental measurements were available. In addition, the maternal exudate should be collected and measured since this would provide a better estimate of uptake.

Chapter 8: Modelling the effect of intervillous flow on solute transfer based on 3D imaging of the human placental microstructure

The following journal paper has been submitted based on the work presented in this chapter:

1) S Perazzolo, RM Lewis, BG Sengers. **Modelling the effect of intervillous flow on solute transfer based on 3D imaging of the human placental microstructure.** Submitted to *Annals of Biomedical Engineering*, 2017.

The following conference paper has been published based on the work presented in this chapter:

1) S Perazzolo, RM Lewis, BG Sengers. **Modelling nutrient transfer based on 3D imaging of the human placental microstructure.** *Engineering in Medicine and Biology Society (EMBC), 38th Annual International Conference of the IEEE*, 2016.

Main contributions:

- Implementation of an imaging-based 3D modelling of placental microstructure
- Modelling of the maternal flow as well as the maternal transport of substances (novelty with respect to previous 3D modelling)
- Simulating the maternal flow at lower or higher than physiological rates (novelty with respect to previous 3D modelling)
- Modelling the villous barrier as diffusive barrier and the fetal capillaries as perfect sinks
- Assessing the importance of maternal flow local conditions on the transfer
- Assessing that different villi have different uptake capacity

8.1 Introduction

The placental structure and function has been described in Chapter 2, and it has been shown to be altered in babies who grow poorly in the womb and in response to maternal disease and lifestyle factors [62]. Understanding whether these changes in placental structure help or impair placental function, particularly in terms of gas and nutrient transfer, is an important question. In particular gas, anaesthetics and other small diffusive solutes are thought to be highly dependent on the flow and placental morphology [185]. Thus, with respect to previous compartmental modelling, the placental structure is now included in the computational characterization of the modelling approach (solving partial differential equations).

Improved imaging techniques are allowing detailed 3D imaging of the placental villi over wider areas that now allow detailed mathematical modelling of these processes to predict how changes in placental structure may affect placental function. A more extensive discussion on previous modelling approaches was presented in Section 2.6.

The objective of this study is to evaluate the effects of maternal blood flow in the intervillous space on the placental transfer of solutes, modelling both maternal flows as well as solute transport, using 3D image based models of the placental microstructure. With the term solute, we will refer to any small molecular species whose transport mechanism can be described by simple diffusion, e.g. anaesthetics and other gases. With respect to previous approaches, the novelty of our approach is to include the solute transport in the maternal circulation. In addition, the hydraulic permeability of the maternal circulation associated with the placental microstructure was estimated and the placental uptake was calculated as a measure of transfer for a generic solute. In particular, the effect on uptake was assessed of different maternal blood flow rates below and above the normal physiological range.

8.2 Methods

8.2.1 3D reconstruction of the placental microstructure

Tissue was collected from healthy term placentas after delivery with written informed consent and ethical approval from the Southampton and Southwest Hampshire Local Ethics Committee (11/SC/0529).

Samples were collected within 30 min of delivery and villous tissue was dissected and fixed in 4% paraformaldehyde in PBS at 4°C overnight and then stored in PBS at 4°C. Villous fragments were dissected from the fixed tissue and permeabilized in 1% triton X-100 for 2 h, washed in PBS, and incubated overnight with 10 µg/ml Biotin-Datura Starmonium Lectin (DSL, Vector laboratories) which binds specific carbohydrates on the syncytiotrophoblast; 10 µg/ml Rhodamin-Pisum Sativum Agglutinin (PSA, Vector laboratories) which binds specific carbohydrates in the stromal tissue; 10 µg/ml FITC-Aleuria Aurantia Lectinto (AAL, Vector laboratories) which binds specific carbohydrates on the fetal capillary endothelium. Samples were washed in PBS and incubated with Strptavidin-680 (Licor) and 11 nmol/l DAPI for 2 h then washed in PBS. Samples were cleared through a series of 10%, 25%, 50% and 3 x 97% 2, 2'-thiodiethanol (TDE, Fisher Scientific, UK) in PBS for at least 30 minutes per step. Samples were stored in 97% TDE at 4°C until imaging.

The placental villous fragments were imaged with a Leica TCS SP5 laser scanning confocal microscope. For each batch, a control sample run without lectin or primary antibody (but including

DAPI and any secondary antibodies) was imaged and this sample was used to determine background fluorescence levels for each channel.

Six confocal fluorescence microscopy samples of placental tissue were collected (N=6). Each sample had dimension of 0.78 x 0.78 x 0.25 mm (height x width x depth). From each sample, images were collected at different depths with sampling space of 1.99 µm (for a total of 125 images in the depth direction). Each image had resolution of 1026 x 1026 pixel with sampling of 0.76 µm between pixels (Example in Fig.8.1A). One additional image sample was collected with resolution of 1.5 x 1.5 x 4.2 µm (height x width x depth) and dimensions of 1.55 x 1.55 x 0.41 mm (height x width x depth, 1033 x 1033 x 100 pixels) to test the simulation for even larger sample volumes. Voxel resolution was reduced to 5 µm in all directions to reduce imaging analysis and computation. The impact of reducing image resolution on the used metrics in this Chapter (permeability and uptake) was carried out (Appendix B). Images were filtered to reduce the background noise (normal Gaussian filter). From the image stack, a 3D structure was segmented using ScanIP (Simpleware Ltd, UK). Post-reconstruction smoothing was employed to improve the volumetric imperfection, e.g. small holes or sharp tips in a domain. Volumetric meshing was carried out by ScanIP (Simpleware Ltd, UK) exploiting its automatic procedure [186]. A mesh reduction was carried out to reduce the computational burden (and let the numerical solution to converge) by the Simpleware' s coarseness factor of -50, which generated the most coarse mesh available [186]. Such coarseness factor reduced the number of mesh elements of about 80%. The impact of reducing the mesh resolution on the used metrics in this Chapter (permeability and uptake) was carried out (Appendix B). The mesh was imported into COMSOL Multiphysics 5.2 (COMSOL Inc., USA) where the model was set up for finite element analysis (FEA) (Example in Fig. 8.1B). The problem was solved in steady state with the GMRES iterative solver optimised with the Incomplete LU preconditioner. Briefly, GMRES provides the numerical solution of a non-symmetric system of linear equations using the linear least square problem at each iteration [187]. Incomplete LU is a matrix optimisation of sparse matrixes that improves the iteration computation of GMRES [188].

Simulations were carried out using the IRIDIS 4 Computing Cluster (University of Southampton, UK) using a 16 core node (2.6 GHz) with 64 GB of memory.

Results were expressed as mean ± SD (N = 6). The relationship between permeability and geometrical properties or uptake was represented by Pearson's correlation coefficient *r*.

8.2.2 Modelling assumptions

The reconstructed 3D solid consisted of three main domains: 1) The intervillous space, i.e., the volume around the villi; 2) The villous barrier, as composed of the syncytiotrophoblast and the stromal layer (DSL+PSA staining); 3) The fetal vessels, represented by the endothelium wrapping

the fetal capillaries (AAL staining). For simplicity, it was assumed that the endothelium was part of the volume of the placental capillaries.

8.2.3 Intervillous space blood flow modelling

Fluid flow in the intervillous space was modelled to represent the maternal blood flow percolating around the villi. The fluid was modelled as Newtonian and incompressible. The fluid flow regime was modelled as Stokes flow (creeping flow) [87, 98] and described by:

$$0 = \nabla[-p\boldsymbol{I} + \mu(\nabla\boldsymbol{u} + (\nabla\boldsymbol{u})^T)] \tag{8.1}$$

$$\nabla \cdot \mathbf{u} = 0. \tag{8.2}$$

$\boldsymbol{u}$ and p were respectively the velocity (m/s) and pressure (Pa). $\boldsymbol{I}$ was the identity tensor. μ = 3.2 mPa·s was the dynamic viscosity representative for blood [189]. The typical pressure gradient in the placental cotyledon has been estimated as 36.2 Pa/cm [87, 97]. Thus, a pressure difference of 2.9 Pa ($P_{in} - P_{out}$) was applied along one of the longest dimensions of the sample (L = 0.76 mm) (Fig. 8.1B). On the remaining outer surfaces of the sample, a no-flux boundary condition was imposed. No-slip boundary conditions were applied for the fluid at the villous boundary walls.

8.2.4 Permeability of the placental structure

The hydraulic permeability of the placental structures κ (m^2) was estimated according to Darcy's law for porous media:

$$\kappa = -a\frac{Q}{\Delta P}, \tag{8.3}$$

where Q (m^3/s) is the volumetric rate and $\Delta P = P_{in} - P_{out}$ (Pa). $a = \mu L/A$, with μ the dynamic viscosity of the fluid (Pa·s), L (m) the length of the sample over which the pressure drop takes place and A (m^2) the cross-sectional area. Q was calculated by integrating the normal fluid velocity over one cross-sectional area.

8.2.5 Solute transport modelling

The solute transport in the intervillous space is governed by the advection-diffusion equation:

$$\frac{\partial C}{\partial t} + \nabla(-D\nabla C) + \boldsymbol{u}\nabla C = R. \tag{8.4}$$

C (mmol/l) was the solute concentration and R (mmol l^{-1} s^{-1}) represented the solute reaction rate that may occur during transport. D (m^2/s) was the diffusivity of the solute. The diffusivities were

considered constant and isotropic. The fluid velocity $\boldsymbol{u}$ was inferred from Eq. 8.1. For simplicity, we chose just one solute and no solute reactions.

A solute input concentration C_{in} was prescribed as a constant value at the same inlet face as the inflow (Fig. 8.2A). The initial concentrations in the intervillous space C_{is} and the villous barrier C_{vb} required by COMSOL 5.2 were set to zero (Note however that the problem was solved in steady state). The model did not include blood flow in the fetal vessels, instead, the effect of the solute uptake by the fetal capillaries was simplified by constraining the solute concentration in the fetal vessels to zero (perfect sink condition). Thus, fetal vessel concentration C_{fv} was set and maintained constant at zero. No solute metabolism was assumed to occur in each domain. Parameters for oxygen were used in Eq. 8.4 as it is a small solute that moves across the plasma membranes and the connective tissue by simple diffusion [185]. The parameters used in Eq. 8.4 for the transport of the solute were taken as: C_{in} = 0.1 mmol/l [87], and diffusivity in the fluid D_f = 1.67 × 10^{-9} m^2/s [87]. The model considered the villous barrier as a purely diffusive barrier with D_{vb} = 0.95 × 10^{-9} m^2/s [52]. Transfer of solute across the villous barrier, denoted as uptake q (mol/s), was calculated as the surface integral of the normal solute flux per area entering the villous barrier surface, based on the internal villous concentration.

The pressure difference was varied over a wide range around the physiological pressure from 1000 fold lower (0.0029 Pa) to 100 fold higher (290 Pa) to study the uptake as a function of the resultant fluid velocity.

An estimate of the total relative placental uptake fraction α_{tot} at the macroscale can be found by taking the average relative uptake (N = 6) for the microstructural samples simulated and repeating this over the length of the flow path through the placenta. Relative uptake is defined here as the uptake q (mol/s) divided by the inlet face flux J_{in} (mol/s), i.e. representing the fraction of influx taken up by the placental villi.

The cotyledon distance between inflow and outflow is around 1.3 cm [97] (Fig. 2.14), which equals to around the length of 16 samples. We can consider the average sample with its average uptake $\bar{q}$ (mol/s) and its average inlet face flux $\overline{J_{in}}$ (mol/s) repeated by 16 times in series to represent the cotyledon uptake α_{tot} from the spiral artery (inlet) and the decidual vein (outlet). Thus:

$$\alpha_{tot} = 1 - \left(1 - \frac{q}{J_{in}}\right)^{16}. \tag{8.6}$$

An additional test was carried out to evaluate the maximum transfer capacity of the placental barrier alone, neglecting the intervillous space blood flow. The concentration was set constant to C_{in} outside the villous barrier and it was kept as a perfect sink condition in the fetal capillaries.

8.3 Results

The reconstructed volume of the villi occupied 28 ± 10% of the overall sample volume. The outer surface of the villi was 1.44 ± 0.38 mm^2, while the fetal capillary surface was 0.66 ± 0.29 mm^2, corresponding to a ratio of 2.18 between the outer villous surface and the fetal capillary surface (Fig. 8.1B). A representative example of simulation results is shown in Fig. 8.2A. Qualitatively, the flow velocity and the solute concentrations were higher in areas with less dense villi, thus highlighting depleted regions in proximity of denser villous structures (Fig. 8.2B). The magnitude of the flux through the villous surface showed areas with higher flux capacity (Fig. 8.2C). Similarly, when the magnitude of the flux entering the fetal capillaries was considered, it showed corresponding areas of higher flux capacity (Fig. 8.2D). In combination, these results indicated that those villi most protruding in the intervillous space displayed a higher flux capacity compared to the bulk of the villous structure.

The sensitivity analysis (Appendix B) demonstrated that reducing the image resolution had no significant impact on the permeability estimate, while it led to under-prediction of the uptake (-15%) for 5 µm voxel compared to full resolution, probably due to a loss of capillary detail. The computational time was reduced by 90% for 5 µm resolution. The mesh coarseness did not have a significant impact on the permeability estimate while reducing the number of elements led to over-prediction of the uptake (+18%) for the coarse mesh, which corresponded to an 80% reduction in the number of elements and a 78% reduction in computational time.

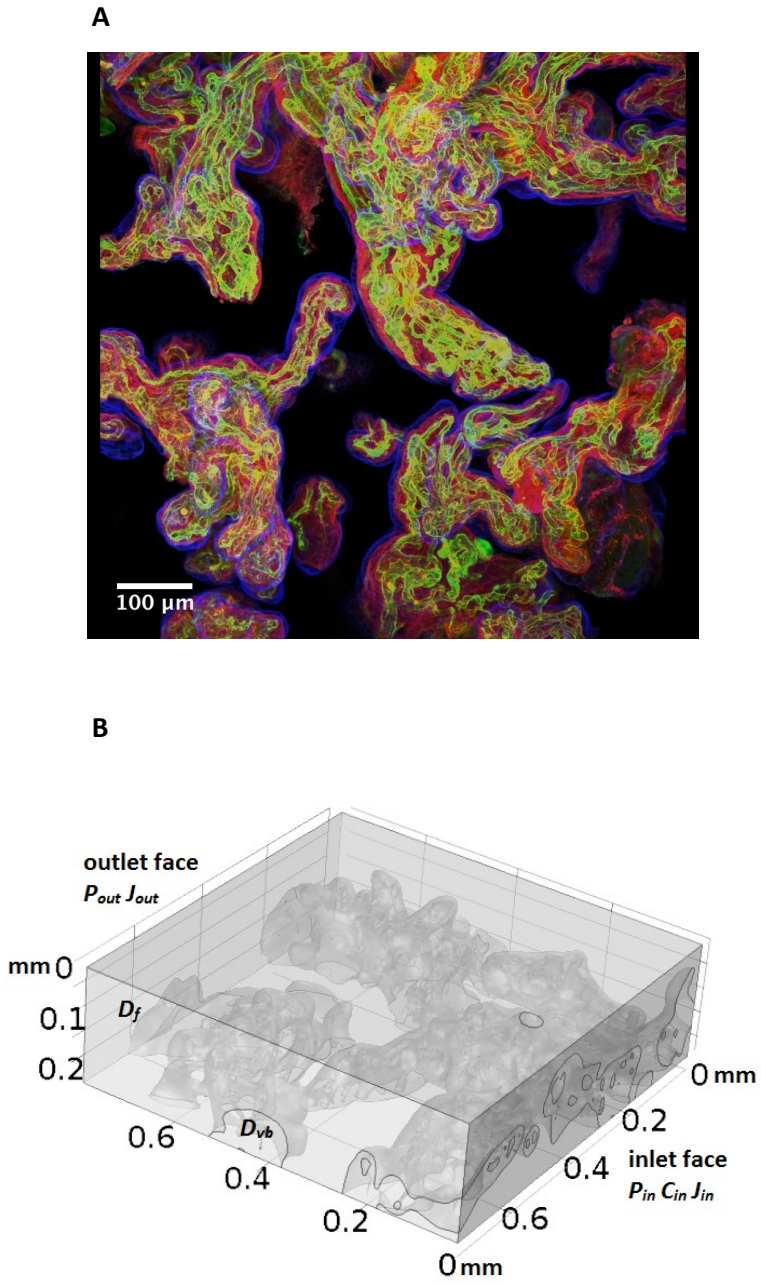

Figure 8.1. *Examples of confocal imaging and 3D placental reconstruction*

(A) Confocal image with tissue-specific labelling of the three villous structures. Blue for the syncytiotrophoblast, red for the stroma and green for the fetal vessel endothelium. (B) Sample showing the 3 domains considered in this study: intervillous space, villous barrier and fetal capillaries (all dimensions in mm). Pressure and concentration boundary conditions were prescribed for an inflow/inlet face. The outflow/outlet surface is the opposite face of the rectangular sample. P_{in}, P_{out}, are the applied pressure, with $P_{in} > P_{out}$. C_{in} is the inlet concentration. J_{in}, J_{out}, are the solute fluxes. D_f, D_{vb}, are the diffusivities in the intervillous space and villous barrier, respectively.

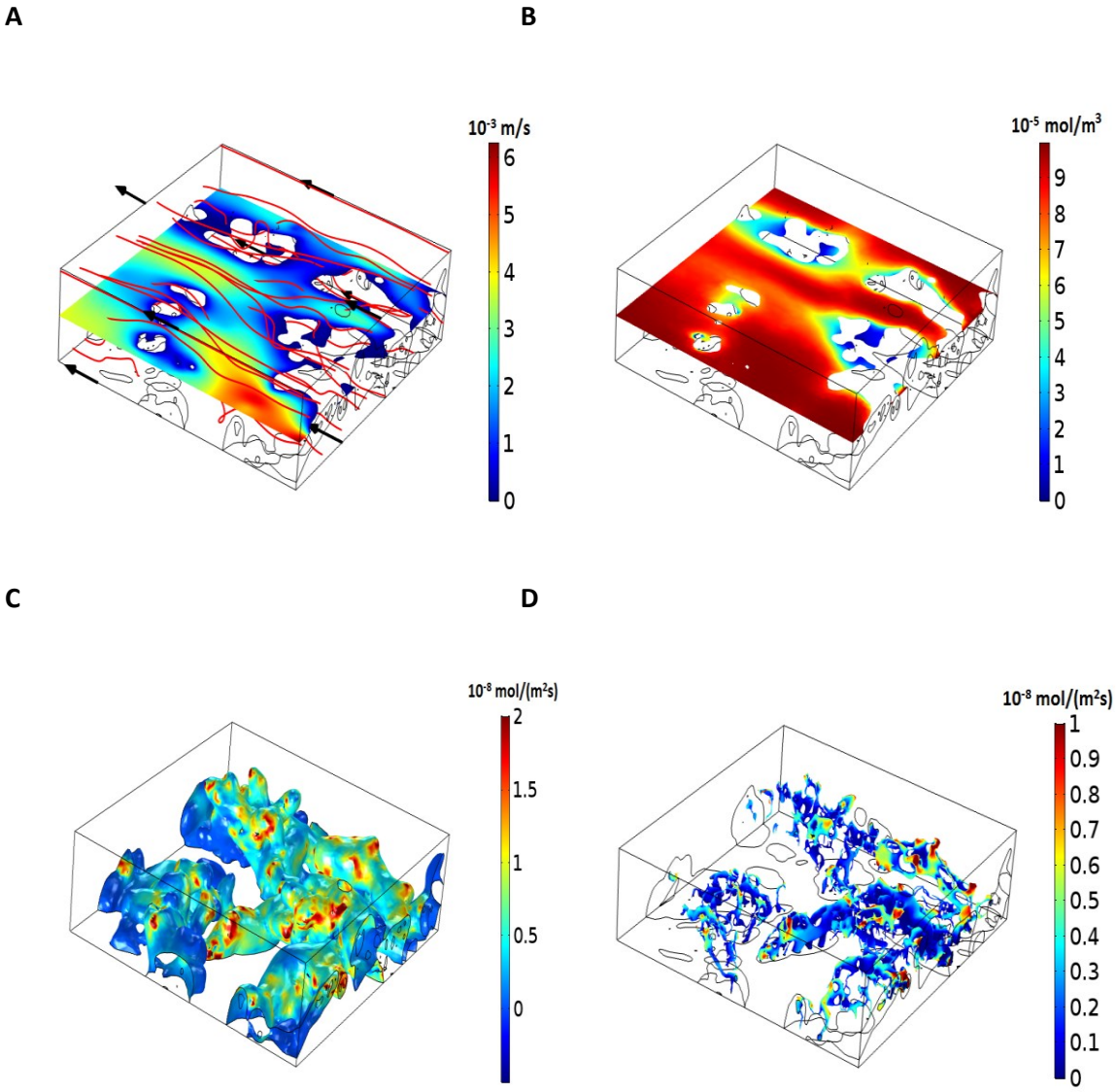

Figure 8.2. *Example of 3D simulation results modelling flow and solute transport. Shades of red represent higher values of units, shades of blue represent lower values of units. (A) Maternal blood absolute velocity field in the intervillous space (m/s) on a plane in the longitudinal direction and red streamlines depicting the main flow routes (flow direction indicated by black arrows). (B) Corresponding concentration distribution on the same plane in the longitudinal direction (mol/m^3). Blue zones correspond to depleted regions. (C) Solute flux through the villous barrier (mol/(m^{2}s)). (D) Solute flux into the fetal capillaries (mol/(m^{2}s)).*

8.3.1 Simulation of physiological conditions

The permeability and uptake values under physiological conditions (ΔP = 2.9 Pa) were reported in Table 8.1. The average hydraulic permeability of the samples was $\kappa = 1.62 \pm 1.35 \times 10^{-9} m^2$. The average total uptake of the samples was $q = 1.98 \pm 0.83 \times 10^{-15}$ mol/s. Permeability and uptake produced similar results when simulations were repeated in different directions (i.e. along the other sample dimension of 0.78 mm: $\kappa = 1.33 \pm 1.10 \times 10^{-9} m^2$, $q = 1.91 \pm 0.67 \times 10^{-15}$ mol/s). Villous volume fractions and villous barrier outer surface showed an inversely proportional trend with permeability (r = -0.68 and r = -0.69 respectively), reflecting the fact that less dense samples have lower resistance to fluid flow. Surprisingly, uptake q was found to be independent from permeability (r = 0.01), despite the lower villous surface area available for uptake in the less dense samples. To investigate this further, also the uptake efficiency of the tissue was evaluated by calculating the uptake per unit of villous volume or surface area. Uptake per unit of villous volume displayed a weak correlation (r = 0.22) with permeability, while uptake per unit of villous outer surface and fetal capillary surface displayed an increasing trend with permeability (r = 0.47 and r = 0.52, respectively). The average relative uptake of the samples was 22 ± 19 % (N = 6), i.e. on average 22% of the solutes entering the sample volume was taken up by the placental structure in the steady state. Thus, the estimate for macroscale uptake from Eq. 8.7, was α_{tot} = 0.98, i.e. on average around 98% of the solute entering the cotyledon is taken up by the placental villi.

Table 8.1. Physiological condition simulation results.

Stack number	Villi volume, % of total volume	Villi barrier surface (mm^2)	Capillaries surface (mm^2)	Permeability κ (10^{-10} m^2)	Uptake q (10^{-15} mol/s)	Relative uptake %
1	22	1.35	0.76	20.5	2.77	50
2	25	1.56	0.24	18.6	1.44	4
3	22	0.89	0.42	39.7	1.56	3
4	31	2.06	0.76	6.5	1.97	18
5	49	1.34	0.73	1.5	0.98	38
6	23	1.46	1.06	10.1	3.15	17

8.3.2 Effect of maternal blood flow rate

Simulations changing the intervillous space pressures generated proportional changes in velocities, as would be expected for Stokes flow. Similarly, permeability did not change with pressure. For pressures higher than physiological the simulations repeated with the full Navier-Stokes equation did not change the results. Absolute uptake *q* increased with the pressure and was observed to level off for very high pressures (Fig. 8.3A). On the contrary, relative uptake showed that the percentage of solute input transferred to the fetus decreased for higher pressure (Fig. 8.3B).

8.3.3 Simulation without maternal blood flow

Simulating the villous barrier alone without modelling the maternal flow resulted in an averaged villous uptake of $4.86 \pm 2.57 \times 10^{-15}$mol/s, which represents 2.45 times higher flux through the villous barrier compared to the simulations including maternal flow.

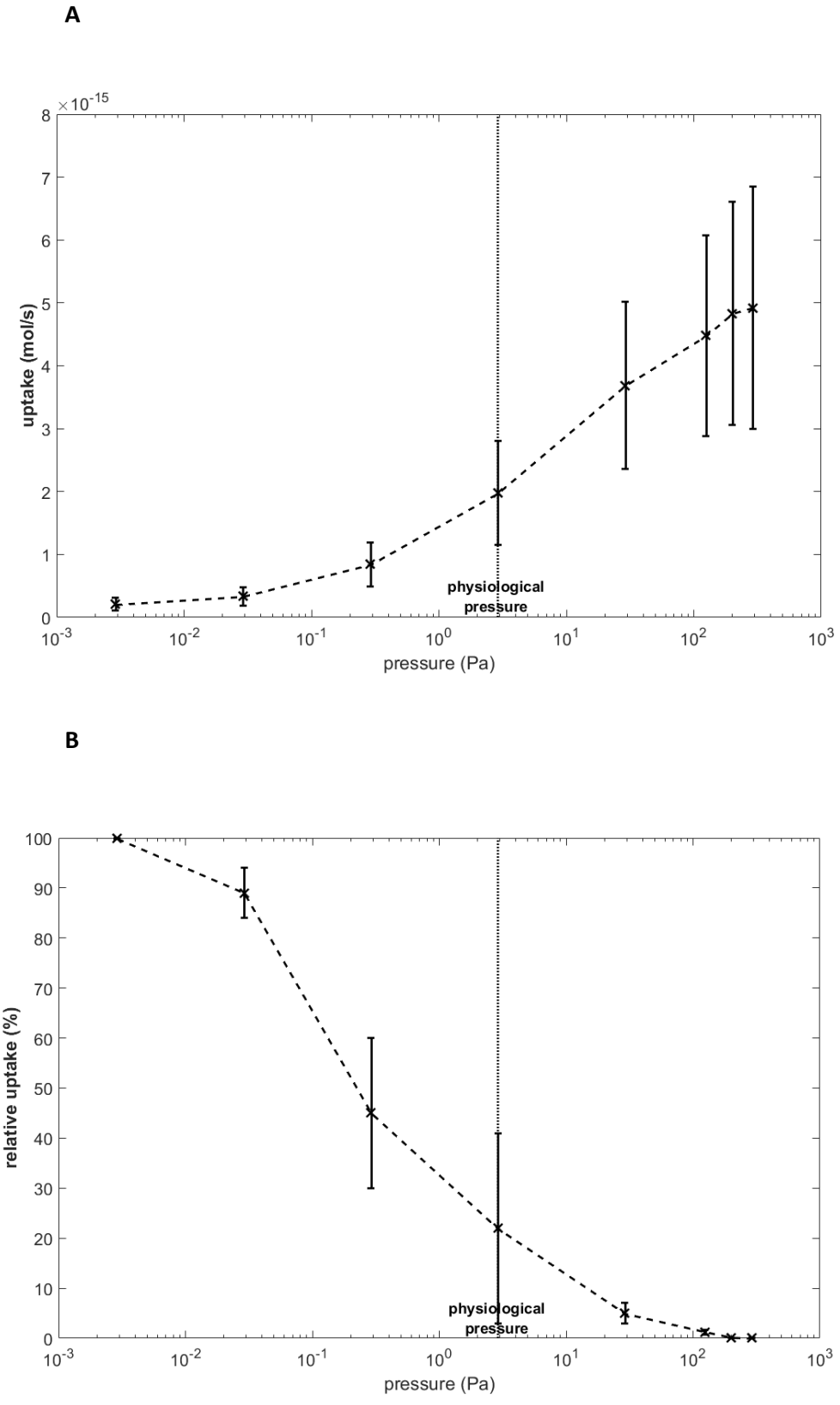

Figure 8.3. *Uptake as a function of inlet pressure*

(***A***) *Absolute uptake of solute into the placental structure q (mol/s).* (***B***) *Relative uptake of solute into the placental structure as the ratio of the uptake q and the inlet flux expressed as a percentage. The vertical dashed line represented the value corresponding to the physiological pressure gradient in the intervillous space. Mean ± SD (N = 6).*

8.3.4 Simulation of larger structures

An example simulation result under physiological conditions for a 1.55 x 1.55 x 0.41 mm sample is reported in Fig. 8.4. Qualitatively the same results found for the smaller volume samples appear to be repeated here, i.e. the protruding villi most exposed to the flow displayed higher flux capacities and similar zones of relative solute depletion were found. Permeability and relative uptake were also in the same range as for the smaller samples.

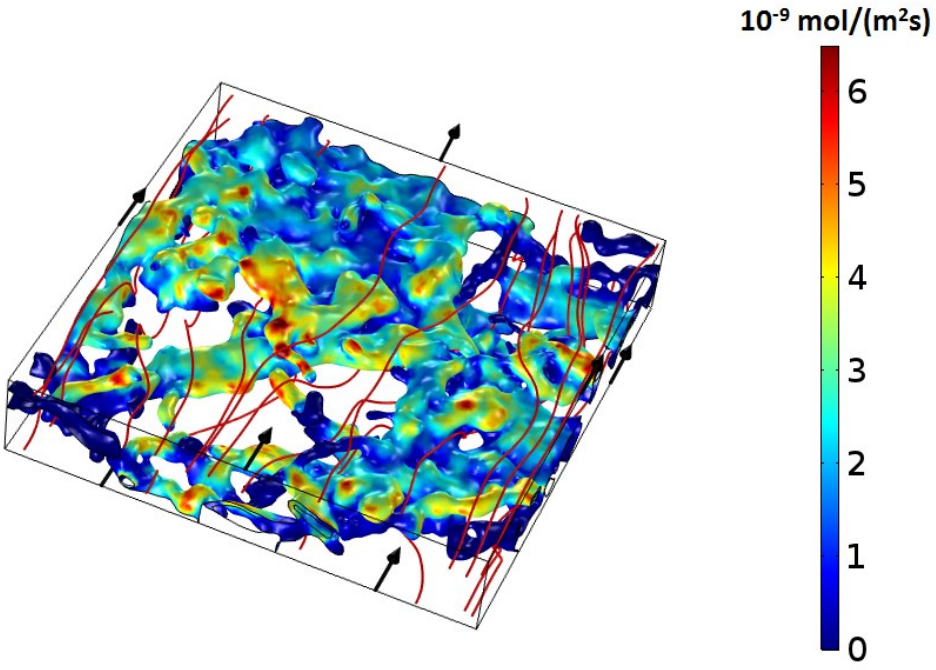

Figure 8.4. *Example simulation of a larger sample.*
Sample with dimension 1.55 x 1.55 x 0.41 mm (height x width x depth). Maternal flow streamlines are represented by red lines (direction given by black arrows). Solute flux per unit of area through the villous barrier is mapped with colours corresponding to high (red) and low (blue) flux intensity, respectively.

8.4 Discussion

This study highlights the importance of the local maternal flow conditions in the placental microstructure for solute transfer to the fetus. By adopting a 3D image based approach this allowed us to model both the detailed flow environment as well as the transport and distribution of solute in the intervillous space. This approach complements previous studies that have assumed uniform maternal concentrations. Testing with uniform maternal concentrations instead of modelling intervillous flow resulted in around 2.5-fold higher uptake and would thus overestimate transfer under physiological flow conditions. This is further illustrated by the fact that only at very high flow rates simulations with or without flow converged to the same maximum uptake values since intervillous concentrations become uniform (Fig. 8.3A).

Flow simulations under physiological conditions resulted in an average blood velocity of 0.1 cm/s in the intervillous space, which is in accordance with previous estimates [90, 97]. Notably, the distribution of solutes in the intervillous space revealed areas of lower concentrations at steady state (Fig. 8.2B). This indicated that the villous bulk may hinder flow resulting in more stagnant regions, while the extended villi may be more exposed and favour transfer. Indeed, by studying the uptake capacity of the villous barrier, the extended terminal parts of the villi displayed a larger uptake capacity (Fig. 8.2C), which would likely be due to a combination of the effects of reduced villous barrier thickness and increased exposure of these villi to the flow. Previous studies have investigated the role of barrier thickness and fetal capillary density [92, 93], but neglected the local effects of maternal flow. Interestingly, the placental transfer was found to be relatively constant for samples with widely varying permeability. The reason for this was that less dense microvillous structures had a lower surface area available for uptake, but this was compensated by increased flow due to their higher permeability. Indeed, less dense samples displayed increased efficiency with higher uptake per unit of villous area. This indicates that local flow exposure and the occurrence of depleted regions play an important role in the overall efficiency of placental transfer. Uptake increased with pressure difference and only levelled off at flow rates well above physiological to a constant level determined by the resistance of the villous barrier (Fig. 8.3A). Thus the maternal flow rate was the main determinant of transfer, in accordance with the literature [51]. Note that while for higher flow rates the absolute uptake increased, the overall efficiency of uptake would be reduced, i.e. the relative uptake decreased (Fig. 8.3B) since the inflow of solutes was so fast that only a smaller fraction could be absorbed by the villi.

Maternal blood flow was assumed to be in in the Stokes regime. The Reynolds number for the samples based on a maximum sample dimension of 0.76 mm is 0.26. Repeating with the full Navier-Stokes equations for the higher flow rates did not change the results. Model parameters were based on oxygen due its small size and diffusive nature as well as its biological importance. However,

haemoglobin binding kinetics were not considered, so results should be considered representative for a generic small solute. Only diffusive transport through the villous barrier was modelled, representing solutes with high membrane permeability. However, by incorporating membrane transporter behaviour (*e.g.* facilitated diffusion), the model could be applied to a wide range of solutes, such as amino acids and fatty acids [47, 169, 190].

The choice to proceed by first choosing the imaging resolution and then chose the coarseness of the mesh was the only method that provided a convergence to the numerical solution. In fact, without decreasing the imaging resolution down to a factor of 5, the imaging and segmentation analysis was impracticable. Nonetheless, getting a lower imaging resolution a villi may become less representative (e.g. blocky) and that would affect the local flow. Thus, by varying the imaging resolution and mesh coarseness within the model simulation, they did not change the permeability (Appendix B Fig.B1, Table B.1) and only had a reduction effect on uptake (Appendix B Fig.B2, Table B.1). In addition, varying the flow direction did not change the results, overall confirming the robustness of the overall image based modelling approach.

For large pressure differences, concentrations in the intervillous space become uniform and it was found this affected the accuracy of the calculated uptake flux when based on external concentrations, therefore uptake was calculated based on the concentration gradient within the villous barrier at all times.

Samples displayed considerable variability (Table 8.1). Modelling larger representative volume sizes would reduce the inter-sample variability and reduce the effect of boundary conditions, although this is not expected to change the overall results (Fig. 8.4).

Importantly, fetal capillaries were treated as a perfect sink, i.e. kept at zero concentration, which was a first practical assumption that allowed us to estimate the efficiency of the transfer in terms of the maximum possible fluxes across the placental barrier. However, in reality, this represents an over-estimation of the transfer and could be solved by modelling specifically the fetal placental blood flow [94-96]. Future work could also include the mechanical movement of the villi in the intervillous space, which may adapt and change their positions with the flow rate intensity and direction.

The model could be applied to compare normal and altered pregnancies, which may have different transfer efficiencies related both to changes in morphological structures and flow patterns. For example, in preeclampsia or intra uterine growth restriction (IUGR) the pressure in the intervillous space was estimated to be 5 to 10-fold higher [91, 97], and diabetic placentas display distinct differences in structure [191, 192].

In conclusion, modelling placental solute transfer based on 3D imaging of the placental morphology provides a quantitative and diagnostic platform to assess placental solute transfer, which will

contribute significantly to our understanding of the impact of placental microstructure in health and disease.

Chapter 9: Discussion

In this thesis, a range of distinct but interrelated modelling approaches has been proposed for the transfer of biological relevant substances between the mother and the fetus across the placenta. Modelling provided a powerful tool to enhance the understanding of the placental system, to predict and interpret experimental results, and has the potential to provide a diagnostic platform in the future.

With the exception of Chapter 8, all models developed as part of this thesis employed the compartmental modelling approach. Compartmental modelling has an excellent trade-off between complexity and predictive power and works well for those systems where the biological spaces can be considered well-mixed [105]. In addition, compartmental modelling is able to provide a prediction of those biological pools that are inaccessible, i.e. those compartments that cannot be directly measured experimentally. For instance, in the placental transfer of fatty acids, the syncytiotrophoblast concentration over time is inferred from the modelling.

One of the main results obtained using compartmental analysis, as reported in this thesis and published [109, 110, 190], was that placental metabolism was found to be a key determinant of transfer. This represents a novel view of placental transfer since the study of placental transfer has mostly focussed on the membrane transporters [108] or blood flows [185]. By the term metabolism in this thesis, we meant the set of processes taking place in the placental tissue that do not directly participate in the transfer. For example, fatty acids undergo irreversible (e.g. oxidation) and reversible pathways (e.g. esterification); amino acids form protein; cortisol is inactivated by conversion into cortisone. From these findings, it can be concluded that placental metabolism may play an important role in buffering the release of nutrients to the fetal circulation (Fig. 9.1). In accordance with this, in the mass balance calculations, an important fraction of the labelled input into the system was found either missing or present in the tissue at the end of the experiment. In addition, fetal concentrations were found to be low and constant over time, even if maternal inputs were much higher and presented abrupt changes.

Overall, compartmental modelling is an effective computational method to investigate biological problems, however, the well-mixed assumption may not always be true and may need to be revisited depending on the physiological question under consideration. For example, when the local flow conditions in the intervillous space are thought to be important, the geometry of the placental structure should be considered [185]. In particular, this could be the case for small solutes that are transferred by simple diffusion rather than membrane transporters, e.g. gases such as anaesthetics. To address this, we proposed a computational modelling approach based on 3D imaging of the actual placental microstructures, focussing on the microvilli as the place of placental exchange

between the maternal and fetal circulations. This consisted of generating a finite element mesh based on the reconstructed geometry from 3D confocal microscopy imaging data, setting up the flow and convection-diffusion problems involved and performing the analysis. The novelty of this approach was that we explicitly modelled the nutrient transport in the maternal circulation in the intervillous space, whereas in previous studies the intervillous space was commonly assumed as homogenous, with the outer villous surface set to a certain uniform reference concentration. It was found that intervillous blood flow did not homogenously perfuse the intervillous space, leading to local differences in concentration. Thus, the efficiency of transfer was influenced by the interaction between the intervillous blood flow and the placental microstructure. Although this approach requires high efforts in terms of imaging and computational resources, it represents the state of the art in modelling the placental transfer of nutrients, leading to improved understanding of the placental structure-function relationships.

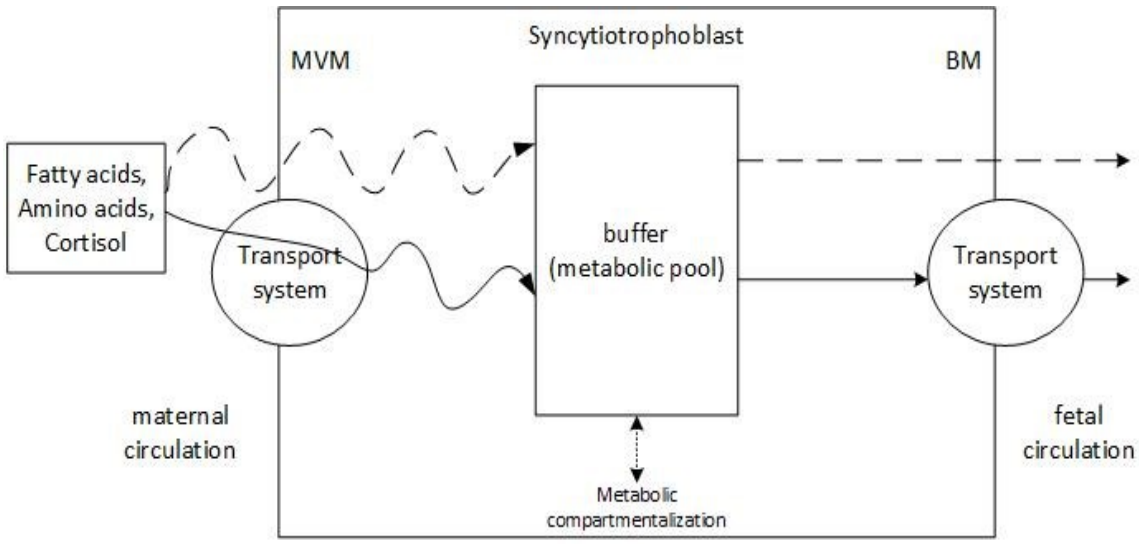

Figure 9.1. *Placental metabolism as a buffer for nutrient delivery to the fetal circulation*. *Schematic of the potential role of the metabolic pool in nutrient transfer. The metabolic pool could function as a buffer modulating uptake to achieve a more favourable delivery to the fetus in terms of release rates, overall quantities and types of compounds. On the MVM the undulating arrows represent any sort of dynamic fluctuations in uptake from the maternal circulation, while the straight arrows on the BM represent a more steady delivery to the fetus. Dashed lines represent diffusive processes.*

9.1 Recommendations for future work and applications

The first recommendation for future work is to focus on the investigation of the role of the placental metabolism. We would propose a sub-compartmentalization of what we called the metabolic pool. For example for fatty acids, the measurement of different labelled lipid classes in the placental tissue, as carried out in Chapter 5, should be included in every perfusion/*in vivo* study of fatty acid transfer from mother to fetus. In this regards, additional placental tissue timepoints, as well as measurement of those irreversible processes (e.g. CO_2 measurement for oxidation), would improve the study. These latest recommendations apply as well for amino acids and cortisol. In fact, certain metabolic pathways may be altered in specific clinical conditions and therefore influence the pregnancy outcomes. For example, altered placental tissue phospholipids metabolism was found in pregnancies of diabetic mothers [150]. Furthermore, oxidation was reduced in favour of esterification into triglycerides in pregnancies of mothers affected by gestational diabetes [151]. If a metabolic pathway will be recognized as a major control point in pregnancy for a certain nutrient (e.g. fatty acid), modelling represents a tool to evaluate the impact of the condition and inform diagnosis and treatment.

The second recommendation for future work would be to extend the model *in vivo* as introduced in Chapter 5. Depending on the available data, the current placental models could be incorporated into whole body physiological-based pharmacokinetics (PBPK) models. This would allow the study of *in vivo* nutrient transfer from administration to specific organ uptake, and therefore this type of modelling is commonly used for preclinical tests of drug kinetics [193]. This is particularly important as due to ethical considerations pregnant populations are scarcely included in such studies [162, 194] and currently detailed modelling of the placenta is missing. Including the models presented in this thesis into PBPK models would thus represent an important step forward in resolving these issues (Fig. 9.2).

A third recommendation is to improve the 3D modelling approach by extending the size and number of placental samples to further capture biological variability. In addition, a range of different solute transport mechanisms can be included (e.g. facilitated transport). Reducing the computational effort will be important though and for this purpose, tissue staining, image analysis and Finite Element Analysis should be further optimised.

The PBPK model has the potential to be implementable on PC or laptop in the clinic. Clinicians can measure clinical parameters, e.g. *in vivo* concentrations and ciculation flows, and then enter this information into the model to potentially diagnose whether the efficiency of solute transfer to the fetus is normal or at risk of being abnormal.

Overall, the present modelling approaches have been designed to be as open as possible to include other substances such as drugs, pathogen or pollutants. The 3D microstructural models also have

the clear potential to be incorporated into multi-scale models to represent transfer for the placenta as a whole. Additionally, lower scale mechanisms can be implemented into these models, such as for example specific kinetics associated with different membrane transport mechanisms.

The visionary objective of this study was to create a range of models as an integrated part in the realisation of a "virtual" placenta. Ultimately, this could even lead to the concept of an artificial placenta to support difficult pregnancies. It is worth to reminding ourselves that not only the baby but also the mother could suffer from pregnancy complications. Realising this vision will have to have the full support of experimentalists and clinicians; because good model outcomes are the results of good modelling and good data.

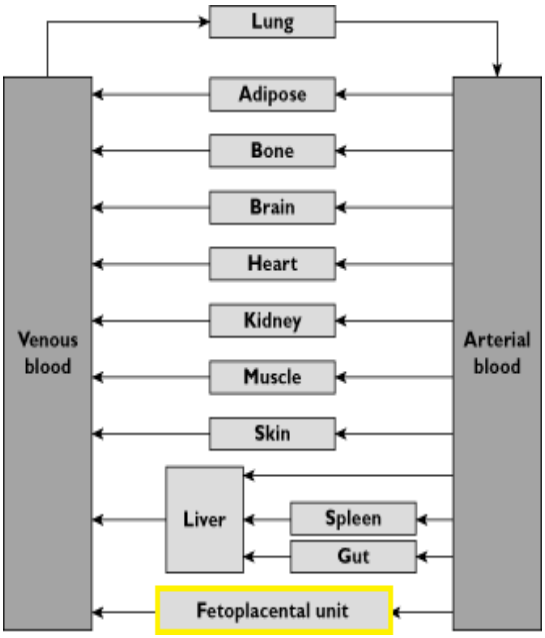

Figure 9.2. *Example schematic for incorporating the current placental model into whole body pharmacokinetic (PBPK) models*.

Schematic of a whole-body physiological model, adapted from commonly employed pharmacokinetic models. The model input is either an intravenous injection (IV dose) or oral dosage. The models discussed in this thesis can be included to extend the generic fetoplacental unit in the schematic, for example with respect to the transfer of fatty acids. Image modified from [162].

Appendix A *In vivo* fatty acid modelling transfer in obese mothers

Clinical and modelling methods are described in Section 5.2, and repeated for a group of 10 obese mothers chosen with BMI > 25 kg/m^2. The clinical parameters are reported below (Table A. 1), as well as the data at birth and modelling results (Table A. 2, Table A. 3) in comparison with the lean group already presented in the main text of Chapter 5. Clinical parameters such as placental weight and flow rates were in general increased for obese subjects. Fatty acid measurements were similar to the lean group when considered at time zero (birth). Comparing the set of estimated model parameters between the lean and obese "average subject" showed similar results. Following the same lines as in the discussion of Chapter 5, the OA, SA and PA results could be estimated adequately with a single set of parameters, while LA and DHA raised similar issues. For OA, SA and PA the obese group showed similar transfer predictions as the lean group, while the lower predicted transfer for LA and DHA in the obese group would need to be confirmed. In addition, the different maternal input scenarios were tested for the obese mothers, which have been found to have higher TG levels in their blood than normal weight mothers [195]. However, Case 1 (input as NEFA + TG + PL + CE) and Case 2 (input as NEFA + TG) produced similar results as found for lean subjects. Statistical assessment between the two groups must be done as part of future work, however, this was presently not possible using the model since some subjects were heavily affected by measurement errors, for example displaying a reversed gradient between umbilical cord artery and vein concentrations, implying uptake from the fetus.

We speculate that any differences in transfer of OA, SA and PA from mother to fetus between lean and obese mothers [196], this may reside in differences in clinical parameters (e.g. higher placenta weight and flow rates) rather than the intrinsic membrane transfer behaviour as represented by the rate constants *k* in the model. Hence, we suggest a wider population study for assessing such factors.

Table A. 1. Parameter used for modelling the lean and obese subjects *in vivo*.

N = 10, Values as mean ± SD

Parameter	Lean Value	Obese Value
Maternal weight	74.6 ± 6.3 Kg	93.6 ± 14 Kg
NEFA oral intake	0.5 or 0.1 mg/kg body weight	0.5 or 0.1 mg/kg body weight
Maternal haematocrit	0.331 ± 0.3	0.345 ± 4.3
Uterine artery blood flow	541 ml/min [161]	598 ml/min [161]
Uterine artery plasma flow	362 ml/min	392 ml/min
Placenta weight	0.61 ± 0.12 kg	0.75 ± 0.1 Kg
Fetal weight	3.24 ± 0.4 Kg	3.51 ± 0.5 Kg
Fetal haematocrit	0.48 ± 0.03	0.45 ± 0.03
Umbilical vein blood flow	347 [164]	376 [164]
Umbilical vein plasma flow	180 ml/min	208 ml/min
Fetal blood volume	0.34 l	0.37 L
Fetal plasma volume	0.18 l [165]	0.21 [165]

Table A. 2. Lean and Obese mothers: Comparison of estimated model parameter for OA, PA, SA.

Results for Case 1 (input as TG + NEFA + PL + CE).

Model parameters	**OA**		**PA**		**SA**	
	Lean	**Obese**	**Lean**	**Obese**	**Lean**	**Obese**
k_{uptake} (ml/min)	4.2	5.1	4.2	5.1	4.2	5.1
$k_{delivery}$ (ml/min)	7.5	9.2	7.5	9.2	7.5	9.2
$k_{fetaltissue}$ (ml/min)	163	219	163	219	163	219
Predicted total fetal tissue metabolism-accumulation (output, µmol)	4.96	5.49	2.28	2.06	0.13	0.13
Experimental amounts*	**OA**		**PA**		**SA**	
	Lean	**Obese**	**Lean**	**Obese**	**Lean**	**Obese**
given to mother (µmol)	132	165	145l	182l	131l	164l
Total maternal delivery to the placenta (input, µmol)	473	465	253	210	25	23l
in placental tissue at birth (µmol)	0.45	0.52	0.87	1.04	0.38	0.46
in fetal plasma at birth (µmol)	0.0065	0.0061	0.0112	0.0126	0.0026	0.0035
estimated placental transfer[$]	**1.05%**	**1.18%**	**0.91%**	**0.98%**	**0.53%**	**0.57%**

*Calculated from data and using assumptions outlined in Table A. 1 (e.g. fetal plasma volume).

[$]Predicted fetal metabolism-accumulation as a fraction of total maternal delivery to placenta

Table A. 3. Lean and Obese mothers: Comparison of estimated model parameter for LA, DHA. Results for Case 1 (input as TG + NEFA + PL + CE).

Model parameters	**LA**		**DHA**	
	Lean	**Obese**	**Lean**	**Obese**
k_{uptake} (ml/min)	0.97	0.96	0.97	0.96
$k_{delivery}$ (ml/min)	0.95	0.81	0.95	0.81
$k_{fetaltissue}$ (ml/min)	20.5	20.6	20.5	20.6
Predicted total fetal tissue metabolism/accumulation (output, µmol)	0.61	0.49	0.08	0.06
Experimental amounts*	**OA**		**PA**	
	Lean	**Obese**	**Lean**	**Obese**
given to mother (µmol)	133l	167	23l	29
Total maternal delivery to the placenta (input, µmol)	133	167l	81	77l
in placental tissue at birth (µmol)	1.02	1.28l	0.23	0.26l
in fetal plasma at birth (µmol)	0.0133	0.0146	0.0020	0.0015
estimated placental transfer[$]	**0.089%**	**0.064%**	**0.095%**	**0.071%**

*Calculated from data and using assumptions outlined in Table A. 1 (e.g. fetal plasma volume).

[$]Predicted fetal metabolism-accumulation as a fraction of total maternal delivery to placenta

Appendix B Impact of imaging and mesh resolutions on modelling of nutrient transfer based on 3D imaging of the human placental microstructure

Assessments about the impact of imaging resolution and mesh coarseness were carried out taking six small placental samples (0.2 x 0.2 x 0.2 mm, length x width x height) randomly and following the protocol for reconstruction stated in methods of Chapter 8. Sensitivity was tasted against permeability and uptake, which are the metric for transfer described in Chapter 8.

Imaging data sensitivity analysis

The image resolution sensitivity had not significant impact on the permeability estimate (Fig. B. 1), while it underpredicts the uptake (-15% for 5µm resolution) (Fig. B. 2). The computational time was reduced of -90% for 5µm resolution.

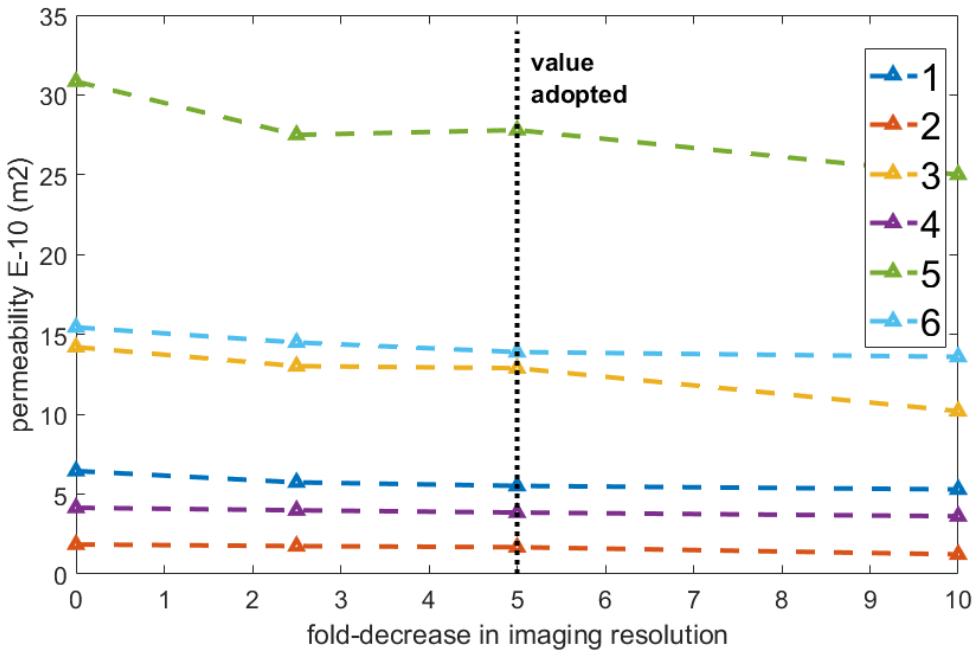

Figure B. 1. *3D Imaging resolution vs. permeability.*

Each placental sample permeability κ (m^2) was studied as a function of the imaging resolution from which it was reconstructed. Moving from left to right the resolution decreased (0 = full resolution). Each colour was a placental sample and each triangle was a sample test result (values interpolated by dashed lines to show a trend). Black dashed vertical line was the imaging resolution chosen for the study.

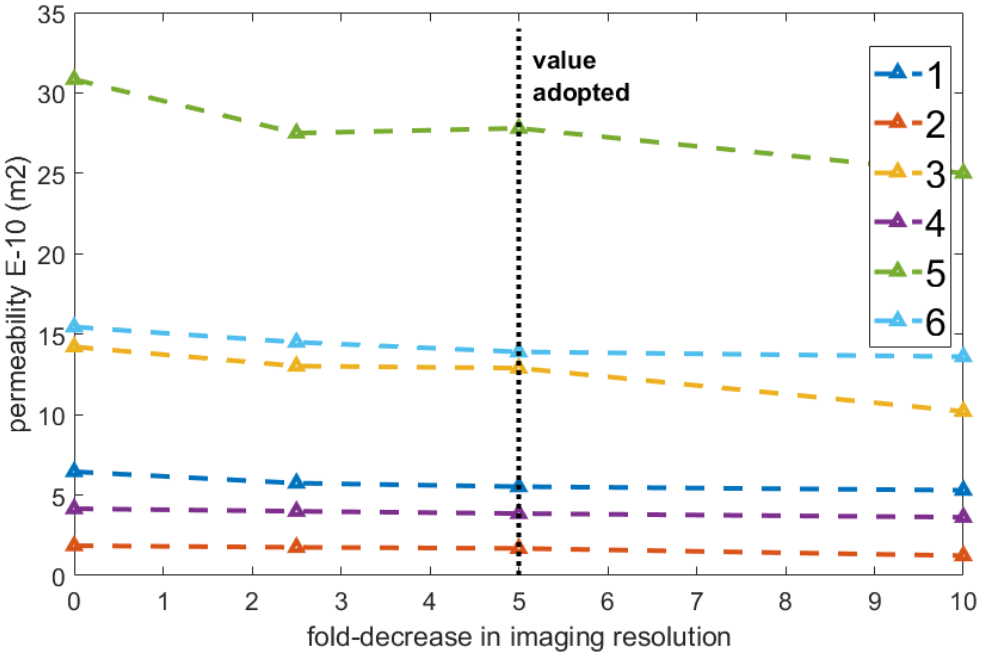

Figure B. 2. *3D Imaging resolution vs. uptake*.

Each placental sample uptake q (mol/s) was studied as a function of the imaging resolution from which it was reconstructed. Moving from left to right the resolution decreased (0 = full resolution). Each colour was a placental sample and each triangle was a sample test result (values interpolated by dashed lines to show a trend). Black dashed vertical line was the imaging resolution chosen for the study.

Mesh sensitivity analysis

Mesh coarseness sensitivity had not significant impact on the permeability estimate while it over-predicts the uptake (+18% for -50 parameter). The computational time was reduced of -78% for -50 parameter (Table B. 1). Note that, without reduction of the imaging resolution, the simulation did not converge. After establishing that a resolution decrease was necessary we studied the coarseness impact.

Table B. 1. 3D imaging study *in vivo* results vs. mesh resolutions.

Mesh coarseness (Simpleware parameter)	*Number of Tetrahedral*	*Permeability (m^2)*	*Uptake (mol/s)*	*Computational time (min)*
-50 (value chosen)	***107e3***	***5.52e-10***	***0.78e-15***	***55***
-25	*143e3*	*5.57e-10*	*0.70e-15*	*90*
0 (not refined)	*544e3*	*5.57e-10*	*0.65e-15*	*240*

Bibliography

[1] G. Desoye, M. Gauster, and C. Wadsack, "Placental transport in pregnancy pathologies," *The American Journal of Clinical Nutrition,* vol. 94, no. 6 Suppl, pp. 1896S-1902S, 2011.

[2] F. J. Korteweg *et al.*, "Diverse placental pathologies as the main causes of fetal death," *Obstetrics & Gynecology,* vol. 114, no. 4, pp. 809-817, 2009.

[3] E. Larqué *et al.*, "Placental fatty acid transfer: a key factor in fetal growth," *Annals of Nutrition and Metabolism,* vol. 64, no. 3-4, pp. 247-253, 2014.

[4] I. A. Arnoldussen *et al.*, "Early intake of long chain polyunsaturated fatty acids preserve brain structure and function in diet induced obesity," *The Journal of Nutritional Biochemistry,* 2016.

[5] P. Haggarty, "Fatty acid supply to the human fetus," *Annual Review of Nutrition,* vol. 30, pp. 237-255, 2010.

[6] E. Larqué, A. Gil-Sánchez, M. T. Prieto-Sánchez, and B. Koletzko, "Omega 3 fatty acids, gestation and pregnancy outcomes," *British Journal of Nutrition,* vol. 107, no. S2, pp. S77-S84, 2012.

[7] C. P. Sibley *et al.*, "Placental phenotypes of intrauterine growth," *Pediatric Research,* vol. 58, no. 5, pp. 827-832, 2005.

[8] C. P. Sibley, P. Brownbill, M. Dilworth, and J. D. Glazier, "Review: adaptation in placental nutrient supply to meet fetal growth demand: implications for programming," *Placenta,* vol. 31, pp. S70-S74, 2010.

[9] M. Johansson, L. Karlsson, M. Wennergren, T. Jansson, and T. Powell, "Activity and protein expression of Na+/K+ ATPase are reduced in microvillous syncytiotrophoblast plasma membranes isolated from pregnancies complicated by intrauterine growth restriction," *The Journal of Clinical Endocrinology & Metabolism,* vol. 88, no. 6, pp. 2831-2837, 2003.

[10] M. Aufdenblatten *et al.*, "Prematurity is related to high placental cortisol in preeclampsia," *Pediatric research,* vol. 65, no. 2, pp. 198-202, 2009.

[11] A. S. Serov, C. Salafia, D. S. Grebenkov, and M. Filoche, "The role of morphology in mathematical models of placental gas exchange," *Journal of Applied Physiology,* p. jap. 00543.2015, 2015.

[12] R. Berger and Y. Garnier, "Pathophysiology of perinatal brain damage," *Brain Research Reviews,* vol. 30, no. 2, pp. 107-134, 1999.

[13] K. B. Benirschke, G J.; Baergen, R N, Springer, Ed. *Pathology of the Human Placenta*. Springer, 2006, p. 941.

[14] J. Kingdom, B. Huppertz, G. Seaward, and P. Kaufmann, "Development of the placental villous tree and its consequences for fetal growth," *European Journal of Obstetrics & Gynecology and Reproductive Biology,* vol. 92, no. 1, pp. 35-43, 2000.

[15] P. Kaufmann and I. Scheffen, "Placental development," *Fetal and neonatal physiology,* vol. 1, pp. 59-70, 1998.

[16] G. J. Van der Vusse, J. F. Glatz, F. A. Van Nieuwenhoven, R. S. Reneman, and J. B. Bassingthwaighte, "Transport of long-chain fatty acids across the muscular endothelium," in *Skeletal Muscle Metabolism in Exercise and Diabetes*: Springer, 1998, pp. 181-191.

[17] D. Elad, R. Levkovitz, A. J. Jaffa, G. Desoye, and M. Hod, "Have we neglected the role of fetal endothelium in transplacental transport?," *Traffic,* vol. 15, no. 1, pp. 122-126, 2014.

[18] P. Haggarty, "Placental regulation of fatty acid delivery and its effect on fetal growth—a review," *Placenta,* vol. 23, pp. S28-S38, 2002.

[19] S. Lager and T. L. Powell, "Regulation of nutrient transport across the placenta," *Journal of Pregnancy,* vol. 2012, 2012.

[20] N. H. Jones, T. L. Powell, and T. Jansson, "Regulation of placental nutrient transport - a review," *Placenta,* vol. 28, pp. 763-74, 1984.

[21] F. Gaccioli, S. Lager, T. Powell, and T. Jansson, "Placental transport in response to altered maternal nutrition," *Journal of Developmental Origins of Health and Disease,* vol. 4, no. 02, pp. 101-115, 2013.

[22] D. Edwards, C. Jones, C. Sibley, and D. Nelson, "Paracellular permeability pathways in the human placenta: a quantitative and morphological study of maternal-fetal transfer of horseradish peroxidase," *Placenta,* vol. 14, no. 1, pp. 63-73, 1993.

[23] G. J. Burton, A. L. Fowden, and K. L. Thornburg, "Placental Origins of Chronic Disease," *Physiological Reviews,* vol. 96, no. 4, pp. 1509-1565, 2016.

[24] G. Nelson, *Dietary fatty acids and lipid metabolism*. NY: Dekker Inc, 1985.

[25] E. Larqué *et al.*, "Placental transfer of fatty acids and fetal implications," *The American Journal of Clinical Nutrition,* vol. 94, no. 6 Suppl, pp. 1908S-1913S, 2011.

[26] L. Sherwood, *Fundamentals of physiology: a human perspective*. Cengage Learning, 2005.

[27] E. Herrera, M. A. Lasunci{\'o}n, D. Gomez-Coronado, P. Aranda, P. L{\'o}pez-Luna, and I. Maier, "Role of lipoprotein lipase activity on lipoprotein metabolism and the fate of circulating triglycerides in pregnancy," *American journal of obstetrics and gynecology,* vol. 158, no. 6, pp. 1575-1583, 1988.

[28] C. D. Fuchs *et al.*, "Absence of adipose triglyceride lipase protects from hepatic endoplasmic reticulum stress in mice," *Hepatology,* vol. 56, no. 1, pp. 270-280, 2012.

[29] M. Crawford, G. Williams, A. Hassam, and W. Whitehouse, "Essential fatty acids and fetal brain growth," *The Lancet,* vol. 307, no. 7957, pp. 452-453, 1976.

[30] A. Magnusson, I. Waterman, M. Wennergren, T. Jansson, and T. L. Powell, "Triglyceride hydrolase activities and expression of fatty acid binding proteins in the human placenta in pregnancies complicated by intrauterine growth restriction and diabetes," *Journal of Clinical Endocrinology \& Metabolism,* vol. 89, no. 9, pp. 4607-4614, 2004.

[31] J. F. Glatz, "Lipids and lipid binding proteins: A perfect match," *Prostaglandins, Leukotrienes and Essential Fatty Acids (PLEFA),* vol. 93, pp. 45-49, 2015.

[32] M. Vork, J. Glatz, and G. Van der Vusse, "Modelling intracellular fatty acid transport: possible mechanistic role of cytoplasmic fatty acid-binding protein," *Prostaglandins, Leukotrienes and Essential Fatty Acids,* vol. 57, no. 1, pp. 11-16, 1997.

[33] G. J. van der Vusse, "Albumin as fatty acid transporter," *Drug Metabolism and Pharmacokinetics,* vol. 24, no. 4, pp. 300-307, 2009.

[34] T. Arts, R. S. Reneman, J. B. Bassingthwaighte, and G. J. van der Vusse, "Modeling Fatty Acid Transfer from Artery to Cardiomyocyte," *PLoS Computational Biology,* vol. 11, no. 12, 2015.

[35] F. Kamp and J. A. Hamilton, "How fatty acids of different chain length enter and leave cells by free diffusion," *Prostaglandins, leukotrienes and essential fatty acids,* vol. 75, no. 3, pp. 149-159, 2006.

[36] J. E. Schaffer, "Fatty acid transport: the roads taken," *American Journal of Physiology-Endocrinology And Metabolism,* vol. 282, no. 2, pp. E239-E246, 2002.

[37] P. Haggarty, K. Page, D. Abramovich, J. Ashton, and D. Brown, "Long-chain polyunsaturated fatty acid transport across the perfused human placenta," *Placenta,* vol. 18, no. 8, pp. 635-642, 1997.

[38] Y. Xu, T. J. Cook, and G. T. Knipp, "Methods for investigating placental fatty acid transport," in *Placenta and Trophoblast*: Springer, 2006, pp. 265-284.

[39] A. K. Duttaroy, "Transport of fatty acids across the human placenta: a review," *Progress in Lipid Research,* vol. 48, no. 1, pp. 52-61, 2009.

[40] F. L. Hanebutt, H. Demmelmair, B. Schiessl, E. Larqu{\'e}, and B. Koletzko, "Long-chain polyunsaturated fatty acid (LC-PUFA) transfer across the placenta," *Clinical Nutrition,* vol. 27, no. 5, pp. 685-693, 2008.

[41] A. Bonen, J. J. Luiken, Y. Arumugam, J. F. Glatz, and N. N. Tandon, "Acute regulation of fatty acid uptake involves the cellular redistribution of fatty acid translocase," *Journal of Biological Chemistry,* vol. 275, no. 19, pp. 14501-14508, 2000.

[42] F. Campbell, P. Bush, J. Veerkamp, and A. Dutta-Roy, "Detection and cellular localization of plasma membrane-associated and cytoplasmic fatty acid-binding proteins in human placenta," *Placenta,* vol. 19, no. 5, pp. 409-415, 1998.

[43] G. V. Richieri, R. T. Ogata, and A. M. Kleinfeld, "Kinetics of fatty acid interactions with fatty acid binding proteins from adipocyte, heart, and intestine," *Journal of Biological Chemistry,* vol. 271, no. 19, pp. 11291-11300, 1996.

[44] S. Broer, "Adaptation of plasma membrane aminop acid transport mechanism to physiologicaldemands," *Pflugers Archiv European The Journal of Physiology,* vol. 20, no. 8, pp. 677-82, 1999.

[45] F.Verrey, "System L:heteromeric exchangers of large, neutral amino acids involved in directional transport," *Journal of Physiology,* vol. 445, no. 5, pp. 529-33, 2003.

[46] J. Cleal and R. Lewis, "The mechanisms and regulation of placental amino acid transport to the human foetus," *Journal of neuroendocrinology,* vol. 20, no. 4, pp. 419-426, 2008.

[47] N. Panitchob *et al.*, "Computational modelling of amino acid exchange and facilitated transport in placental membrane vesicles," *Journal of Theoretical Biology,* vol. 365, pp. 352-364, 2015.

[48] A. C. R. Benediktsson, C. Edwards, J. Secki, "Placental 11beta-hydroxysteroid dehydrogenase: a key regulator of fetal glucocorticoid exposure. Clinical Endocrinology " *Clinical Endocrinology,* vol. 46, pp. 161-165, 1997. .

[49] E. V. d. A. K.Yam, E. van Rossum, A. van Mullem, T. Visser, "Is transport of cortisol in liver cells carrier-mediated?," *Erasmus Journal of Medicine,* vol. 3, no. 1, 2012.

[50] R. Benediktsson, A. A. Calder, C. R. Edwards, and J. R. Seckl, "Placental 11β-hydroxysteroid dehydrogenase: a key regulator of fetal glucocorticoid exposure," *Clinical Endocrinology,* vol. 46, no. 2, pp. 161-166, 1997.

[51] J. J. Faber, "Review of flow limited transfer in the placenta," *International Journal of Obstetric Anesthesia,* vol. 4, no. 4, pp. 230-237, 1995.

[52] M. H. Friedman, "Principles and models of biological transport," ed: Springer, 2012.

[53] N. M. Gude, C. T. Roberts, B. Kalionis, and R. G. King, "Growth and function of the normal human placenta," *Thrombosis research,* vol. 114, no. 5, pp. 397-407, 2004.

[54] J. Stulc, "Placental transfer of inorganic ions and water," *Physiological reviews,* vol. 77, no. 3, pp. 805-836, 1997.

[55] G. E. Ringler and J. F. Strauss III, "In Vitro Systems for the Study of Human Placental Endocrine Function*," *Endocrine reviews,* vol. 11, no. 1, pp. 105-123, 1990.

[56] B. K. Patterson *et al.*, "Leukemia inhibitory factor inhibits HIV-1 replication and is upregulated in placentae from nontransmitting women," *The Journal of Clinical Investigation,* vol. 107, no. 3, pp. 287-294, 2001.

[57] J. Marin, R. Macias, and M. Serrano, "The hepatobiliary-like excretory function of the placenta. A review," *Placenta,* vol. 24, no. 5, pp. 431-438, 2003.

[58] M. Pasanen, "The expression and regulation of drug metabolism in human placenta," *Advanced Drug Delivery Reviews,* vol. 38, no. 1, pp. 81-97, 1999.

[59] F. Barut *et al.*, "Research Intrauterine growth restriction and placental angiogenesis," 2010.

[60] S. M. Almasry and A. K. Elfayomy, "Morphometric analysis of terminal villi and gross morphological changes in the placentae of term idiopathic intrauterine growth restriction," *Tissue and Cell,* vol. 44, no. 4, pp. 214-219, 2012.

[61] T. Mayhew, C. Ohadike, P. Baker, I. Crocker, C. Mitchell, and S. Ong, "Stereological investigation of placental morphology in pregnancies complicated by pre-eclampsia with and without intrauterine growth restriction," *Placenta,* vol. 24, no. 2, pp. 219-226, 2003.

[62] R. Lewis *et al.*, "The Placental Exposome: Placental Determinants of Fetal Adiposity and Postnatal Body Composition," *Annals of Nutrition and Metabolism,* vol. 63, no. 3, pp. 208-215, 2013.

[63] T. M. Mayhew and G. J. Burton, "Stereology and its impact on our understanding of human placental functional morphology," *Microscopy Research and Technique,* vol. 38, no. 1-2, pp. 195-205, 1997.

[64] P. Sastry, "Lipids of nervous tissue: composition and metabolism," *Progress in lipid research,* vol. 24, no. 2, pp. 69-176, 1985.

[65] L. Lauritzen, H. S. Hansen, M. H. o. r. J{\o}rgensen, and K. F. Michaelsen, "The essentiality of long chain omega-3 fatty acids in relation to development and function of the brain and retina," *Progress in lipid research,* vol. 40, no. 1, pp. 1-94, 2001.

[66] M. Neuringer, G. J. Anderson, and W. E. Connor, "The essentiality of n-3 fatty acids for the development and function of the retina and brain," *Annual review of nutrition,* vol. 8, no. 1, pp. 517-541, 1988.

[67] D. J. P. Barker *et al.*, "Relation of birth weight and childhood respiratory infection to adult lung function and death from chronic obstructive airways disease.," *BMJ,* vol. 303, pp. 671-75, 1993.

[68] D. Lane, W. J. McConathy, M. A. McCafree, and H. M, "Cord serum lipid and apolipoprotein levels in preterm infants with neonatal respiratory distress syndrome," *Metern. Fetal Neonatal Med.,* vol. 11, pp. 118-25, 2002.

[69] C. H. Fall *et al.*, "Relation of infant feeding to adult serum cholesterol concentration and death from ischaemic heart disease," *BMJ,* vol. 304, pp. 801-05, 1992.

[70] R. Uauy, D. R. Hoffman, P. Peirano, D. G. Birch, and E. E. Birch, "Essential fatty acids in visual and brain development," *Lipids,* vol. 36, no. 9, pp. 885-895, 2001.

[71] C. L. Paolini *et al.*, "Placental transport of leucine, phenylanine, glycine, and proline in intrauterine growth-restricted pregnancies," *J Clin Endocrinology,* vol. 86, pp. 5427-32, 2001.

[72] M. B. M.Aufdenblatten, L.Raio, . Dick, B. Frey, H. Schneider, D.Surbek, B.Hocher, M.Mohaupt, "Prematurity is related to high placental cortisol in Preeclampsia," *Pediatric Research,* vol. 65, no. 2, 2009.

[73] R. Lewis *et al.*, "L-serine uptake by human placental microvillous membrane vesicles," *Placenta,* vol. 28, no. 5, pp. 445-452, 2007.

[74] J. Glazier and C. Sibley, "In vitro methods for studying human placental amino acid transport: placental plasma membrane vesicles," *Methods in molecular medicine,* vol. 122, pp. 241-252, 2005.

[75] K. Page, "Perfusion of isolated human placenta," *Proceedings of the Nutrition Society,* vol. 50, no. 02, pp. 345-347, 1991.

[76] H. Schneider, "Tolerance of human placental tissue to severe hypoxia and its relevance for dual ex vivo perfusion," *Placenta,* vol. 30 Suppl A, pp. S71-6, Mar 2009.

[77] H. Schneider, "IFPA senior award lecture: Energy metabolism of human placental tissue studied by ex vivo perfusion of an isolated cotyledon," *Placenta,* Dec 23 2014.

[78] R. M. Lewis *et al.*, "Review: Modelling placental amino acid transfer - From transporters to placental function," *Placenta,* vol. 34, pp. S46-S51, MAR 2013 2013.

[79] K. A. Rejniak, H. J. Kliman, and L. J. Fauci, "A computational model of the mechanics of growth of the villous trophoblast bilayer," *Bulletin of mathematical biology,* vol. 66, no. 2, pp. 199-232, 2004.

[80] Q. Xia and C. Salafia, "Transport efficiency of the human placenta," *Journal of Coupled Systems and Multiscale Dynamics,* vol. 2, no. 1, pp. 1-8, 2014.

[81] D. M. Moorcroft, J. D. Stitzel, G. G. Duma, and S. M. Duma, "Computational model of the pregnant occupant: predicting the risk of injury in automobile crashes," *American journal of obstetrics and gynecology,* vol. 189, no. 2, pp. 540-544, 2003.

[82] H. Thoumsin, A. Albert, and J. Duvivier, "Preliminary clinical application of a mathematical model for interpreting dehydroepiandrosterone-sulfate loading test in late pregnancy," *Journal of Perinatal Medicine-Official Journal of the WAPM,* vol. 6, no. 1, pp. 32-38, 1978.

[83] F. Mac Gabhann and A. S. Popel, "Model of competitive binding of vascular endothelial growth factor and placental growth factor to VEGF receptors on endothelial cells," *American Journal of Physiology-Heart and Circulatory Physiology,* vol. 286, no. 1, pp. H153-H164, 2004.

[84] P. G. Walker, F. O. ter Kuile, T. Garske, C. Menendez, and A. C. Ghani, "Estimated risk of placental infection and low birthweight attributable to Plasmodium falciparum malaria in Africa in 2010: a modelling study," *The Lancet Global Health,* vol. 2, no. 8, pp. e460-e467, 2014.

[85] S.-p. Gong, Y.-T. Zhao, and Y.-H. Yu, "Vascular network modeling reveals significant differences in vascular morphology in growth-restricted placentas," *Reviews in Obstetrics and Gynecology,* vol. 4, no. 3-4, p. 103, 2011.

[86] J. Faber and D. F. Anderson, "Model study of placental water transfer and causes of fetal water disease in sheep," *American Journal of Physiology-Regulatory, Integrative and Comparative Physiology,* vol. 258, no. 5, pp. R1257-R1270, 1990.

[87] I. Chernyavsky, O. Jensen, and L. Leach, "A mathematical model of intervillous blood flow in the human placentone," *Placenta,* vol. 31, no. 1, pp. 44-52, 2010.

[88] A. Serov, C. Salafia, P. Brownbill, D. Grebenkov, and M. Filoche, "Optimal villi density for maximal oxygen uptake in the human placenta," *Journal of theoretical biology,* vol. 364, pp. 383-396, 2015.

[89] A. Serov, C. Salafia, M. Filoche, and D. Grebenkov, "Analytical theory of oxygen transport in the human placenta," *Journal of theoretical biology,* vol. 368, pp. 133-144, 2015.

[90] E. Lecarpentier *et al.*, "Computational Fluid Dynamic Simulations of Maternal Circulation: Wall Shear Stress in the Human Placenta and Its Biological Implications," *PloS one,* vol. 11, no. 1, p. e0147262, 2016.

[91] C. J. Roth *et al.*, "Dynamic modeling of uteroplacental blood flow in IUGR indicates vortices and elevated pressure in the intervillous space–a pilot study," *Scientific Reports,* vol. 7, 2017.

[92] J. Gill, C. Salafia, D. Grebenkov, and D. Vvedensky, "Modeling oxygen transport in human placental terminal villi," *Journal of theoretical biology,* vol. 291, pp. 33-41, 2011.

[93] C.-J. D. Mayo RP, Burton GJ, Oyen ML, "Three-dimensional modelling of human placenta terminal villi," *Placenta,* 2016.

[94] R. P. Mayo, J. Olsthoorn, D. Charnock-Jones, G. Burton, and M. Oyen, "Computational modeling of the structure-function relationship in human placental terminal villi," *Journal of Biomechanics,* vol. 49, no. 16, pp. 3780-3787, 2016.

[95] A. T. Shannon and P. Mirbod, "Three-dimensional flow patterns in the feto-placental vasculature system of the mouse placenta," *Microvascular Research,* vol. 111, pp. 88-95, 2017.

[96] P. Pearce *et al.*, "Image-Based Modeling of Blood Flow and Oxygen Transfer in Feto-Placental Capillaries," *arXiv,* 2016.

[97] G. Burton, A. Woods, E. Jauniaux, and J. Kingdom, "Rheological and physiological consequences of conversion of the maternal spiral arteries for uteroplacental blood flow during human pregnancy," *Placenta,* vol. 30, no. 6, pp. 473-482, 2009.

[98] A. Sengupta, P. Biswas, G. Jayaraman, and S. Guha, "Understanding utero-placental blood flow in normal and hypertensive pregnancy through a mathematical model," *Medical and Biological Engineering and Computing,* vol. 35, no. 3, pp. 223-230, 1997.

[99] A. D. Kaplan, A. J. Jaffa, I. E. Timor, and D. Elad, "Hemodynamic analysis of arterial blood flow in the coiled umbilical cord," *Reproductive Sciences,* vol. 17, no. 3, pp. 258-268, 2010.

[100] J. Alastruey, S. J. Sherwin, K. H. Parker, and D. D. Rubens, "Placental transfusion insult in the predisposition for SIDS: A mathematical study," *Early human development,* vol. 85, no. 7, pp. 455-459, 2009.

[101] D. Talbert and N. Sebire, "The dynamic placenta: I. Hypothetical model of a placental mechanism matching local fetal blood flow to local intervillus oxygen delivery," *Medical hypotheses,* vol. 62, no. 4, pp. 511-519, 2004.

[102] M. Beall, J. Van Den Wijngaard, M. Van Gemert, and M. Ross, "Amniotic fluid water dynamics," *Placenta,* vol. 28, no. 8, pp. 816-823, 2007.

[103] W. J. Wilbur, G. G. Power, and L. Longo, "Water exchange in the placenta: a mathematical model," *American Journal of Physiology-Regulatory, Integrative and Comparative Physiology,* vol. 235, no. 3, pp. R181-R199, 1978.

[104] N. Sebire, V. Jain, and D. Talbert, "Spiral artery associated restricted growth (SPAARG): a computer model of pathophysiology resulting from low intervillous pressure having fetal programming implications," *Pathophysiology,* vol. 11, no. 2, pp. 87-94, 2004.

[105] E. Carson and C. Cobelli, *Modeling methodology for physiology and medicine*, Second Edition ed. (Elsevier Insights). Elsevier, 2013.

[106] J. A. Jacquez, *Compartmental analysis in biology and medicine*. JSTOR, 1985.

[107] B. G. Sengers, C. P. Please, and R. M. Lewis, "Computational modelling of amino acid transfer interactions in the placenta," *Experimental physiology,* vol. 95, no. 7, pp. 829-840, 2010.

[108] N. Panitchob, R. Lewis, and B. Sengers, "Computational modelling of placental amino acid transfer as an integrated system," *Biochimica et Biophysica Acta (BBA) - Biomembranes,* vol. 1858, no. 7-A, pp. 1451-1461, 2016.

[109] S. Perazzolo, B. Hirschmugl, C. Wadsack, G. Desoye, R. Lewis, and B. Sengers, "Computational modelling of fatty acid transport in the human placenta," in *Engineering in Medicine and Biology Society (EMBC), 2015 37th Annual International Conference of the IEEE*, 2015, pp. 8054-8057: IEEE.

[110] E. M. Lofthouse *et al.*, "Phenylalanine transfer across the isolated perfused human placenta: an experimental and modelling investigation," *American Journal of Physiology-Regulatory, Integrative and Comparative Physiology,* p. ajpregu. 00405.2015, 2015.

[111] L. Hummel, T. Zimmermann, W. Schirrmeister, and H. Wagner, "Synthesis, turnover and compartment analysis of the free fatty acids in the placenta of rats," *Acta biologica et medica Germanica,* vol. 35, no. 10, pp. 1311-1316, 1976.

[112] K. Vyska *et al.*, "Fatty acid uptake in normal human myocardium.," *Circulation research,* vol. 69, no. 3, pp. 857-870, 1991.

[113] P. Eaton, M. Bernman, and D. Steinberg, "Kinetic studies of plasma Free fatty acids and tryglyceride metabolism in man," *The Journal of Clinical Investigation,* vol. 48, p. 1560, 1969.

[114] R. P. Eaton, M. Berman, and D. Steinberg, "Kinetic studies of plasma free fatty acid and triglyceride metabolism in man," *Journal of Clinical Investigation,* vol. 48, no. 8, p. 1560, 1969.

[115] J. Dancis, V. Jansen, and M. Levitz, "Transfer across perfused human placenta. IV. Effect of protein binding on free fatty acids," *Pediatric research,* vol. 10, no. 1, pp. 5-10, 1976.

[116] S. Lager, V. I. Ramirez, F. Gaccioli, B. Jang, T. Jansson, and T. L. Powell, "Protein expression of fatty acid transporter 2 is polarized to the trophoblast basal plasma membrane and increased in placentas from overweight/obese women," *Placenta,* vol. 40, pp. 60-66, 2016.

[117] P. Cunningham and L. McDermott, "Long chain PUFA transport in human term placenta," *The Journal of nutrition,* vol. 139, no. 4, pp. 636-639, 2009.

[118] J. Luiken, F. Van Nieuwenhoven, G. America, G. Van der Vusse, and J. Glatz, "Uptake and metabolism of palmitate by isolated cardiac myocytes from adult rats: involvement of sarcolemmal proteins," *Journal of Lipid Research,* vol. 38, no. 4, pp. 745-758, 1997.

[119] J. R. Araújo, A. Correia-Branco, C. Ramalho, E. Keating, and F. Martel, "Gestational diabetes mellitus decreases placental uptake of long-chain polyunsaturated fatty acids: involvement of long-chain acyl-CoA synthetase," *The Journal of nutritional biochemistry,* vol. 24, no. 10, pp. 1741-1750, 2013.

[120] N. J. Faergman and J. Knudsen, "Role of long-chain fatty acyl-CoA esters in the regulation of metabolism and in cell signalling," *Biochemical Journal,* vol. 323, no. 1, pp. 1-12, 1997.

[121] E. Larqué, H. Demmelmair, B. Berger, U. Hasbargen, and B. Koletzko, "In vivo investigation of the placental transfer of 13C-labeled fatty acids in humans," *Journal of Lipid Research,* vol. 44, no. 1, pp. 49-55, 2003.

[122] A. Pathmaperuma *et al.*, "Fatty acids alter glycerolipid metabolism and induce lipid droplet formation, syncytialisation and cytokine production in human trophoblasts with minimal glucose effect or interaction," *Placenta,* vol. 31, no. 3, pp. 230-239, 2010.

[123] P. Shekhawat, M. J. Bennett, Y. Sadovsky, D. M. Nelson, D. Rakheja, and A. W. Strauss, "Human placenta metabolizes fatty acids: implications for fetal fatty acid oxidation disorders and maternal liver diseases," *American Journal of Physiology-Endocrinology and Metabolism,* vol. 284, no. 6, pp. E1098-E1105, 2003.

[124] D. Rakheja, M. Bennett, B. Foster, R. Domiati-Saad, and B. Rogers, "Evidence for fatty acid oxidation in human placenta, and the relationship of fatty acid oxidation enzyme activities with gestational age," *Placenta,* vol. 23, no. 5, pp. 447-450, 2002.

[125] D. C. Kuhn and M. Crawford, "Placental essential fatty acid transport and prostaglandin synthesis," *Progress in lipid research,* vol. 25, pp. 345-353, 1986.

[126] P. Day, J. Cleal, E. Lofthouse, M. Hanson, and R. Lewis, "What factors determine placental glucose transfer kinetics?," *Placenta,* vol. 34, no. 10, pp. 953-958, 2013.

[127] H. L. Barrett *et al.*, "Placental lipases in pregnancies complicated by gestational diabetes mellitus (GDM)," *PloS one,* vol. 9, no. 8, p. e104826, 2014.

[128] E. Herrera and G. Desoye, "Maternal and fetal lipid metabolism under normal and gestational diabetic conditions," *Hormone molecular biology and clinical investigation,* 2015.

[129] H. Schneider and A. Huch, "Dual in vitro perfusion of an isolated lobe of human placenta: method and instrumentation," in *In vitro perfusion of human placental tissue*: Karger Publishers, 1985, pp. 40-47.

[130] V. Matyash, G. Liebisch, T. V. Kurzchalia, A. Shevchenko, and D. Schwudke, "Lipid extraction by methyl-tert-butyl ether for high-throughput lipidomics," *Journal of lipid research,* vol. 49, no. 5, pp. 1137-1146, 2008.

[131] F. L. Hanebutt, H. Demmelmair, B. Schiessl, E. Larqué, and B. Koletzko, "Long-chain polyunsaturated fatty acid (LC-PUFA) transfer across the placenta," *Clinical Nutrition,* vol. 27, no. 5, pp. 685-693, 2008.

[132] A. J. Kilbane, T. Petroff, and W. W. Weber, "Kinetics of acetyl CoA: arylamine N-acetyltransferase from rapid and slow acetylator human liver," *Drug metabolism and disposition,* vol. 19, no. 2, pp. 503-507, 1991.

[133] R. C. Boston and P. J. Moate, "A novel minimal model to describe NEFA kinetics following an intravenous glucose challenge," *American Journal of Physiology-Regulatory, Integrative and Comparative Physiology,* vol. 294, no. 4, pp. R1140-R1147, 2008.

[134] A. Pagán *et al.*, "Materno-fetal transfer of docosahexaenoic acid is impaired by gestational diabetes mellitus," *American Journal of Physiology-Endocrinology and Metabolism,* vol. 305, no. 7, pp. E826-E833, 2013.

[135] L. F. Shampine, I. Gladwell, and S. Thompson, *Solving ODEs with matlab*. Cambridge University Press, 2003.

[136] T. F. Coleman and A. Verma, "A preconditioned conjugate gradient approach to linear equality constrained minimization," *Computational Optimization and Applications,* vol. 20, no. 1, pp. 61-72, 2001.

[137] D. Sorensen, "Minimization of large {scale quadratic functions subject to an ellipsoidal constraint," *Department of Computational and Applied Mathematics,* 1994.

[138] C. B. Moler, *Numerical computing with MATLAB*. SIAM, 2004.

[139] N. Abumrad, J. Park, and C. Park, "Permeation of long-chain faty acid into adipocytes," *J Biol Chem,* vol. 14, pp. 1945-1953, 1984.

[140] P. J. Trotter, S. Y. Ho, and J. Storch, "Fatty acid uptake by Caco-2 human intestinal cells," *Journal of lipid research,* vol. 37, no. 2, pp. 336-346, 1996.

[141] E. Neufeld, D. Wilson, H. Sprecher, and P. Majerus, "High affinity esterification of eicosanoid precursor fatty acids by platelets," *Journal of Clinical Investigation,* vol. 72, no. 1, p. 214, 1983.

[142] W. Schwieterman *et al.*, "Uptake of oleate by isolated rat adipocytes is mediated by a 40-kDa plasma membrane fatty acid binding protein closely related to that in liver and gut," *Proceedings of the National Academy of Sciences,* vol. 85, no. 2, pp. 359-363, 1988.

[143] J. Storch, C. Lechene, and A. M. Kleinfeld, "Direct determination of free fatty acid transport across the adipocyte plasma membrane using quantitative fluorescence microscopy," *Journal of Biological Chemistry,* vol. 266, no. 21, pp. 13473-13476, 1991.

[144] W. Stremmel, G. Strohmeyer, and P. D. Berk, "Hepatocellular uptake of oleate is energy dependent, sodium linked, and inhibited by an antibody to a hepatocyte plasma membrane fatty acid binding protein," *Proceedings of the National Academy of Sciences,* vol. 83, no. 11, pp. 3584-3588, 1986.

[145] W. Stremmel, "Fatty acid uptake by isolated rat heart myocytes represents a carrier-mediated transport process," *Journal of Clinical Investigation,* vol. 81, no. 3, p. 844, 1988.

[146] G. V. Richieri and A. M. Kleinfeld, "Unbound free fatty acid levels in human serum," *Journal of lipid research,* vol. 36, no. 2, pp. 229-240, 1995.

[147] M. T. Prieto-Sánchez *et al.*, "Placental MFSD2a transporter is related to decreased DHA in cord blood of women with treated gestational diabetes," *Clinical Nutrition,* 2016.

[148] A. Malassine *et al.*, "Ultrastructural visualization of the internalization of low density lipoprotein by human placental cells," *Histochemistry,* vol. 87, no. 5, pp. 457-464, 1987.

[149] K. Kolahi, S. Louey, O. Varlamov, and K. Thornburg, "Real-Time Tracking of BODIPY-C12 Long-Chain Fatty Acid in Human Term Placenta Reveals Unique Lipid Dynamics in Cytotrophoblast Cells," *PLOS ONE,* vol. 11, no. 4, p. e0153522, 2016.

[150] D. C. Kuhn, M. A. Crawford, M. J. Stuart, J. J. Botti, and L. M. Demers, "Alterations in transfer and lipid distribution of arachidonic acid in placentas of diabetic pregnancies," *Diabetes,* vol. 39, no. 8, pp. 914-918, 1990.

[151] F. Visiedo, F. Bugatto, V. Sánchez, I. Cozar-Castellano, J. L. Bartha, and G. Perdomo, "High glucose levels reduce fatty acid oxidation and increase triglyceride accumulation in human placenta," *American Journal of Physiology-Endocrinology and Metabolism,* vol. 305, no. 2, pp. E205-E212, 2013.

[152] M. Crawford, "Placental delivery of arachidonic and docosahexaenoic acids: implications for the lipid nutrition of preterm infants," *The American journal of clinical nutrition,* vol. 71, no. 1, pp. 275S-284S, 2000.

[153] W. Schlörmann *et al.*, "Foetal cord blood contains higher portions of n-3 and n-6 long-chain PUFA but lower portions of trans C18: 1 isomers than maternal blood," *Food & nutrition research,* vol. 59, 2015.

[154] S. M. Nelson, P. Matthews, and L. Poston, "Maternal metabolism and obesity: modifiable determinants of pregnancy outcome," *Human reproduction update,* vol. 16, no. 3, pp. 255-275, 2010.

[155] N. J. Sebire *et al.*, "Maternal obesity and pregnancy outcome: a study of 287 213 pregnancies in London," *International Journal of Obesity & Related Metabolic Disorders,* vol. 25, no. 8, 2001.

[156] J. M. Baeten, E. A. Bukusi, and M. Lambe, "Pregnancy complications and outcomes among overweight and obese nulliparous women," *American journal of public health,* vol. 91, no. 3, p. 436, 2001.

[157] R. M. Lewis and G. Desoye, "Placental Lipid and Fatty Acid Transfer in Maternal Overnutrition," *Annals of Nutrition and Metabolism,* 2017.

[158] C. Osmond and D. Barker, "Fetal, infant, and childhood growth are predictors of coronary heart disease, diabetes, and hypertension in adult men and women," *Environmental Health Perspectives,* vol. 108, no. Suppl 3, p. 545, 2000.

[159] D. K. Waller *et al.*, "Prepregnancy obesity as a risk factor for structural birth defects," *Archives of pediatrics & adolescent medicine,* vol. 161, no. 8, pp. 745-750, 2007.

[160] A. Gil-Sánchez *et al.*, "Maternal-fetal in vivo transfer of [13C] docosahexaenoic and other fatty acids across the human placenta 12 h after maternal oral intake," *The American Journal of Clinical Nutrition,* vol. 92, no. 1, pp. 115-122, 2010.

[161] K. Abduljalil, P. Furness, T. N. Johnson, A. Rostami-Hodjegan, and H. Soltani, "Anatomical, physiological and metabolic changes with gestational age during normal pregnancy," *Clinical pharmacokinetics,* vol. 51, no. 6, pp. 365-396, 2012.

[162] L. Gaohua, K. Abduljalil, M. Jamei, T. N. Johnson, and A. Rostami-Hodjegan, "A pregnancy physiologically based pharmacokinetic (p-PBPK) model for disposition of drugs metabolized by CYP1A2, CYP2D6 and CYP3A4," *British journal of clinical pharmacology,* vol. 74, no. 5, pp. 873-885, 2012.

[163] C. Cobelli, G. Toffolo, and D. M. Foster, "Tracer-to-tracee ratio for analysis of stable isotope tracer data: link with radioactive kinetic formalism," *American Journal of Physiology-Endocrinology And Metabolism,* vol. 262, no. 6, pp. E968-E975, 1992.

[164] A. A. Nouh, A. M. Alanwar, and A. E. Diab, "Effect of umbilical vein blood flow on perinatal outcome of fetuses with lean and/or hypo-coiled umbilical cord," *Archives of gynecology and obstetrics,* vol. 283, no. 1, pp. 53-58, 2011.

[165] A. C. Yao and J. Lind, "Blood volume in the asphyxiated term neonate," *Neonatology,* vol. 21, no. 3-4, pp. 199-209, 1972.

[166] P. Haggarty, J. Ashton, M. Joynson, D. Abramovich, and K. Page, "Effect of maternal polyunsaturated fatty acid concentration on transport by the human placenta," *Neonatology,* vol. 75, no. 6, pp. 350-359, 1999.

[167] C. L. Paolini *et al.*, "Placental transport of leucine, phenylalanine, glycine, and proline in intrauterine growth-restricted pregnancies," *J Clin Endocrinol Metab,* vol. 86, no. 11, pp. 5427-32, Nov 2001.

[168] J. K. Cleal and R. M. Lewis, "The mechanisms and regulation of placental amino acid transport to the human foetus," (in eng), *J Neuroendocrinol,* Research Support, Non-U.S. Gov't

Review vol. 20, no. 4, pp. 419-26, Apr 2008.

[169] K. L. Widdows *et al.*, "Integration of computational modeling with membrane transport studies reveals new insights into amino acid exchange transport mechanisms," *The FASEB Journal,* vol. 29, no. 6, pp. 2583-2594, 2015.

[170] I. Cetin *et al.*, "Maternal and fetal amino acid concentrations in normal pregnancies and in pregnancies with gestational diabetes mellitus," (in eng), *Am J Obstet Gynecol,* vol. 192, no. 2, pp. 610-7, Feb 2005.

[171] J. K. Cleal *et al.*, "Facilitated transporters mediate net efflux of amino acids to the fetus across the basal membrane of the placental syncytiotrophoblast," *J Physiol,* vol. 589, no. 4, pp. 987-997, February 15, 2011 2011.

[172] U. Lichter-Konecki, C. M. Hipke, and D. S. Konecki, "Human phenylalanine hydroxylase gene expression in kidney and other nonhepatic tissues," *Mol Genet Metab,* vol. 67, no. 4, pp. 308-16, Aug 1999.

[173] A. F. Philipps, I. R. Holzman, C. Teng, and F. C. Battaglia, "Tissue concentrations of free amino acids in term human placentas," (in eng), *Am J Obstet Gynecol,* vol. 131, no. 8, pp. 881-7, Aug 15 1978.

[174] R. M. Lewis *et al.*, "L-serine uptake by human placental microvillous membrane vesicles," (in eng), *Placenta,* Research Support, Non-U.S. Gov't vol. 28, no. 5-6, pp. 445-52, May-Jun 2007.

[175] P. E. L. Day *et al.*, "Partitioning of glutamine synthesised by the isolated perfused human placenta between the maternal and fetal circulations," *Placenta,* vol. 34, no. 12, pp. 1223-1231, DEC 2013 2013.

[176] N. Panitchob *et al.*, "Computational modelling of amino acid exchange and facilitated transport in placental membrane vesicles," *Journal of Theoretical Biology,* vol. 365, pp. 352-364, JAN 21 2015 2015.

[177] M. J. Carroll and M. Young, "The relationship between placental protein synthesis and transfer of amino acids," *Biochem J,* vol. 210, no. 1, pp. 99-105, Jan 15 1983.

[178] S. W. S.Nussey, *Endocrinology*. London, Uk: BIOS Scientific Publisher, 2001.

[179] M. Aufdenblatten *et al.*, "Prematurity is related to high placental cortisol in Preeclampsia," *Pediatric Research,* vol. 65, no. 2, 2009.

[180] R. Brown *et al.*, "Cloning and production of antisera to human placenta 11beta-hds type 2," *J. of Biochemestry,* vol. 313, pp. 1007-17, 1996.

[181] R. Benediktsson, A. Calder, C. Edwards, and J. Secki, "Placental 11beta-hydroxysteroid dehydrogenase: a key regulator of fetal glucocorticoid exposure. Clinical Endocrinology," *Clinical Endocrinology,* vol. 46, pp. 161-165, 1997.

[182] K. Yam, E. Van den Akker, E. van Rossum, A. v. Mullem, and T. Visser, "Is transport of cortisol in liver cells carrier-mediated?," *Erasmus Journal of Medicine,* vol. 3, no. 1, 2012.

[183] B. Murphy, "The influence of serum proteins on the metabolism of cortisol by the human placenta.," *J. Steroid Biochem.,* vol. 10, no. 4, pp. 387-92, 1979.

[184] E. Couturier, O. D. Bruno, P. Metzger, R. Leclercq, and G. Copinschi, "Transport of cortisol, progesterone and cholesterol across isolated mesentery," *The Journal of membrane biology,* vol. 13, no. 1, pp. 89-96, 1973.

[185] A. S. Serov, S. C., D. S. Grebenkov, and M. Filoche, "The role of morphology in mathematical models of placental gas exchange," *Journal of Applied Physiology,* p. 543, 2015.

[186] F.-J. Pettersen and J. O. Høgetveit, "From 3D tissue data to impedance using Simpleware ScanFE+ IP and COMSOL Multiphysics–a tutorial," *Journal of Electrical Bioimpedance,* vol. 2, no. 1, pp. 13-32, 2011.

[187] Y. Saad and M. H. Schultz, "GMRES: A generalized minimal residual algorithm for solving nonsymmetric linear systems," *SIAM Journal on scientific and statistical computing,* vol. 7, no. 3, pp. 856-869, 1986.

[188] H. C. Elman, "A stability analysis of incomplete LU factorizations," *Mathematics of Computation,* pp. 191-217, 1986.

[189] P. K. Kundu and I. M. Cohen, Dowling, D.R., *Fluid Mechanics*. Oxford, UK: Elsevier Inc., 2012.

[190] S. Perazzolo, B. Hirschmugl, C. Wadsack, G. Desoye, R. M. Lewis, and B. G. Sengers, "The influence of placental metabolism on fatty acid transfer to the fetus," *Journal of Lipid Research,* p. jlr. P072355, 2016.

[191] M. Jirkovská, L. Kubínová, J. Janáček, M. Moravcová, V. Krejčí, and P. Karen, "Topological properties and spatial organization of villous capillaries in normal and diabetic placentas," *Journal of vascular research,* vol. 39, no. 3, pp. 268-278, 2002.

[192] M. Higgins, P. Felle, E. Mooney, J. Bannigan, and F. McAuliffe, "Stereology of the placenta in type 1 and type 2 diabetes," *Placenta,* vol. 32, no. 8, pp. 564-569, 2011.

[193] P. L. Bonate and J.-L. Steimer, *Pharmacokinetic-pharmacodynamic modeling and simulation*. Springer, 2006.

[194] A. Vinks, "The future of physiologically based pharmacokinetic modeling to predict drug exposure in pregnant women," *CPT: pharmacometrics & systems pharmacology,* vol. 2, no. 3, pp. 1-3, 2013.

[195] M. Gauster *et al.*, "Dysregulation of placental endothelial lipase in obese women with gestational diabetes mellitus," *Diabetes,* vol. 60, no. 10, pp. 2457-2464, 2011.

[196] E. Brass, E. Hanson, and P. F. O'Tierney-Ginn, "Placental oleic acid uptake is lower in male offspring of obese women," *Placenta,* vol. 34, no. 6, pp. 503-509, 2013.